Filler-hydrates Adhesion Properties in Cement Paste System
Development of Sustainable Building Materials

Ouyang, Xiaowei

DOI
10.4233/uuid:4d613364-6f2e-4a61-be9f-a71a6c05ebdc

Publication date
2017

Document Version
Final published version

Citation (APA)
Ouyang, X. (2017). *Filler-hydrates Adhesion Properties in Cement Paste System: Development of Sustainable Building Materials*. [Dissertation (TU Delft), Delft University of Technology]. https://doi.org/10.4233/uuid:4d613364-6f2e-4a61-be9f-a71a6c05ebdc

Filler-hydrates Adhesion Properties in Cement Paste System

Development of Sustainable Building Materials

Xiaowei Ouyang

Filler-hydrates Adhesion Properties in Cement Paste System

Development of Sustainable Building Materials

Filler-hydrates Adhesion Properties in Cement Paste System

Development of Sustainable Building Materials

Proefschrift

ter verkrijging van de graad van doctor
aan de Technische Universiteit Delft,
op gezag van de Rector Magnificus prof. ir. K.C.A.M. Luyben;
voorzitter van het College voor Promoties,
in het openbaar te verdedigen op
Maandag 25 september 2017 om 10.00 uur

door

Xiaowei OUYANG

Master of Engineering in Structure Engineering
Jinan University, P.R.China
geboren te Hunan, P.R.China

Dit proefschrift is goedgekeurd door de

Promotor: Prof. dr. ir. K. van Breugel

Copromotor: Dr. G. Ye
Copromotor: Dr. D. A. Koleva

Samenstelling promotiecommissie:

Rector Magnificus,	voorzitter
Prof. dr. ir. K. van Breugel,	Technische Universiteit Delft, promotor
Dr. G. Ye,	Technische Universiteit Delft, copromotor
Dr. D. A. Koleva,	Technische Universiteit Delft, copromotor

Onafhankelijke leden:

Prof. dr. Stephen Picken,	Technische Universiteit Delft
Dr. Jorge S. Dolado,	TECNALIA Research & Innovation, Spain
Prof. Kefei Li,	Tsinghua University, P. R. China
Prof. dr. ir. H.E.J.G. Schlangen	Technische Universiteit Delft

ISBN: 978-94-6186-842-8

Keywords: filler, adhesion, cement paste, limestone powder, micronized sand, contact area, strength.

Printing: Gildeprint

Cover design: Xiaowei Ouyang

Printed in the Netherlands.

To my family

Table of Contents

List of Figures

List of Tables

List of Symbols

Roman lower case letters

a	Intrinsic strength of material at zero capillary porosity	[MPa]
$a(t)$	Degree of hydration	[-]
a_N	Normal force influence factor	[-]
a_M	Bending influence factor	[-]
c	The quantity of binder	[g]
f_c	Compressive strength	[MPa]
f_t	Tensile strength	[MPa]
f^e	The local force vector	[kN]
g	The ratio of filler to binder	[-]
k_s	The shear correction factor	[-]
k^e	The element stiffness matrix in the local domain	[-]
l	Length	[m]
x	Solid-space ratio	[-]
r_K	Meniscus radius	[m]
t	Time	[s]
u	Displacement	[m]
ν	Poisson's ratio	[-]
w	Cross sectional moment of resistance	[m^3]

Roman capital letters

A	The cross-sectional area of element	[m^2]
A_s	The shear cross-sectional area	[m^2]
D	Distance	[m]
E	Elastic modulus	[GPa]
G	Shear modulus	[GPa]
K	The shear correction factor	[-]
I	The moments of inertia	[-]
J	Polar moment of inertia	[-]
M	Bending moments	[kN·m]
N	Normal force	[kN]
$\Delta P_{Laplace}$	Laplace pressure	[MPa]
T	Temperature	[°C]
W	The non-evaporable water of hydration of the cement	[g]

Greek letters

ρ	The ionic concentrations in the solution	[mmol/l]
ε_r	Dielectric constant	[-]
Φ_1, Φ_2	The shear effect adjustment factors	[-]
σ	Surface charge density	[C/m^2]
σ_t	The maximum tensile stress	[kPa]
γ_{LV}	Surface tension	[J/m^2]

List of Abbreviations

AFM	Atomic-force microscopy
CH	Calcium hydroxide
C-S-H	Calcium silicate hydrate
C_3S	Tricalcium silicate $3CaO \cdot SiO_2$
C_2S	Dicalcium silicate $2CaO \cdot SiO_2$
C_3A	Tricalcium aluminate $3CaO \cdot Al_2O_3$
C_4AF	Calcium ferroaluminate $4CaO \cdot Al_2O_3 \cdot Fe_2O_3$
CO_2	Carbon dioxide
CC-SECA	Specific effective contact area between cement particles
CF-SECA	Specific effective contact area between cement particle and filler particle
DLVO	Derjaguin, Landau, Verwey, and Overbeek
DTG	Differential thermogravimetric
EDL	Electrical double layer
EDS	Energy dispersive spectroscopy
ECA	Effective contact area
ITZ	Interfacial transition zone
IEP	Iso-electric point
LP	Limestone powder
MS	Micronized sand
N-A-S-H	Sodium aluminosilicate hydrate
OPC	Ordinary Portland cement
PSD	Particle size distribution
PZC	Point of zero charge
SEM	Scanning electron microscope
SE	Secondary electrons
SECA	Specific effective contact area
SI	Strong interface
TG	Thermogravimetric
TGA	Thermogravimetric analysis
TEM	Transmission electron microscopy
w/c	Water-to-cement ratio
w/b	Water-to-binder ratio
WI	Weak interface
XRD	X-ray diffraction

1

General Introduction

This chapter starts with a presentation of the background of the research. Then the objectives, scope and methodology of this research are explained. Finally, the coherence between the chapters is given.

1.1 Research background

Concrete is by far the most widely used building material in the world. A basic component of concrete that binds the aggregate particles together is Portland cement paste. This binder is produced in a process in which natural lime-bearing rocks and other materials (such as clay) are burned at around 1500 °C, quenched and ground to a fine powder that can react with water. This process is responsible for a high CO_2 emission and high energy consumption. To make concrete more environment friendly, and possible cheaper, part of the Portland cement can be replaced by fillers, such as limestone or quartz powder [1-3]. Additions of limestone or quartz powder have been reported to exert a limited chemical effect on cement hydration [4, 5]. The main quasi-chemical effect of added limestone and quartz powder is that they accelerate cement hydration by facilitating nucleation and growth of reaction products at their surfaces [1, 5-7]. These effects are most important in the early stage of hydration when the microstructure is rapidly developing. The hydrates, mainly calcium silicate hydrate (C-S-H), which precipitate and constitute at least 60% of the fully hydrated cement paste, form connections between the cement and filler grains, leading to setting and strength development.

Finer fillers in cement paste can result in improvements in strength because of a lower porosity and a denser packing [8, 9]. However, the use of fillers also results in dilution of Portland cement particles and their strength-providing reaction products in the paste for keeping water-to-binder ratio consistent. This ‘dilution’ effect will lead to an increased porosity. Above a critical amount of filler, the effect of dilution exceeds the effect of packing, resulting in a lower strength of the hardened paste or concrete [1, 10]. These ‘packing’ and ‘dilution’ effects on the strength of the hardened paste or concrete mainly depend on the replacement level of the filler and its fineness. It is well known that reducing porosity will increase the interparticle connections in the cement paste and hence increase the strength of the binder [1, 11, 12]. These effects (porosity, packing and dilution) on the strength of cement paste have been studied intensively. However, they (porosity, packing and dilution) cannot explain the difference in performance of different fillers.

The affinity of filler particles for cement hydrates, which depends on the physical and chemical properties of the filler, also influences the strength of blended cement paste by affecting the adhesion strength between filler particles and reaction products. However, the role of filler-hydrates adhesion properties in the strength of blended cement paste attracted very little attention yet. This is attributed to the fact that the gel-space ratio is assumed to play a primary role in strength of cement paste and the contact area between filler particles and reaction products is very small (the contact area between gel particles is approximately 5% of the cross section of a paste having a porosity of 50% [13], and the contact area between gel particles and filler particles even smaller). Various studies [14-16] report on the effect of the chemical and physical nature of fillers on the adhesion strength. However, the basic questions how the chemistry and surface characteristics of fillers affect this adhesion, and why filler particles and reaction products adhere to each other in cement paste are rarely addressed yet.

Improvement of the effect of fillers in cementitious materials, especially their effect on the properties of the interface between filler particles and hydration products, is a big issue and challenge today. Clarifying the role of filler-hydrates adhesion properties in the strength of cement paste and understanding the adhesion mechanisms between filler particles and hydration products are, therefore, important. The knowledge acquired in this research will provide a stimulus to the search for new fillers.

1.2 Objectives of this research

The main goal of this research is to get a better understanding of the adhesion mechanisms between fillers and hydration products in blended cement paste. The study contains the following objectives:

- As the cement particles continue to hydrate, more particles become connected, and the strength of cement paste increases. A parameter, i.e. the contact area, has been introduced to describe the interparticle connections. This numerical contact area can be related directly to the measured compressive strength of cement paste. However, the validation of the concept of contact area in case of blended systems is still lacking. Therefore, one of the objectives is to validate the concept of contact area as strength parameter.
- The role of filler-hydrates adhesion properties (quality of contact area between filler particles and reaction products) in the strength of blended cement paste is not well described. Therefore, the second objective of this research is to elucidate and quantify the influence of the filler-hydrates adhesion properties on the strength of blended cement paste.
- The third objective is to quantify the mechanical properties of filler-hydrates interface or the strength of filler-hydrates adhesion at the microscale.
- The fourth objective of this research is to investigate the effect of chemical surface properties on filler-hydrates adhesion properties in order to better understand the bond between filler surface and cement hydrates.
- Even though the influence of structural features (shape, surface roughness, etc.) of *aggregates* on the mechanical properties of concrete is well studied, the influence of structural features of *fillers* on the strength of hardened blended cement paste is still not clear because of the difference in size scale. The filler (1-100 µm) is much finer than the aggregate (1-100 mm). The fifth objective is, therefore, to investigate the effect of microstructural features (shape, surface roughness, etc.), particle size distribution and volume fraction of fillers on the strength of hardened blended cement paste and the filler-hydrates adhesion properties.

1.3 Scope of this research

In this research only two types of filler will be used, i.e. limestone powder and micronized sand. No other fillers or additives are considered. The effect of fillers will be studied up to an age of 90 days. The fillers are considered as quasi-inert mineral powders with an average grain size similar to that of Portland cement.

It is known that calcium silicate hydrate (C-S-H) gel, representing around 60% of the fully hydrated cement paste, plays the role as the glue that binds the original cement particles together into a cohesive whole. Calcium hydroxide (CH) constitutes 20 to 25% of the volume of solids in the hydrated cement paste. It tends to form large crystals with a distinctive hexagonal-prism morphology. Compared to C-S-H, the strength-contributing potential of CH is limited as a result of a considerably lower surface area. All the other hydration products are intrinsically strong but do not form strong connections to the solid phases they are in contact with and so cannot contribute much to the overall strength [14]. Therefore, the term ‘hydrates’ in this research mainly refers to C-S-H and the filler-hydrates adhesion refers to the adhesion between filler surfaces and C-S-H gel.

1.4 Strategy of this research

The strategy to achieve the objectives of this research is as follows:

- First, the compressive strength of cement paste blended with limestone powder and micronized sand is studied experimentally. The contact area between different solid phases in these blended cement pastes is quantified numerically. The relationship between the measured compressive strength and simulated contact area is then analysed. Based on this relationship, the influence of the filler-hydrates adhesion properties on the strength of blended cement paste is investigated.
- Second, microscopic observations of the crack paths and fracture surfaces of loaded blended cement pastes are proposed to experimentally evaluate the micromechanical properties of the filler-hydrates interface. Lattice type modelling is used to explain the experimentally observed features of cracks. The mechanical properties of the filler-hydrates interface at microscale are quantified.
- The influence of the chemical properties of filler on the interaction between main ions in the pore solution of blended cement paste and filler surfaces is studied via zeta potential measurements in model solutions. Meanwhile, microscopic studies of the nucleation and growth of C-S-H on the surface of these filler particles are performed by scanning electron microscopy (SEM) to further elucidate these interactions. Then the effect of surface chemical properties on filler-hydrates adhesion properties is studied. Based on these studies, the adhesion mechanisms between C-S-H and fillers are analysed.

- The lattice model is also used to investigate the effect of microstructural features (shape, surface roughness, etc.), particle size distribution and volume fraction of fillers on the strength and fracturing of hardened blended cement paste and the filler-hydrates adhesion properties.

1.5 Research outline

As shown in Fig. 1.1, this dissertation consists of 7 chapters. This current chapter presents the general introduction. Chapter 2 gives a literature survey of the fundamental knowledge and background of the effects of fillers on the cement-based materials and cohesion or adhesion between particles or reaction products in the cement-based materials, and specifies the knowledge gaps that have to be bridged by this research.

In chapter 3, the compressive strength of cement paste blended with limestone powder and micronized sand is studied experimentally. Parallel with this experimental study, the contact area between different solid phases in these blended cement paste is quantified numerically. The relationship between the measured compressive strength and the simulated contact area is then analysed. With this relationship, the role of the filler-hydrates adhesion properties in the strength of blended cement paste is investigated and hence better understood.

To explain the results of mesoscale investigations in chapter 3, the micromechanical properties of the filler-hydrates interface, i.e. the strength of filler-hydrates adhesion, are evaluated in chapter 4. The microscopic observations of the crack paths and fracture surfaces of loaded cement pastes, together with lattice type modelling of cracking behaviour are performed in this investigation.

In chapter 5, the effect of chemical properties of fillers on filler-hydrates adhesion properties is studied by investigating the interaction between filler surfaces and main ions in the pore solution of blended cement paste. This interaction is investigated using zeta potential measurements of fillers in model solutions, together with microscopic observations of the nucleation and growth of C-S-H on the surface of these filler particles. This study leads to a deeper understanding of the adhesion mechanisms between C-S-H and filler surfaces.

To understand the fracture behaviour of cement paste with different filler-hydrates adhesion properties, the effect of microstructural features (shape, surface roughness, etc.), particle size distribution and volume fraction of fillers on the crack patterns and strength of blended cement paste is investigated using a lattice model. This is discussed in chapter 6.

Chapter 7 summarizes the results of this research and gives recommendations for further research.

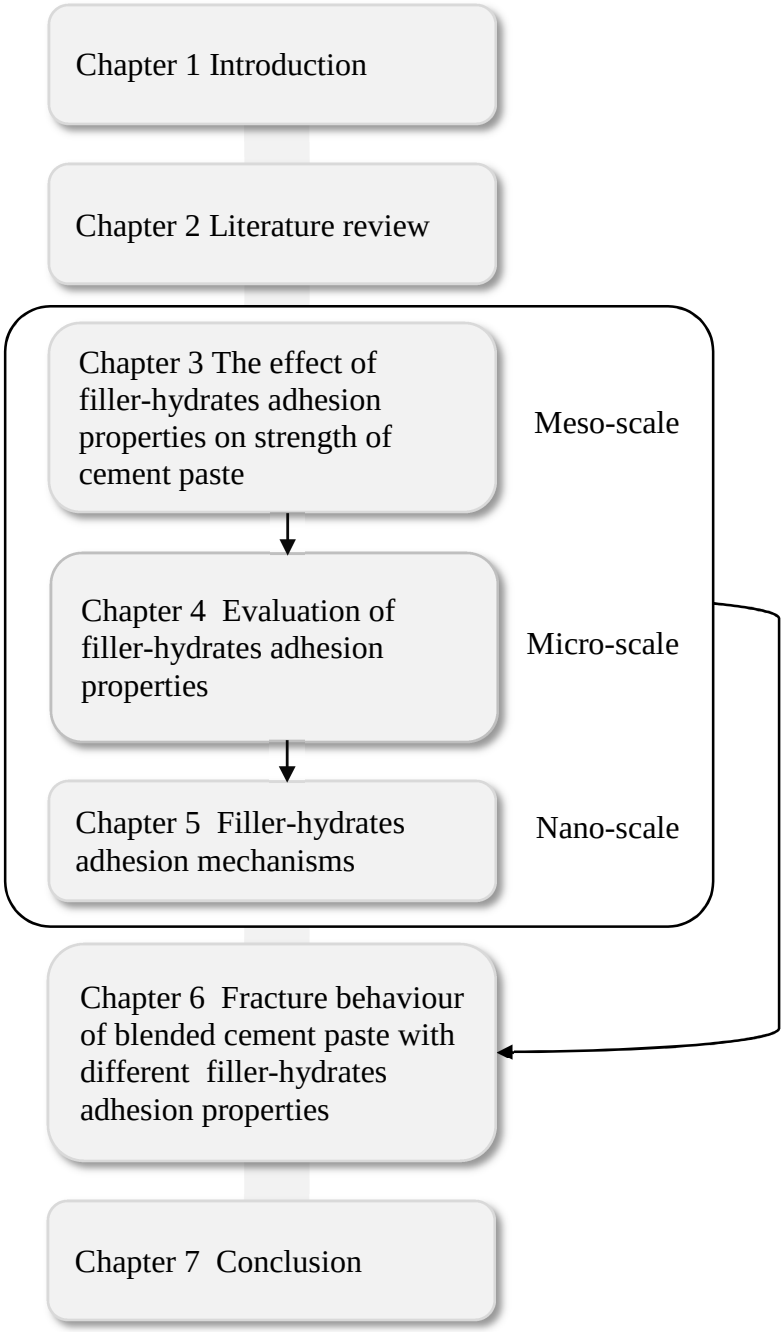

Fig. 1.1 Outline of this thesis.

References

1. Bonavetti, V., et al., *Limestone filler cement in low w/c concrete: A rational use of energy.* Cement and Concrete Research, 2003. **33**(6): p. 865-871.
2. Nehdi, M., S. Mindess, and P.C. Aitcin, *Optimization of high strength limestone filler cement mortars.* Cement and Concrete Research, 1996. **26**(6): p. 883-893.
3. Justnes, H., et al., *Microstructure and performance of energetically modified cement (EMC) with high filler content.* Cement & Concrete Composites, 2007. **29**(7): p. 533-541.
4. Lothenbach, B., et al., *Influence of limestone on the hydration of Portland cements.* Cement and Concrete Research, 2008. **38**(6): p. 848-860.
5. Bentz, D.P., *Modeling the influence of limestone filler on cement hydration using CEMHYD3D.* Cement & Concrete Composites, 2006. **28**(2): p. 124-129.
6. Gutteridge, W.A. and J.A. Dalziel, *Filler cement: The effect of the secondary component on the hydration of Portland cement.* Cement and Concrete Research, 1990. **20**(5): p. 778-782.
7. Soroka, I. and N. Stern, *Calcareous fillers and the compressive strength of portland cement.* Cement and Concrete Research, 1976. **6**(3): p. 367-376.
8. Moosberg-Bustnes, H., B. Lagerblad, and E. Forssberg, *The function of fillers in concrete.* Materials and Structures, 2004. **37**(2): p. 74-81.
9. Kronlöf, A., *Filler effect of inert mineral powder in concrete.* VTT PUBLICATIONS, 1997.
10. Lawrence, P., M. Cyr, and E. Ringot, *Mineral admixtures in mortars - Effect of inert materials on short-term hydration.* Cement and Concrete Research, 2003. **33**(12): p. 1939-1947.
11. Taylor, H.F., *Cement chemistry*1997: Thomas Telford.
12. Igarashi, S., V. Kawamura, and A. Watanabe, *Analysis of cement pastes and mortars by a combination of backscatter-based SEM image analysis and calculations based on the Powers model.* Cement & Concrete Composites, 2004. **26**(8): p. 977-985.
13. Soroka, I., *Portland cement paste and concrete.* 1980.
14. Mehta, P. and P.J.M. Monteiro, *Concrete: Microstructure, Properties, and Materials*2006: McGraw-Hill Education.
15. French, C.W. and A. Mokhtarzadeh, *High strength concrete: Effects of materials, curing and test procedures on short-term compressive strength.* PCI Journal, 1993. **38**(3): p. 76-87.
16. Bentz, D.P., et al., *Multi-scale investigation of the performance of limestone in concrete.* Construction and Building Materials, 2015. **75**: p. 1-10.

2

Literature Review

This chapter gives a brief overview on Portland cement paste and the effect of filler on blended cement paste in view of strength. First, a literature survey of the strength of cement paste is presented. This is done by presenting the characteristics of the main phase (C-S-H) responsible for the strength of cement paste and the forces controlling the cohesion of C-S-H. Moreover, the effects (i.e., dilution, packing density and nucleation) of filler on the strength of cement paste are highlighted.

2.1 Introduction

According to CEMBUREAU, cement production has undergone a tremendous development. In 1900, the total world production of cement was about 10 million tonnes; in 1998 it was 1.6 billion tonnes; in 2015, it reached 4.6 billion tonnes. Meanwhile, the cement industry is facing challenges, e.g., the increase of energy costs, needs to reduce CO_2 emissions, and the supply of raw materials in sufficient qualities and amounts. The concrete of tomorrow should be more durable and has to satisfy socio-economic needs at the lowest environmental impact. The binders of tomorrow will probably contain less clinker. It should be possible to make more concrete with the same amount of binder [1].

In order to make a more efficient use of the cement in concrete, many pozzolanic mineral admixtures (fly ash, slag etc.) and inert fillers (limestone powder, quartz powder etc.) have been used in the cement industry. This research focuses on the inert fillers. Fillers are here defined as quasi-inert mineral powders with an average grains size similar to that of Portland cement. Such fillers are used as a replacement for Portland cement to make concrete more sustainable. The implementation for this replacement requires in-depth knowledge of the effect of fillers on the properties of cementitious materials. Their effect on the strength of the blended cement paste is the main topic of this research.

Understanding the strength of Portland cement paste and the nature of cohesion forces in hardened cement-based materials is the first step towards understanding the effect of filler on the strength of blended cement paste and the adhesion mechanisms between filler particles and hydration products.

2.2 Strength of cement paste

When cement is mixed with water, it undergoes a dissolution reaction generating calcium, silicate and aluminate ions. New products (hydrates) then precipitate when their solubility limit is reached. The most important products are calcium silicate hydrate (C-S-H) and calcium hydroxide (CH) [2]. As the hydration reaction proceeds, more and more anhydrous cement is converted into hydrates. At the same time, the porosity decreases since the volume of hydrates (including interlayer water) is more than twice than that of the initial anhydrous cement [3]. The ‘soft’ state of a cement paste is transformed to the hardened state (setting). It involves two fundamental processes, namely coagulation and rigidification [4]. The coagulation of the slurry results from the attractive forces between particles and leads to the formation of a mechanically reversible connected network. The setting appears to be caused by a continuous reinforcing process at the connections between particles [2]. This leads to a mechanically irreversible network of particles [5]. Over time, hardening leads to an increase in strength due to a continuously filling up the pore space.

According to Powers [3] and Taylor [6], porosity is a key factor in deciding the strength of hardened cement pastes. An assumption that the relative strength of the paste

depends on the degree to which gel fills the space available for it gives an empirical relationship between the porosity and the strength of a paste [3]. The degree to which gel fills available space can be expressed as a ratio of the volume of gel to the volume of available space. A typical relationship between compressive strength and the gel-space ratio is shown in Fig. 2.1. Powers [3] found that the compressive strength f_c of the hardened cement paste or mortar was related to the cube of the gel-space ratio:

$$f_c = ax^3 \tag{2.1}$$

where a is the intrinsic strength of the material at zero capillary porosity, and x the gel-space ratio. The coefficient a is assumed to be different for different cement [7].

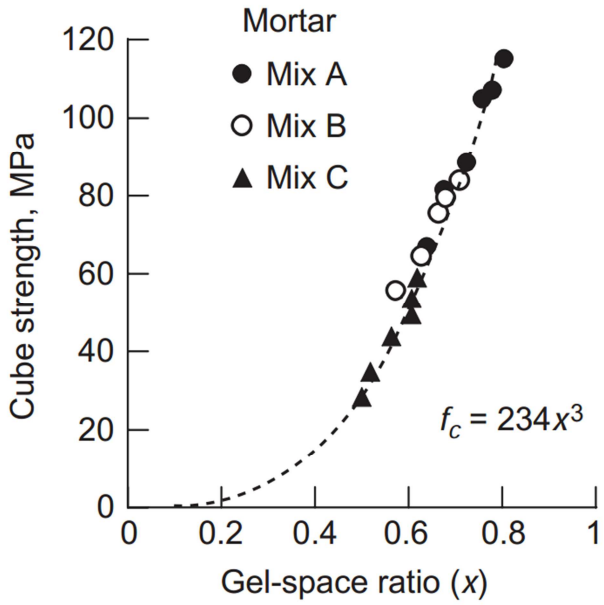

Fig. 2.1 Porosity-strength relation in solids: Portland cement mortars with different mix proportions [3, 7].

From a micro structural point of view, the hydration process is a process of micro-structure formation [8]. As the hydration reaction proceeds, the hydrating particles start to make contact and the number of contact points will increase with increasing hydration. Gradually the earlier formed contact points will change into contact areas. Over time, the number of contact points and the size of the contact surface area between hydrating particles will increase. At the same time, the porosity will decrease and the strength will increase. Several researchers have pointed out that strength develops due to the increasing number of contact points and the increasing size of the contact surface area between hydrating particles during the hydration process [8-11]. A strong correlation between the summarized contact area of a virtual microstructure and the compressive strength of cement paste was found [12-14] (Fig. 2.2). The numerical

coefficient of this correlation depends principally on the intrinsic strength of the gel, and would be different for different cement.

As to the origin of the strength of the gel itself, Powers [3] assumed that strength arises from two general kinds of cohesive bonds: (1) physical attraction between solid surfaces and (2) chemical bonds. Since gel pores are only about 0.8 nm wide, it seems that London-van der Waals forces tend to draw the surfaces together or at least to hold the particles in positions of the least potential energy. Since water cannot disperse gel particles, it seems that the particles are chemically bonded to each other (cross-linked). Such bonds, much stronger than the van der Waals bonds, add significantly to the overall strength. There is a good reason to believe, however, that only a small fraction of the surface of a gel particle is chemically bonded to neighboring particles and that physical bonds are more important. Since Powers hypothesis, which dates back to the fifties of the paste century, considerable progress has been made in this field (i.e., the origin of the strength of the cement gel). In the following section, a brief overview of the research on the strength of C-S-H gel is given.

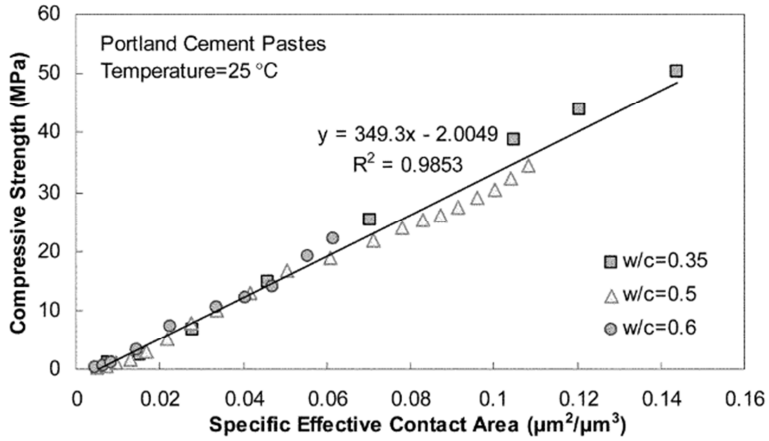

Fig. 2.2 Relationship between the calculated contact area of a virtual microstructure and measured compressive strength of cement paste [13].

2.3 Cohesion of cement paste

Among the precipitated hydrated phases, the hydrated calcium silicate (C-S-H) accounts for more than 60% in the hydrated Portland cement paste. It is responsible for setting and hardening of cement and also for the mechanical performances of the cement pastes [6, 15]. Hardened cement paste has a high compressive strength, whereas its tensile strength is extremely low [15]. It has been suggested that this is because the cohesion of the network of hydration products is due to short-range surface forces between C-S-H particles [16-19]. A closer look at the main hydrate (C-S-H) and at the interparticle forces controlling the cohesion in cement pastes is taken in what follows.

2.3.1 Structure of C-S-H

C-S-H is the most important hydrate responsible for cohesion in hardened cement paste [2]. Morphologically, C-S-H is assumed to be made of ordered stacks of up to several tens or even hundreds of nm-thick lamellae. A TEM observation of the ordered stacks is presented in Fig. 2.3. Over the years, several models for this hydrate have been proposed [3, 20-26], but debates about the structure of C-S-H are still ongoing. Today, it is generally accepted that the average structure of C–S–H is similar to that of tobermorite and/or jennite. It has been assumed that silicate anion layers have a net negative charge and are held together by Ca^{2+} cations in the interlayer region (Fig. 2.4).

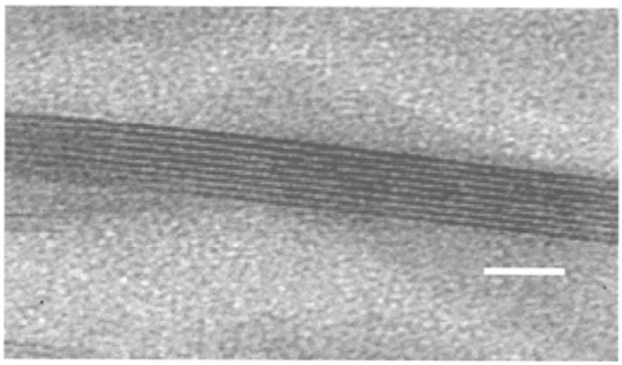

Fig. 2.3 TEM micrograph of C-S-H (scale bar: 15 nm) [27].

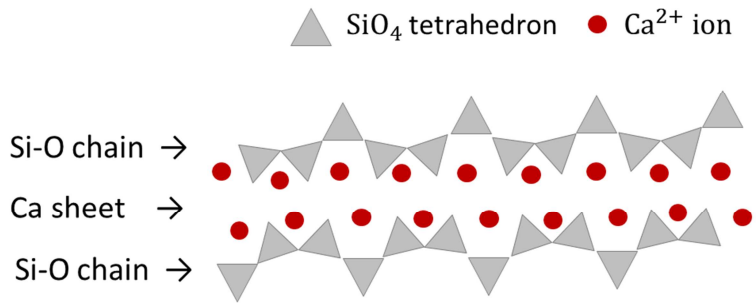

Fig. 2.4 Schematic diagram showing the structure of tobermorite-based C–S–H (adapted from [28]).

In smectite clays, similar structural arrangements can be found. Both smectite clays and C-S-H have individual negatively charged nm-thick layers that can accommodate cations to compensate the deficit in charge in the interlayer space [27]. It has been pointed out that the surface charge of the thick layers for smectite clays is 2 to 5 times less significant in comparison to C-S-H (depending on the Ca/Si ratio) [29]. When they are immersed in water, a compact of cement hydrates does not disintegrate, while smectite clays exhibit a quasi-unlimited increase of the interlamellar distance due to electrical double layer repulsion. However, with high valence ions, such as Ca^{2+}, smectite clays exhibit restricted swelling [27]. These parallel comparative studies between smectite clays and C-S-H may provide a clue for understanding the cohesion of cement paste.

2.3.2 Origin of cohesion at the (sub)nanoscale

Pellenq and van Damme [2] pointed out that atomic-level cohesion of C-S-H can be simulated at this small length scale. The results of atomic-level simulations indicate the ionic character of the bonds in the lamellae is close to 60%. The charge of the interlamellar calcium ions is +1.38. This is slightly higher than for the ions within the lamellae (+1.29), but is still much lower than the value (+2.0) expected for a purely ionic bond. This indicates that the interlayer calcium ions are linked to the lamellae by a strong ionic-covalent bond[*]. This may be considered as the reason for the non-exchangeable character of these ions, contrary to the mobile and exchangeable character of interlamellar ions in smectite clays [27, 30, 31].

At the (sub)nanoscale, the inter-layer calcium ions are linked to the tobermoritic C-S-H lamellae by a strong ionic-covalent bond. This ionic-covalent bond enable C-S-H lamellae to be compactly stacked and form a C-S-H particle with typical dimensions 60 × 30 × 5 nm^3. At the nanoscale, these nanoparticles are compacted and form a gel. The origin of cohesion between these nano C-S-H particles is addressed in what follows.

2.3.3 Origin of cohesion at the nanoscale

Sereda and Soroka [32] conducted an experiment of ‘compacts’. These authors first synthesized hydrates by dispersing anhydrous cement powder in a large volume of water and let the hydration reaction take place. The powder was then filtered and compacted. For the same hydration levels and porosities, this compacted sample and a sample prepared by mixing cement with water in the usual way developed essentially the same strength, as shown in Fig. 2.5. It indicates that surface forces are considered responsible for the interparticle cohesion of cement paste. Several interparticle surface forces are described in what follows. It includes van der Waals force, electric double layer force, capillarity force and ion-ion correlation force.

[*] Ionic-covalent bond is the bond having both ionic and covalent character.

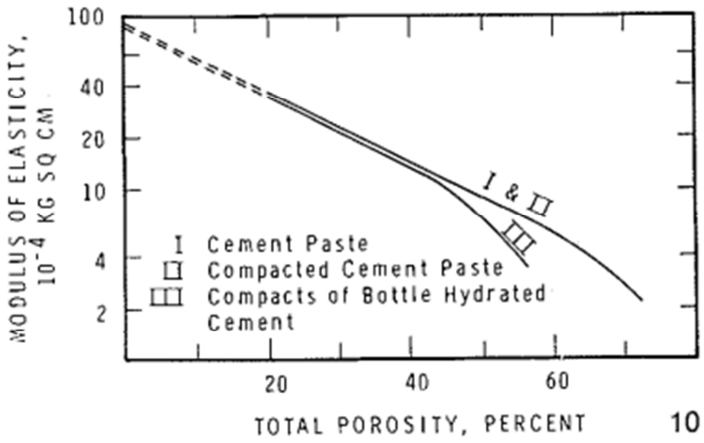

Fig. 2.5 Young's modulus vs porosity relations for various hydrated cement specimens [32].

2.3.3.1 Van der Waals force

Van der Waals forces include the forces between permanent dipoles (Keesom force), the forces between a permanent dipole and a corresponding induced dipole (Debye force), and the forces between instantaneously induced dipoles (London dispersion force) [33]. Van der Waals forces differ from chemical bond because they result from fluctuations in charge density of particles. Van der Waals force can be measured by atomic-force microscopy (AFM). The Hamaker constant can be roughly defined as a material property that represents the strength of van der Waals interactions between particles. Table 2.1 summarises reported values for the Hamaker constants for fillers and C-S-H, as well as the related adhesion forces between these particles as measured by AFM. It has been assumed that the van der Waals forces between different particles are similar. If van der Waals forces were the main forces ensuring the cohesion of hardened cement paste, then many kinds of particles with a roughly similar composition and particle size distribution would have, at the same density, a comparable cohesion. This is not confirmed by common experience. Gmira et al [19], Pellenq et al [2] and Jonsson et al [15] suggested that the van der Waals force has only a marginal contribution to the cohesion of cement pastes.

Table 2.1 Adhesion forces measured between the silica tip and atomically smooth mineral surfaces and Hamaker constants of materials [17, 34].

Substrate/tip	Calcite/silica	C-S-H/silica	C-S-H/calcite	C-S-H/C-S-H
Adhesion force measured in air (nN)	36.8	39.4	48.8	60.0
Hamaker constant of tip in air (10^{-20}J)	6.6	6.6	10.1	14
Hamaker constant of tip in water (10^{-20}J)	1.9	1.9	2.5	-

2.3.3.2 Electric double layer force

Most solids bear electrical charges on their surfaces if put in a liquid environment. In contact with a liquid, surface groups dissociate and ions are released into solution. This results in the development of a surface potential, which will attract counterions from the surrounding solution and exclude co-ions (Fig. 2.6). In equilibrium, the surface charge is balanced by an equal but opposite charge of counterions. The region of counterions is called the electrical double layer. According to the Stern model [35], the electrical double layer (EDL) is composed of the Stern layer and the diffuse layer (Fig. 2.6).

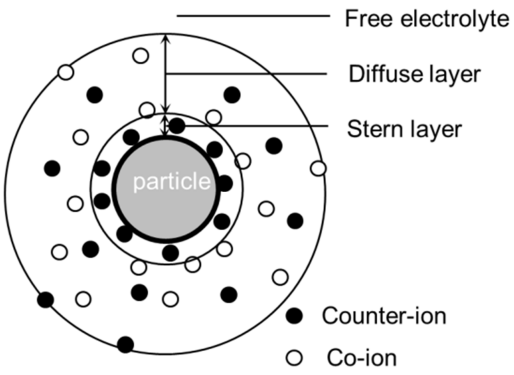

Fig. 2.6 Schematic illustration of the electrical double layer (adapted from [36]).

Electric double layer forces occur between two charged surfaces when counterions are present (Fig. 2.7). The strength of these forces increases with the magnitude of the surface charge density (σ). For two similarly charged objects, this force is repulsive and decays exponentially at larger distances [37].

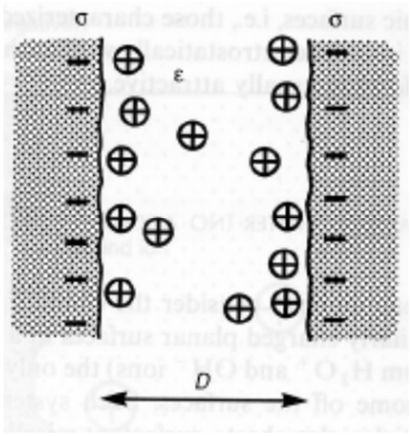

Fig. 2.7 Two negatively charged surfaces of surface charge density σ separated by a distance D (a); the counterions density profile ρ_x and electrostatic potential ψ_x (b) [38].

DLVO theory is a framework for the balance between the repulsive double layer forces and the attractive van der Waals forces [39, 40] (Fig. 2.8). The theory assumes that the interaction forces can be approximated by a superposition of electric double layer forces and van der Waals forces. In a symmetric system, van der Waals forces are attractive and electric double layer forces are repulsive. Although DLVO theory works fairly well for particles with a low surface charge in the presence of monovalent counterions, e.g., K^+ and Na^+, there is now ample evidence that it fails to account correctly for interparticle forces at short distances and in the presence of divalent or multivalent ions, e.g., Ca^{2+} and Al^{3+}, in the electrolytic solution [19, 41, 42].

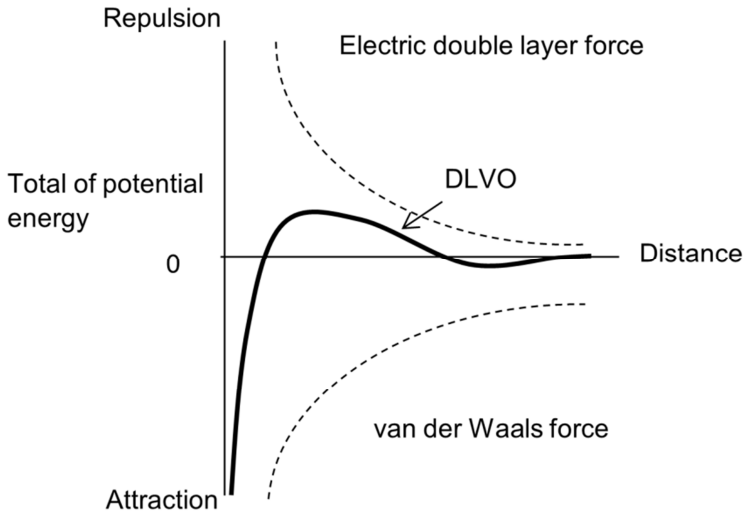

Fig. 2.8 Energy diagram for DLVO theory (description of two types of interactive force: van der Waals attractive and electric double layer repulsive forces).

2.3.3.3 Capillary force

Some cohesion may be detected in finely divided materials, or in a thin tube (Fig. 2.9), due to microscopic capillary bridges. The attractive capillary force is related to the Laplace pressure across the air/water meniscus [19, 42, 43]:

$$\Delta P_{Laplace} = 2\,\gamma_{LV}/r_K \qquad (2.2)$$

where γ_{LV} is the surface tension of the liquid, r_K is the meniscus radius (Fig. 2.9a). As the vapour pressure increases, the meniscus radius decreases, so that cohesion goes through a maximum. In a piece of hardened cement paste, the pressure in the residual water is negative with respect to the atmospheric pressure, which leads to (drying) shrinkage. In narrow pores, this negative pressure may reach very high value. At a spacing of 1.5 nm between the platelets (Fig. 2.9b), it can be as high as -100 MPa [19]. In saturated materials capillary forces are, however, not present. Because hardened cement paste keeps its strength quasi-indefinitely in water, capillary forces are unable to provide the general explanation for the cohesion of cement hydrates [19].

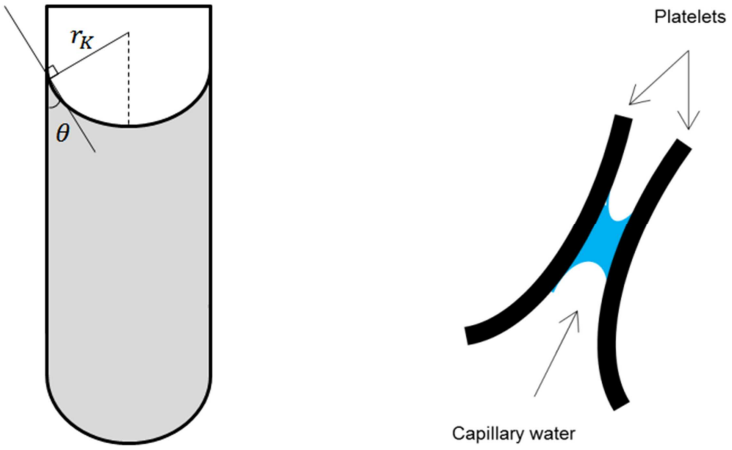

(a) (b)

Fig. 2.9 Example of capillary bridges formed on the top water surface in a tube (a) and formed between two finely divided platelets (b).

2.3.3.4 Ion-ion correlation force

Cohesion of cement paste is mainly controlled by purely physical surface forces acting on a short range [32]. Moreover, neither the van der Waals force, electrical double layer force nor capillary force can individually provide a reasonable explanation for cement paste cohesion [19, 41, 42]. From molecular simulation studies and direct-force measurements by atomic force microscopy, it has been found that the cohesion between C-S-H particles is a consequence of ion-ion correlation forces [2, 15, 17, 19, 44].

In previous simulation studies [15, 18, 45, 46], the surfaces of C-S-H particles are treated as homogeneously charged walls. A dielectric continuum water and ions are in between these walls, as shown in Fig. 2.10. In these two charged walls with an intervening electrolyte solution, the overwhelming majority of instantaneous ionic configurations lead to polarizations of the ionic clouds. For example, the charges of the excess of Ca^{2+} ions in the left of the mid-plane (Fig. 2.10) lead to a deficit in the right, which results in an overall positive charge in the left, and an overall negative charge in the right. These polarizations of the ionic clouds give rise to an attractive force, in the same way as correlations between fluctuating electronic dipoles give rise to the London dispersion force. These attractive electrostatic forces, or ion-ion correlation forces, mainly depend on the surface charge density and the valence of the counterions.

The existence of these attractive forces was confirmed by direct-force measurements using a CSH-covered AFM tip and a CSH-covered single crystal calcite surface [17, 47]. In these studies, when the tip-substrate system was immersed in a sodium chloride or hydroxide solution, only long-range repulsive forces were measured, as expected from the DLVO theory. However, when the tip was immersed in a lime solution in chemical equilibrium with the C-S-H, a strongly attractive force, much larger than the expected van der Waals forces, was measured.

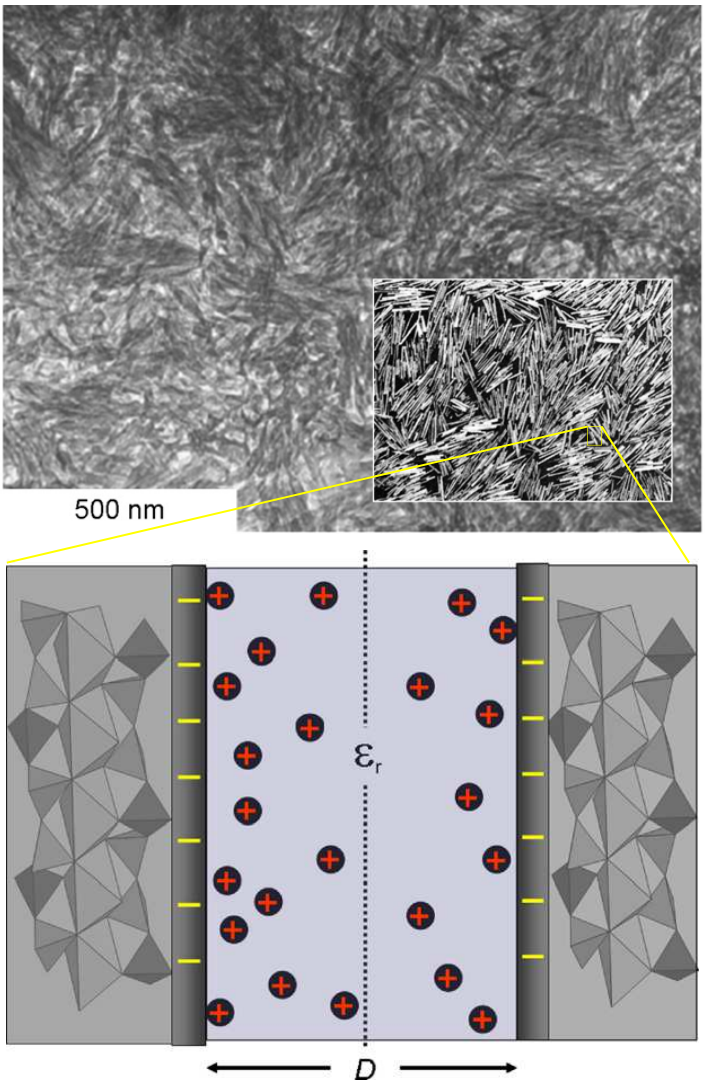

Fig. 2.10 Top: TEM micrograph of the inner product C–S–H in a hardened OPC paste. Inset: cartoon illustrating the type of imperfect liquid crystalline structure. Bottom: configuration for attractive electrostatic interactions between two C-S-H particles. Two charged C-S-H surfaces are separated by a dielectric continuum in which ions are free to move. ε_r is dielectric constant. D is the interlayer (adapted from [31, 48]).

2.4 Effect of filler on the strength of cement paste

Filler as replacement of cement may influence the performance of both the fresh paste and the hardened paste. The hydration kinetics will change and the microstructure of the bulk system will change as well. Consequently, the mechanical properties will be different. Four main effects, i.e., dilution effect, dense packing effect, nucleation effect and the effect of filler surface properties on the strength of cement paste are reviewed below.

2.4.1 Dilution effect

When a filler is used as a cement replacement and the water-to-binder ratio is constant, the amount of cement in the mixture is reduced. It is equivalent to an increase in the water-to-cement ratio. This is defined as the dilution effect of filler (Fig. 2.11). It may lead to a higher porosity in the hardened paste. Above a critical amount of filler, this dilution effect will also lead to a lower strength of the hardened paste [49, 50]. To maintain a certain strength, the critical amount of filler ranges between 5 to 20%, depending on the grain size distributions of both the cement and filler, and the water-to-binder ratio of the mixture [49, 51].

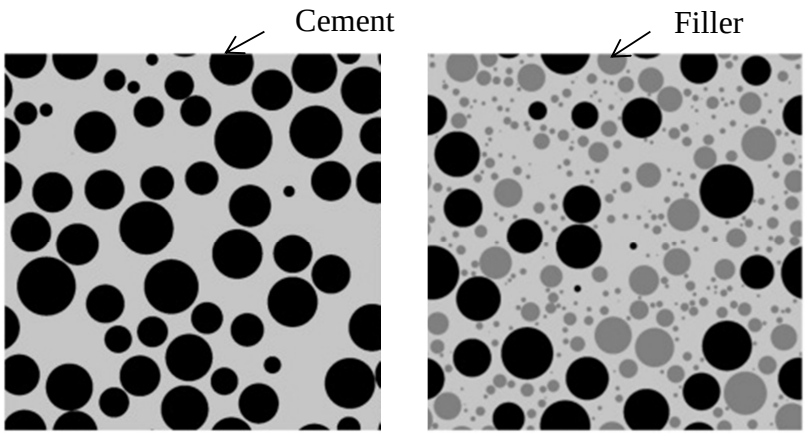

Fig. 2.11 Schematic particle dilution effect of filler. The particle distribution after mixing for a 100% Portland cement system at a water to cement ratio of 0.4 (left) and for the same system but with 40% of the clinker grains replaced by fillers (right) [52].

2.4.2 Packing effect

A fine filler in cement paste can improve the strength of blended cement paste due to a denser packing (Fig. 2.12). The packing effect of fillers on the strength of blended cement paste comes from the improvement of the pore structure and a denser packing structure [53, 54]. Lagerblad and Vogt [55] investigated the effect of very fine fillers on concrete strength. It was found that the strength did not reduce by replacing cement up to 40% with ultrafine filler particles.

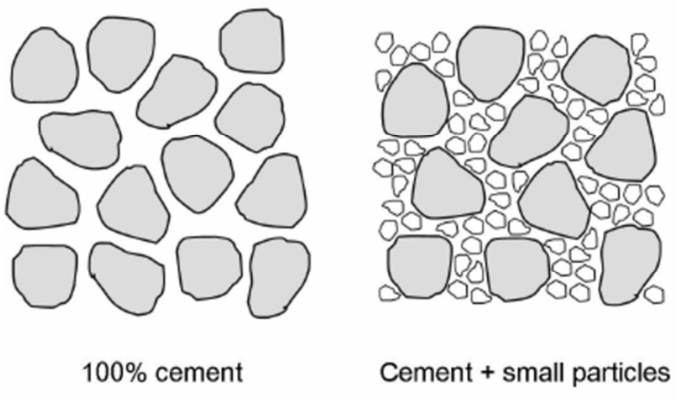

Fig. 2.12 Schematic particle packing effect. Small particles fit in the voids between the cement particles, thus increase maximum packing density [54].

2.4.3 Nucleation effect

The presence of filler particles facilitates C-S-H nucleation and, hence, accelerates the hydration of the clinker component [56, 57]. It has a positive effect on the strength at an early age. This effect depends on the fineness, the replace percentage and the surface properties of the fillers [58, 59].

2.4.4 Effect of filler surface properties

The surface properties have a significant influence on the bond strength between filler particles and hydration products. This affects the strength of the blended cement paste as well. Mehta and Monteiro [7], French and Mokhtarzadeh [60] and Bentz et al [61] found that limestone exhibited superior bond characteristic with cement paste compared to silica. This is due to the favourable physical and chemical properties of the limestone surfaces. However, the effect of the fillers' chemical properties on interfacial bond and the overall strength has not been fundamentally addressed yet. Understanding the exact nature of the fillers' effect in a cement-based matrix, and improving the performance of filler as replacement of cement in view of strength are challenges nowadays.

2.5 Conclusions and outlook

A brief literature survey focusing on the strength of Portland cement paste and the effect of filler on the paste strength has been presented in this chapter. The mechanisms of strength development of cement paste were briefly described. The 'gel-space ratio' theory on the strength development of cement paste was mentioned. Strength increases with the cube of the gel-space ratio. From a micro structural point of view, the strength of cement paste is directly related to the number of contact points and the magnitude of

the contact surface area between hydrating particles. Furthermore, the origin of cohesion between hydrates particles in cement paste has been discussed. It is concluded that at the (sub)nanoscale the cohesion of cement paste is because of the ionic-covalent bond. At the nanoscale the cohesion of cement paste is the consequence of attractive ion-ion correlation forces. Moreover, the effects of dilution, packing, nucleation and filler surface properties on the strength of cement paste were addressed.

Various studies report [7, 60, 61] on the effect of the chemical and physical nature of the filler on the adhesion strength. The basic questions how the chemistry and surface characteristics of fillers affect the adhesion between filler particles and reaction products, and why filler particles and reaction products adhere to each other in cement paste, are rarely addressed yet. Remaining challenges, e.g., understanding the filler-hydrates adhesion mechanisms in blended cement paste system, and quantification of the influence of filler-hydrates adhesion properties on the strength of blended cement paste, need further study.

In the following chapters, the influence of the filler-hydrates adhesion properties on the strength of blended cement paste will be investigated by analysing the relationship between the measured compressive strength and simulated contact area. Microscopic observations of the crack paths and fracture surfaces of loaded blended cement pastes and lattice type modelling will be used to evaluate the micromechanical properties of the filler-hydrates interface. The effect of surface chemical properties on filler-hydrates adhesion properties and the adhesion mechanisms between C-S-H and filler particles will be studied based on zeta potential measurements and microscopic studies of the nucleation and growth of C-S-H on the surface of these filler particles.

References

1. Aïtcin, P.-C., *Cements of yesterday and today: Concrete of tomorrow.* Cement and Concrete Research, 2000. **30**(9): p. 1349-1359.
2. Pellenq, R.J.M. and H. Van Damme, *Why does concrete set?: The nature of cohesion forces in hardened cement-based materials.* Mrs Bulletin, 2004. **29**(5): p. 319-323.
3. Powers, T.C., *Structure and physical properties of hardened Portland cement paste.* Journal of the American Ceramic Society, 1958. **41**(1): p. 1-6.
4. Nachbaur, L., et al., *Dynamic mode rheology of cement and tricalcium silicate pastes from mixing to setting.* Cement and Concrete Research, 2001. **31**(2): p. 183-192.
5. Jiang, S., J. Mutin, and A. Nonat, *Studies on mechanism and physico-chemical parameters at the origin of the cement setting II. Physico-chemical parameters determining the coagulation process.* Cement and Concrete Research, 1996. **26**(3): p. 491-500.
6. Taylor, H.F., *Cement chemistry*1997: Thomas Telford.
7. Mehta, P. and P.J.M. Monteiro, *Concrete: Microstructure, Properties, and Materials*2006: McGraw-Hill Education.
8. van Breugel, K., *simulation of hydration and formation of structure in harding cement-based materials*, 1991, Delft University: Delft.
9. Collepardi, M. and B. Marchese, *Morphology and surface properties of hydrated tricalcium silicate pastes.* Cement and Concrete Research, 1972. **2**(1): p. 57-65.
10. GRANJU, J. and J. MASO, *LAW OF RESISTANCE IN SIMPLE COMPRESSION OF WATER CURED PORTLAND-CEMENT PASTES.* Cement and Concrete Research, 1980. **10**(5): p. 611-621.
11. Lawrence, F. and J. Young, *Studies on the hydration of tricalcium silicate pastes I. Scanning electron microscopic examination of microstructural features.* Cement and Concrete Research, 1973. **3**(2): p. 149-161.
12. Sun, Z., et al. *Early age properties of Portland cement pastes investigated with ultrasonic shear waves and numerical simulation*. in *Proceedings of the RILEM International Symposium on Advances in Concrete through Science and Engineering*. 2004.
13. Sun, Z.H., G. Ye, and S.P. Shah, *Microstructure and early-age properties of portland cement paste - Effects of connectivity of solid phases.* Aci Materials Journal, 2005. **102**(2): p. 122-129.
14. Xiaowei Ouyang, Guang Ye, and K.v. Breugel, *Effect of Inert Additives on Compressive Strength of Cement Paste:Results from Numerical Analysis of Connectivity of Solid Phases*, in *The 14th International Congress on the Chemistry of Cement (ICCC 2015)* 2015: Beijing, China.
15. Jonsson, B., et al., *Controlling the cohesion of cement paste.* Langmuir, 2005. **21**(20): p. 9211-9221.
16. Rueb, C. and C. Zukoski. *Interpartical Attractions and the Mechanical Properties of Colloidal Gels*. in *MRS Proceedings*. 1991. Cambridge Univ Press.
17. Plassard, C., et al., *Nanoscale experimental investigation of particle interactions at the origin of the cohesion of cement.* Langmuir, 2005. **21**(16): p. 7263-7270.
18. Jonsson, B., et al., *Onset of cohesion in cement paste.* Langmuir, 2004. **20**(16): p. 6702-6709.
19. Gmira, A., et al., *Microscopic physical basis of the poromechanical behavior of cement-based materials.* Materials and Structures, 2004. **37**(265): p. 3-14.
20. Bernal, J., J. Jeffery, and H. Taylor, *Crystallographic research on the hydration of Portland cement. A first report on investigations in progress.* Magazine of Concrete Research, 1952. **4**(11): p. 49-54.
21. Taylor, H. and J. Howison, *Relationships between calcium silicates and clay minerals.* Clay Minerals Bull, 1956. **3**(16): p. 98-111.
22. Stade, H. and D. Müller, *On the coordination of Al in ill-crystallized CSH phases formed by hydration of tricalcium silicate and by precipitation reactions at ambient temperature.* Cement and Concrete Research, 1987. **17**(4): p. 553-561.
23. Taylor, H.F., *Proposed structure for calcium silicate hydrate gel.* Journal of the American Ceramic Society, 1986. **69**(6): p. 464-467.
24. Glasser, F.P., E.E. Lachowski, and D.E. Macphee, *Compositional Model for Calcium Silicate Hydrate (C‐S‐H) Gels, Their Solubilities, and Free Energies of Formation.* Journal of the American Ceramic Society, 1987. **70**(7): p. 481-485.

25. Taylor, H., *Nanostructure of C ・ S ・ H: Current status.* Advanced Cement Based Materials, 1993. **1**(1): p. 38-46.
26. Chen, J.J., et al., *Solubility and structure of calcium silicate hydrate.* Cement and Concrete Research, 2004. **34**(9): p. 1499-1519.
27. Gmira, A., et al., *Microscopic physical basis of the poromechanical behavior of cement-based materials.* Materials and Structures, 2004. **37**(1): p. 3-14.
28. Minet, J., et al., *Organic calcium silicate hydrate hybrids: a new approach to cement based nanocomposites.* Journal of Materials Chemistry, 2006. **16**(14): p. 1379-1383.
29. Hamid, S., *The crystal structure of the 11 Ä natural tobermorite Ca2. 25 [Si3O7. 5 (OH) 1.5]· 1H2O.* Zeitschrift für Kristallographie-Crystalline Materials, 1981. **154**(1-4): p. 189-198.
30. Gmira, A., et al. *Molecular engineering of the cohesion in neat and hybrid cement hydrates*. in *American Concrete Institute*. 2008.
31. Pellenq, R.J.M., N. Lequeux, and H. van Damme, *Engineering the bonding scheme in C-S-H: The iono-covalent framework.* Cement and Concrete Research, 2008. **38**(2): p. 159-174.
32. Sereda, R.F.F.a.P.J., *A New Model for Hydrated Portland Cement and its Practical Implications.* 1970.
33. Parsegian, V.A., *Van der Waals forces: a handbook for biologists, chemists, engineers, and physicists*2005: Cambridge University Press.
34. Lomboy, G., et al., *A test method for determining adhesion forces and Hamaker constants of cementitious materials using atomic force microscopy.* Cement and Concrete Research, 2011. **41**(11): p. 1157-1166.
35. Stern, O., *The theory of the electrolytic double-layer.* Z. Elektrochem, 1924. **30**(508): p. 1014-1020.
36. Talero, R., C. Pedrajas, and V. Rahhal, *Performance of fresh Portland cement pastes-Determination of some specific rheological parameters*2013: INTECH Open Access Publisher.
37. Russel, W.B., D.A. Saville, and W.R. Schowalter, *Colloidal dispersions*1989: Cambridge university press.
38. Itul, A., *Interactions entre organo-silanes et client: conséquences sur l'hydratation et les propriétés mécaniques*, 2010, Dijon.
39. Churaev, N.V., B.V. Derjaguin, and V.M. Muller, *Surface forces*2013: Springer Science & Business Media.
40. Verwey, E.J.W., J.T.G. Overbeek, and J.T.G. Overbeek, *Theory of the stability of lyophobic colloids*1999: Courier Corporation.
41. Israelachvili, J.N., *Intermolecular and surface forces: revised third edition*2011: Academic press.
42. Evans, D.F. and H. Wennerstrom, *Colloidal domain*1999: Wiley-Vch.
43. Israelachvili, J.N., *Intermolecular and surface forces*2011: Academic press.
44. Lesko, S., et al., *Investigation by atomic force microscopy of forces at the origin of cement cohesion.* Ultramicroscopy, 2001. **86**(1-2): p. 11-21.
45. Pellenq, R.-M., J. Caillol, and A. Delville, *Electrostatic attraction between two charged surfaces: A (N, V, T) Monte Carlo simulation.* The Journal of Physical Chemistry B, 1997. **101**(42): p. 8584-8594.
46. Pellenq, R.-M., A. Delville, and H. Van Damme, *Cohesive and swelling behaviour of charged interfaces: a (NVT) Monte-Carlo study.* SPECIAL PUBLICATION-ROYAL SOCIETY OF CHEMISTRY, 1997. **213**(1): p. 596-603.
47. Lesko, S., et al., *Investigation by atomic force microscopy of forces at the origin of cement cohesion.* Ultramicroscopy, 2001. **86**(1): p. 11-21.
48. Richardson, I., *Tobermorite/jennite-and tobermorite/calcium hydroxide-based models for the structure of CSH: applicability to hardened pastes of tricalcium silicate, β-dicalcium silicate, Portland cement, and blends of Portland cement with blast-furnace slag, metakaolin, or silica fume.* Cement and Concrete Research, 2004. **34**(9): p. 1733-1777.
49. Bonavetti, V., et al., *Limestone filler cement in low w/c concrete: A rational use of energy.* Cement and Concrete Research, 2003. **33**(6): p. 865-871.
50. Lawrence, P., M. Cyr, and E. Ringot, *Mineral admixtures in mortars - Effect of inert materials on short-term hydration.* Cement and Concrete Research, 2003. **33**(12): p. 1939-1947.
51. Bentz, D.P., *Modeling the influence of limestone filler on cement hydration using CEMHYD3D.* Cement & Concrete Composites, 2006. **28**(2): p. 124-129.

52. Scrivener, K.L., P. Juilland, and P.J.M. Monteiro, *Advances in understanding hydration of Portland cement.* Cement and Concrete Research, 2015. **78, Part A**: p. 38-56.
53. Moosberg-Bustnes, H., B. Lagerblad, and E. Forssberg, *The function of fillers in concrete.* Materials and Structures, 2004. **37**(2): p. 74-81.
54. Fennis, S., J.C. Walraven, and J.A. den Uijl, *The use of particle packing models to design ecological concrete.* Heron, 2009. **54**(2/3): p. 185-204.
55. Lagerblad, B. and C. Vogt, *Ultrafine particles to save cement and improve concrete properties*2004: Cement och Betong Institutet.
56. Gutteridge, W.A. and J.A. Dalziel, *Filler cement: The effect of the secondary component on the hydration of Portland cement.* Cement and Concrete Research, 1990. **20**(5): p. 778-782.
57. Garrault-Gauffinet, S. and A. Nonat, *Experimental investigation of calcium silicate hydrate (C-S-H) nucleation.* Journal of Crystal Growth, 1999. **200**(3–4): p. 565-574.
58. Stumm, W., *Chemistry of the solid-water interface: processes at the mineral-water and particle-water interface in natural systems*1992: John Wiley & Son Inc.
59. Lawrence, P., M. Cyr, and E. Ringot, *Mineral admixtures in mortars: effect of inert materials on short-term hydration.* Cement and Concrete Research, 2003. **33**(12): p. 1939-1947.
60. French, C.W. and A. Mokhtarzadeh, *High strength concrete: Effects of materials, curing and test procedures on short-term compressive strength.* PCI Journal, 1993. **38**(3): p. 76-87.
61. Bentz, D.P., et al., *Multi-scale investigation of the performance of limestone in concrete.* Construction and Building Materials, 2015. **75**: p. 1-10.

3

Effect of Filler-hydrates Adhesion Properties on Strength of Cement Paste*

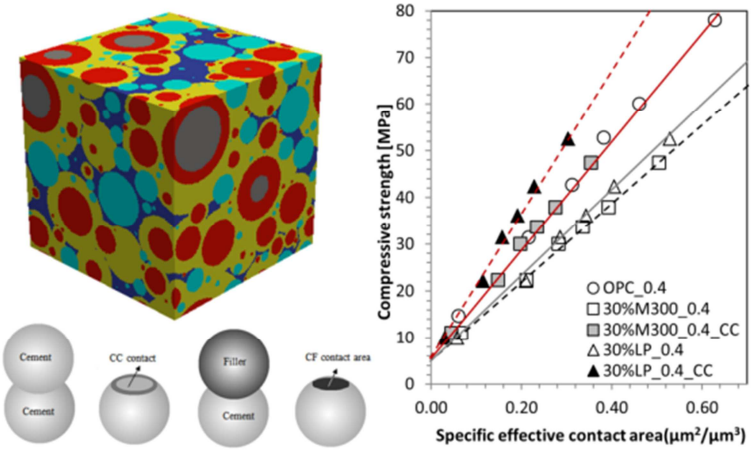

The study presented in this chapter is to investigate the effect of filler-hydrates adhesion properties on strength of cement paste. In this chapter, the development of compressive strength of Portland cement paste and the cement paste blended with limestone powder and micronized sand was studied experimentally. In parallel with this experimental study, the contact area between different solid phases in these cement pastes was quantified numerically. The relationship between the measured compressive strength and simulated contact area was analysed. With this relationship, the effect of filler-hydrates adhesion properties on strength of cement paste was quantified.

* This chapter based on:

1. Xiaowei Ouyang, Peng Gao, Guang Ye and Klaas van Breugel. Effect of Filler-Hydrates Adhesion Properties on Cement Paste Strength. *ACI Materials Journal*, accepted.

2. Xiaowei Ouyang, Guang Ye and Klaas van Breugel. Effect of Inert Additives on Compressive Strength of Cement Paste: Results from Numerical Analysis of Connectivity of Solid Phases. *The 14th International Congress on the Chemistry of Cement (ICCC 2015)*. Beijing, China 2015.

3.1 Introduction

Adding a fine filler to cement paste can result in improvements in strength because of a dense packing. The 'packing' effect of a filler on concrete properties involves improvement of the pore structure and a denser packing structure [1]. At the same time, however, the use of fillers also results in dilution of Portland cement particles in the paste. Above a critical amount of fillers, this 'dilution' effect will lead to an increased porosity, and thus a lower strength of the hardened paste [2, 3]. In cement paste the effect of porosity on the strength has been studied intensively. The adhesion strength between filler particles and reaction products, which depends on the physical and chemical properties of the filler, also has an influence on the strength of blended cement paste. However, the role of filler-hydrates adhesion properties in strength of blended cement paste attracted very little attention and was not well described yet. The objective of the study in this chapter is to investigate the effect of filler-hydrates adhesion properties on the strength of blended cement paste.

The approach of combined experimental measurements and microstructural modelling will be used in this study. The development of the compressive strength of Portland cement paste and the cement paste blended with fillers was studied experimentally. The development of the mechanical properties (compressive strength) is the result of the microstructure evolution due to cement hydration. The microstructural evolution of Portland cement pastes and the blended cement pastes was simulated by a numerical model, called HYMOSTRUC3D. This model was developed in 1991 and has been further extended since then [4-7]. In this model, hydrated cement particles, unhydrated cement particles and filler particles are considered as the solid phase. The interparticle connections of the solid phase is a crucial factor that dominates the development of the mechanical properties of cement-based materials [8]. A parameter, the contact area, was adopted to describe this connection. Correlations between the development of the contact area of different solid phases simulated by the model and the development of compressive strength were investigated. Based on these correlations, mechanical properties of cement paste can be directly related to its microstructure and more particularly related to the simulated contact area in cement paste. In this model the simulated contact area can be divided into two types, i.e., the contact area between hydrating cement particles and the contact area between hydrating cement particle and filler particle. Based on this concept, the effect of filler-hydrates adhesion properties on strength of cement paste can be quantified.

3.2 Materials and experimental methods

3.2.1 Materials and mixture

3.2.1.1 Raw materials

The cement used in this study is OPC CEM I 42.5 N, produced by ENCI, The Netherlands. The fillers used are limestone powder (LP) and two types of micronized

sand (M6 and M300). The chemical composition and physical characteristics of these materials are listed in Table 3.1. The mineral composition of OPC was calculated by the Bogue equation [9] and is reported in Table 3.2. Measured and fitted particle size distribution (PSD) data of materials are shown in Fig. 3.1.

Table 3.1 Chemical compositions (% by mass) and physical characteristics of Portland cement and fillers.

Name	OPC	LP	M6	M300
Chemical composition				
CaO	64.40	-	0.02	0.02
SiO_2	20.36	0.34	99.5	99.5
Al_2O_3	4.96	0.2	0.20	0.20
Fe_2O_3	3.17	0.07	0.03	0.03
K_2O	0.64	0.01	0.04	0.05
Na_2O	0.14	0.02	-	-
SO_3	2.57	0.05	-	-
MgO	2.09	0.27	-	-
$CaCO_3$	-	97.46	-	-
Physical properties				
Density (g/cm^3)	3.15	2.67	2.65	2.65
Surface area (m^2/g)	0.80	0.75	0.81	1.20
D_{50}(μm)	44.5	34.6	62.3	23.9

Table 3.2 Mineral compositions of Portland cement (% by weight).

Phase	C_3S	C_2S	C_3A	C_4AF
Weight (%)	67.1	5.9	7.8	9.6

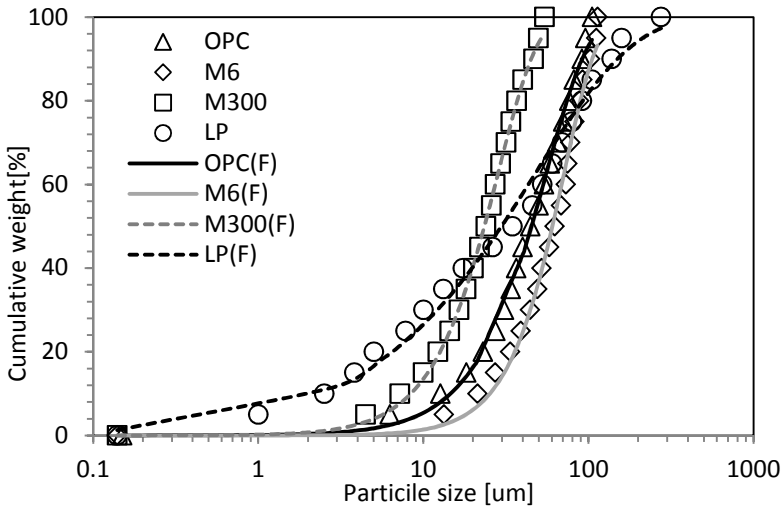

Fig. 3.1 Particle size distribution of cement and fillers (M: measured; F: fitted).

3.2.1.2 Mix design

Eight series of specimens were prepared with different types of fillers, replacement level of fillers and water-to-binder (w/b) ratio. The percentage of different filler and the w/b ratio are given in Table 3.3. In order to identify the different mixtures easily, mixtures are denoted by their substitution level, type of materials and w/b ratio. For example, 30%M300_0.3 corresponds to the mixture containing 30% M300 with a water-to-binder ratio of 0.3. Finally, this study comprises:

i) Two control series of Portland cement paste samples and six blended compositions.
ii) For blended compositions, six samples were prepared by varying the substitution level, filler size and type, and water-to-binder ratio, systematically.

Table 3.3 Mixture compositions of OPC and the blended cement pastes.

Mixtures	OPC*(%)	M300*(%)	M6*(%)	LP*(%)	w/b
OPC_0.3	100	-	-	-	0.3
OPC_0.4	100	-	-	-	0.4
30%M300_0.3	70	30	-	-	0.3
30%M300_0.4	70	30	-	-	0.4
50%M300_0.3	50	50	-	-	0.3
50%M300_0.4	50	50	-	-	0.4
30%M6_0.4	70	-	30	-	0.4
30%LP_0.4	70	-	-	30	0.4

* Percentage of the total mass of binder by weight.

3.2.2 Experimental methods

Particle size distribution
To determine the PSD, laser diffraction method (DIPA 2000) was applied. Three measurements were done and the average value was used.

Experimental procedures
The mixtures were prepared in a Hobart mixer according to the standard procedure described in ASTM C305 [10]. After mixing and casting, cement pastes were covered with a plastic sheet and stored in the laboratory at 20 ± 2 °C. After 24 hours, all the specimens were demolded and then stored in the curing room with a constant temperature of 20 ± 2 °C and a relative humidity of 95 ± 5% until the designated testing age.

Compressive strength test
The compressive strength of cubic (40 × 40 × 40 mm^3) specimens was measured as described in ASTM C109 [11] at 1, 3, 7, 14, 28 and 90 days. The compressive strength value reported is the average of three specimens.

Degree of hydration test

Degree of hydration is defined as the fraction of cement that has fully reacted with water relative to the total amount of cement in the sample [12]. It can be obtained by determining the non-evaporable water content as follows [13]:

$$a(t) = \left[\frac{W_n(t)}{c}\right] / \left[\left(\frac{W_n}{c}\right)_{complete}\right] \quad (3.1)$$

$(w_n/c)_{complete}$ is the non-evaporable water content per gram of the fully hydrated sample. The non-evaporable water content for the major phases of Portland cement at full hydration can be found in [14]. Based on the mineral composition of the plain Portland cement (Table 3.2), the value 0.25 was determined as $(w_n/c)_{complete}$ here. $w_n(t)/c$ is the non-evaporable water per gram of the sample at the curing age of t.

For Portland cement paste and the cement paste blended with micronized sand, $w_n(t)/c$ can be calculated as follows:

$$\frac{W_n(t)}{c} = \frac{W_{105°C} - W_{1000°C}}{(1-g)W_{1000°C}} \quad (3.2)$$

Because CO_2 is leaving the limestone filler at ignition, for the cement paste blended with limestone powder, the Eq. (3.2) is corrected as follows:

$$\frac{W_n(t)}{c} = \frac{W_{105°C} - W_{1000°C}\left(1 + \frac{0.44 \cdot g}{1-0.44 \cdot g}\right)}{(1-g)\frac{W_{1000°C}}{1-0.44 \cdot g}} \quad (3.3)$$

where $w_{105°C}$ is the weight of paste sample after drying in an oven at 105 °C for at least 12 hours; $w_{1000°C}$ is the weight of dried paste after igniting at 1000 °C in a furnace for 3 hours. g is the ratio of filler to binder. If the sample is Portland cement paste, g is equal to 0.

X-ray diffraction analysis (XRD)

X-ray diffraction (XRD) data were collected on the powder samples using a Philips X'Pert diffractometer applying CuK_α radiation (λ = 1.54 Å). The samples were scanned between 5° and 70° 2-theta, with a step size of 0.02° 2-theta and a dwell time of 2 seconds per step.

Thermogravimetric analysis (TGA)

Thermogravimetric analysis (TGA) on the powder samples was done using a heating rate of 10 °C/min from 40 °C to 1100 °C with a thermoanalyzer TG-449-F3-Jupiter instrument. The measurements were carried out in an argon atmosphere at 1.5 bars. The TGA curve can provide the weight loss of each individual phase with increasing temperature. For the interpretation of TGA and DTG results of cement paste, most researchers [15-18] point out that:

- 30-105 °C: the evaporation of adsorbed water. It is generally considered that the evaporable water is completely evaporated at 120 °C.
- 110-170 °C: the decomposition of ettringite and the loss of water from part of the carboaluminate hydrates take place.
- 180-300 °C: the loss of bound water from the decomposition of the C-S-H and carboaluminate hydrates undergoes.
- 450-500 °C: the dehydroxylation of the portlandite, $Ca(OH)_2 \rightarrow CaO + H_2O$.
- 500-700 °C: a further dehydration and/or dehydroxylation occurs.
- 700-900 °C: the decarbonation of calcium carbonate ($CaCO_3 \rightarrow CaO + CO_2$) with CO_2 escaping. The amount of CO_2 escaping from the cement paste can be calculated exactly from TGA tests. Compared with mixture composition of limestone powder (Table 3.3) and its chemical composition (Table 3.1), the amount of limestone powder participated in the chemical reaction during cement hydration can be calculated.

3.3 Numerical simulation

3.3.1 HYMOSTRUC3D

In this study, the HYMOSTRUC3D model was used to simulate the development of the microstructure in cement pastes. In this model, the evolution of the degree of hydration is modelled as a function of the particle size distribution, the phase composition of cement, the water-to-cement ratio, and the reaction temperature. The cement particles are modelled as spheres, randomly distributed in a three-dimensional body and the hydrating cement grains are simulated as growing spheres. Particles of the same size are considered to hydrate at the same rate. At first, hydration reactions are assumed to be phase-boundary reactions. At later stages, when the shells of reaction products around the particles have reached a certain predefined thickness, the reactions become diffusion-controlled. The simulation starts from a random distribution of cement particles in a cubic cell. During hydration, the cement particles gradually dissolve, and a porous shell of hydration products is formed around each particle. Neighbouring particles grow together and smaller particles may become embedded in the outer shells of larger ones to form a ‘cluster’ (Fig. 3.2). As hydration proceeds, the growing particles become more and more connected, and the material changes from the state of a suspension to the state of a porous solid. For a complete description of the original HYMOSTRUC3D model, details can be found in [4] and [7].

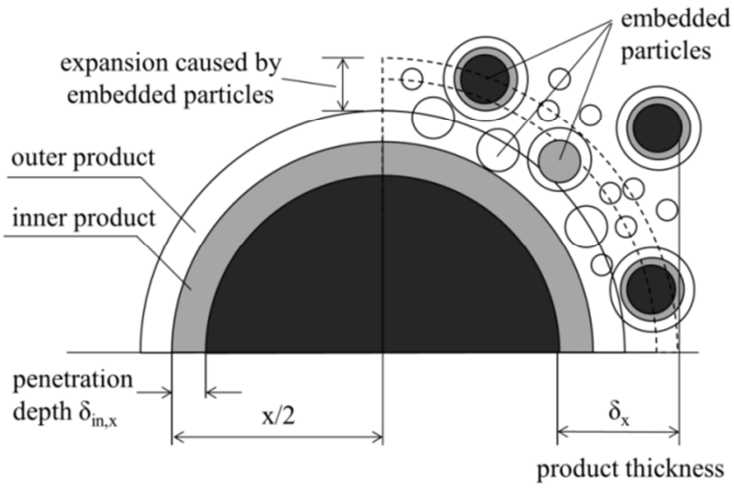

Fig. 3.2 Principle of the basic HYMOSTRUC model. Interaction mechanism for expanding particles: free expansion and formation of inner and outer product (left); embedding of small particles (right).

3.3.2 HYMOSTRUC3D simulation incorporating fillers

In the HYMOSTRUC3D model, the effect of physical interactions between hydrating cement particles is taken into account explicitly. For the resulting kinetic formula the term 'integrated kinetic' was proposed [4]. This integrated particle kinetics model was applied to investigate the microstructure development, the effect of small inert grains on cement hydration, and the inert particles contact surfaces. Based on this integrated kinetics model, the hydration process and the microstructural development of cement pastes blended with filler were simulated.

As the fillers are considered as inert grains, they are represented by non-reacting particles in the model. Filler particles do not grow during hydration but may act as an accelerator during cement hydration. This 'accelerating effect' is supposed to affect the degree of hydration of cement particles. The aim of this study is to quantify the effect of filler-hydrates adhesion properties on strength of cement paste by analyzing the relationship between the measured compressive strength and the simulated contact area. In order to obtain reliable information from the relationship between the measured compressive strength and the simulated contact area, we have to know the exact degree of hydration of cement particles and adjust the simulation results to measured results. After adjusting the simulated degree of hydration is in good agreement with the measured degree of hydration, as shown in Fig. 3.3.

A detailed description of the HYMOSTRUC3D simulation incorporating fillers can be found in [19]. Fig. 3.4 shows examples of the simulated microstructure of the cement paste blended with 30% of M300 filler and that of the reference OPC paste.

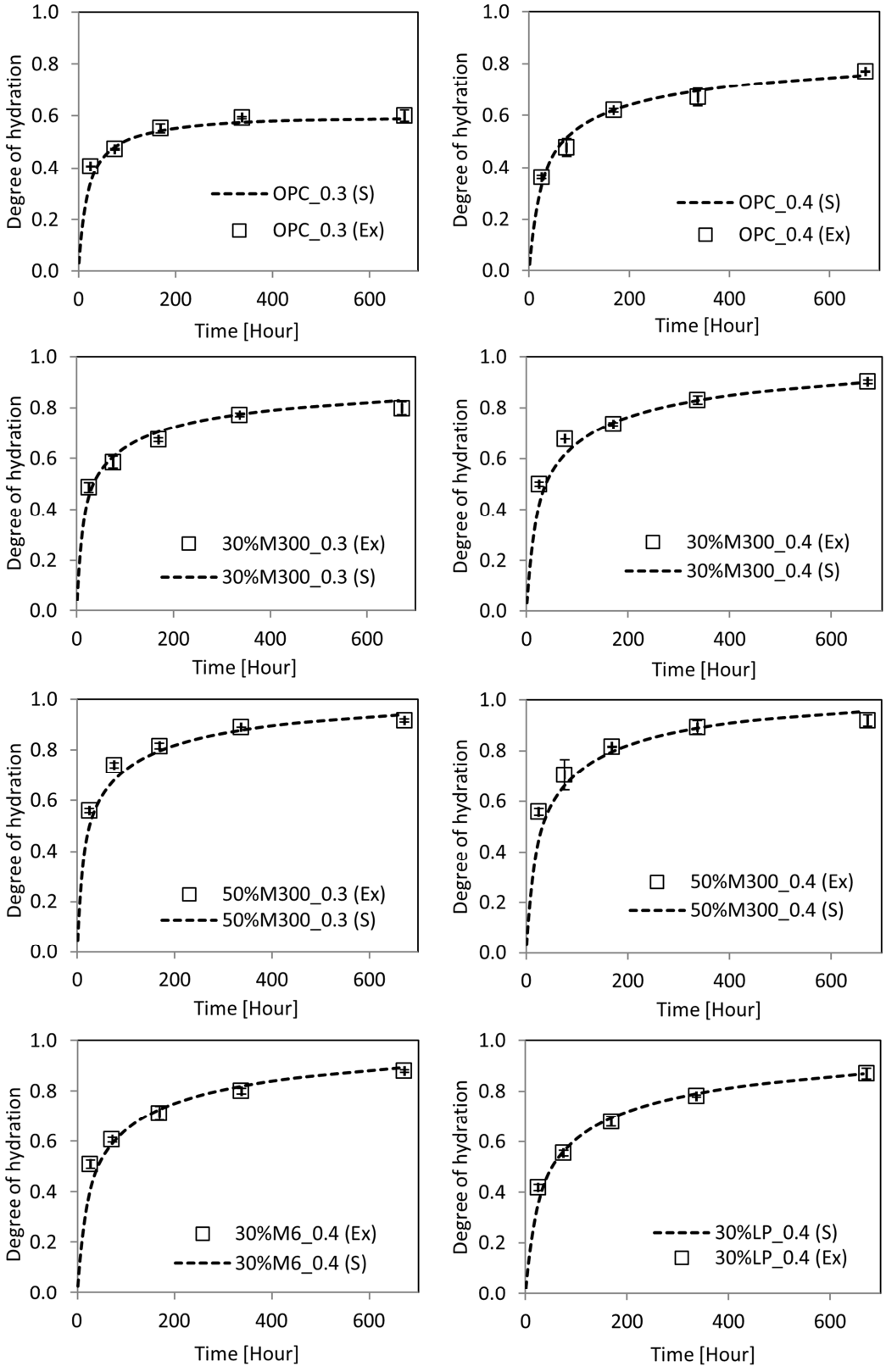

Fig. 3.3 Degree of hydration of cement as a function of time of mixtures listed in Table 3.3 (S: simulation; Ex: experiment).

Portland cement paste Blended cement paste

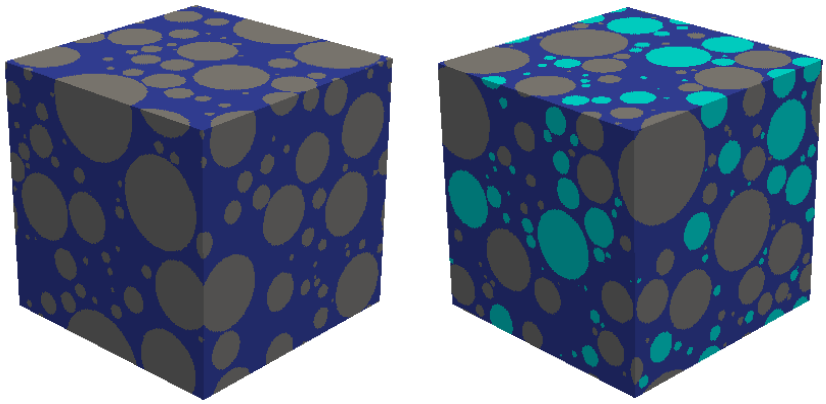

t = 0 hours The cement and M300 particles are modelled as spheres randomly distributed.

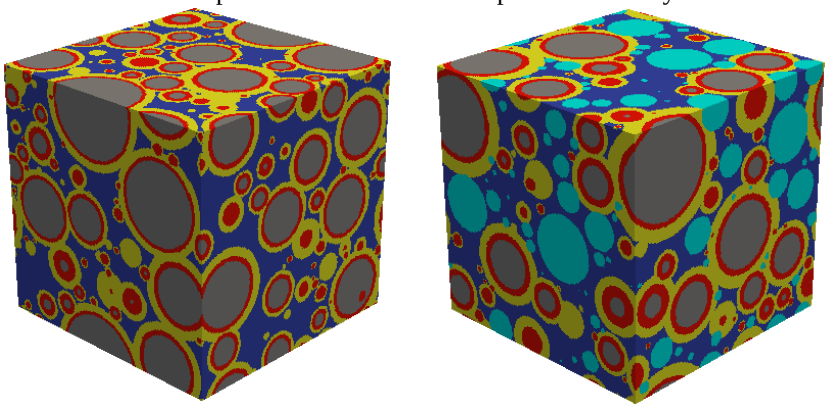

t = 25 hours The cement particles are hydrating. The hydration products around the cement grains firstly cause the formation of small isolated clusters.

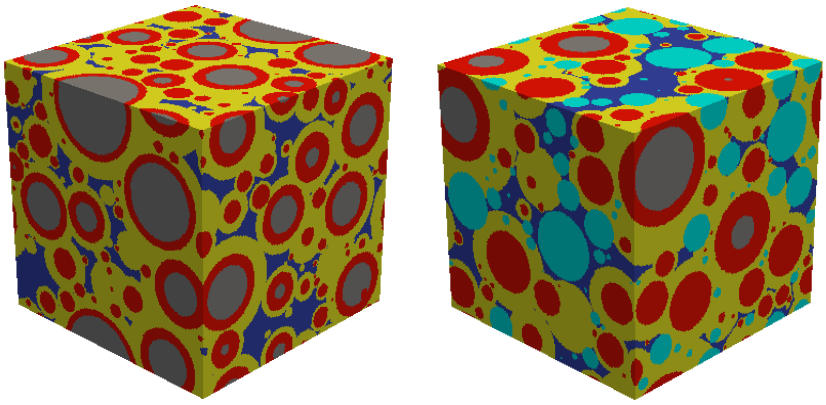

t = 28 days Neighbouring particles grow together, and smaller particles become embedded in the outer shells of larger ones to form a ‘cluster’. The growing particles become more and more strongly connected, and an increasingly rigid porous structure is formed.

Fig. 3.4 Simulated microstructures of OPC paste (left) and the cement paste blended with 30% of M300 filler (right) with w/b=0.3. Cyan particles are M300 filler and grey particles are cement. Yellow layer is outer products, and red layer is inner products.

3.3.3 Concept of contact area

As shown in Fig. 3.4, at time t = 0 hours the filler and cement particles are separated from each other. In this stage the cement paste does not have strength. With progress of the hydration process, the volume of hydrating cement particles grows and the initially separated particles become connected with each other. The cement paste starts to gain strength. As the cement particles continue to hydrate, more particles become connected, and the strength of cement paste then increases. To describe this connection, a parameter, i.e. the contact area, was introduced. As pointed out by several researchers the strength increases due to the increasing number of contact points and the increasing magnitude of the contact surface area between hydrating particles during the hydration process [20-23]. The linear relationship between the measured compressive strength of cement paste and the calculated contact area has already been confirmed in several studies [8, 24, 25].

The strength of cement paste results from the connections between particles, but these connections do not necessarily yield strength. For example, a dense packing of micronized sand or limestone powder, which has a large amount of connections, has almost no strength. Therefore, the contribution of different types of connection to the strength is different. In blended cement paste, there are two types of connection. One is the connection between hydration products and another is the connection between hydration products and filler particles. Accordingly, there are two types of contact area in the cement paste blended with inert filler, as shown in Fig. 3.5:

i) CC contact area: the contact area between hydrating cement particles (Fig. 3.5a);
ii) CF contact area: the contact area between a hydrating cement particle and a filler particle (Fig. 3.5b).

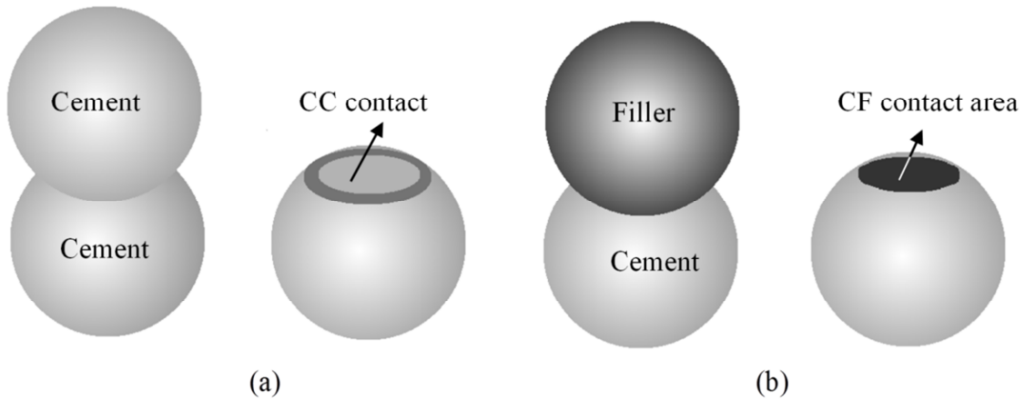

Fig. 3.5 Concept of the contact area between hydrating cement particles (a) and the contact area between a hydrating cement particle and a filler particle (b).

The contact area is defined as the circular area at the intersection of two spherical surfaces. Effective Contact Area (ECA) is defined as the contact area in the direction normal to the direction of the applied load. Taking a load applied in the y direction as an example, the algorithm and criteria for calculating the effective contact area are shown in Fig. 3.6.

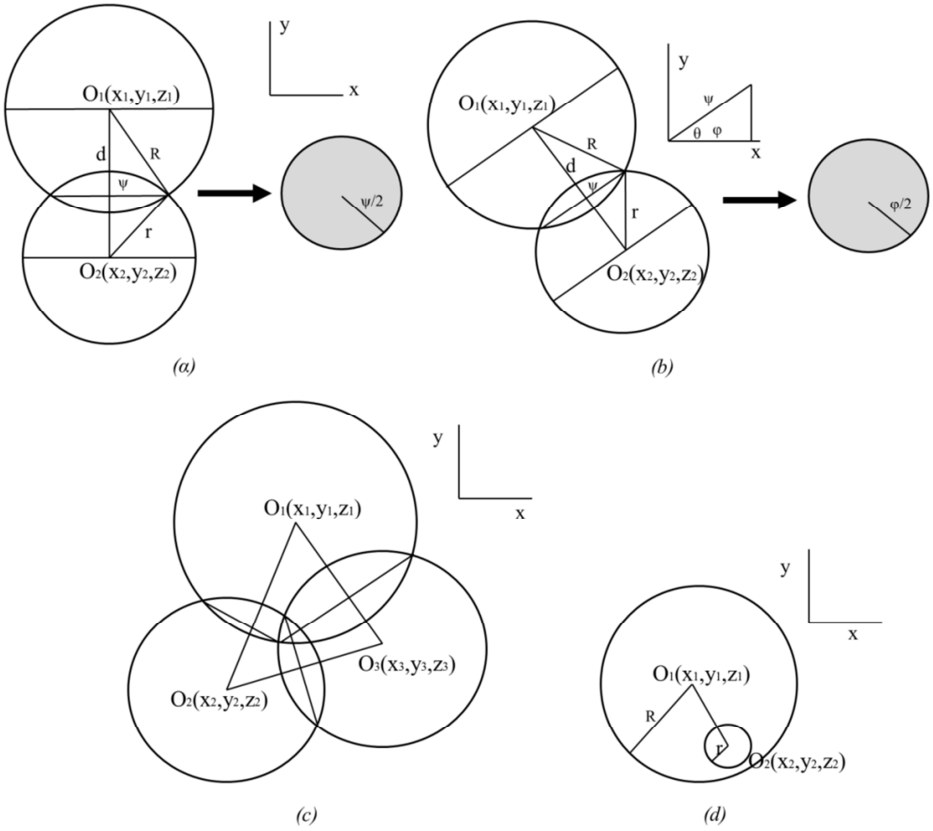

Fig. 3.6 Effective contact area between different particles [8].

As shown in Fig. 3.6, the phenomenon of particle connection can be divided into four cases that are taken into consideration in calculations of the ECA normal to direction y.

- In case (a), when two particles are interconnected in a direction normal to the y axis, ECA(y) equals the area of the contact circle.
- In case (b), when the two particles are not interconnected in a plane normal to the y direction, ECA(y) is calculated by mapping the contact area onto a plane normal to the y direction.
- In case (c), when three or more particles are interconnected the double overlapping contact area has to be subtracted from the total contact area.

- In case (d), when a larger and a smaller particle are close together, the larger particle may grow sufficiently as hydration proceeds for it to completely encapsulate the smaller. In this case, the encapsulated particle has no direct contribution to the connection. Therefore, ECA is 0.

The total ECA in a specific direction is the sum of the ECA in that direction for all particles within the cubic cell. [ECA(x) + ECA(y) + ECA(z)]/3 is the final ECA. For convenience in the data analysis, the concept of Specific Effective Contact Area (SECA) is introduced; it is defined as the ECA per unit volume of cement paste at a given age. A more detailed description of the contact area can be found in [8].

3.4 Results and discussion

3.4.1 Reactivity of fillers in cement paste

In the model, the fillers are considered as inert grains. They do not grow during cement hydration. In reality the fillers may not be inert and possibly participate in a chemical reaction in cement paste. This will affect the strength of blended cement paste. In order to obtain reliable information from the relationship between the measured compressive strength and the simulated contact area, it is important to know the reactivity of fillers in cement paste. X-ray diffraction analysis combined with thermals analysis was carried out to investigate possible reactivity of fillers.

3.4.1.1 X-ray diffraction analysis

Micronized sand is believed to be an inert filler in cement paste. As shown in Fig. 3.7, compared with the pure Portland cement paste, there are no different products found in cement paste blended with micronized sand, no matter at an early age or at an age of 28 days.

As has been reported [26], the dissolution of limestone in Portland cement paste is very low. Substantial reactions between C_3A and carbonate provided by carbonate-based fillers in Portland cement paste are not expected [27, 28]. These reported observations are confirmed by the XRD patterns shown in Fig. 3.7. The formation of monocarbonate in the cement paste blended with LP was not observed at the age of 7 days. At the age of 28 days, there is a very weak intensity of monocarbonate, which indicates the presence of monocarbonate in minute quantities.

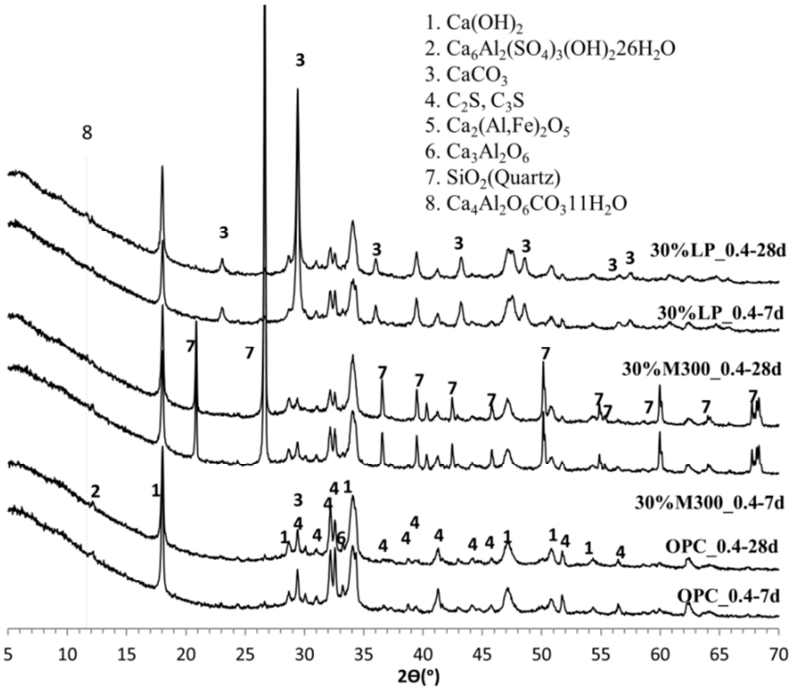

Fig. 3.7 XRD patterns of Portland cement paste and the blended cement pastes at 7 and 28 days.

3.4.1.2 Thermals analysis

TGA curves can provide the weight loss of each individual phase on heating of the samples. Results of the thermal decomposition of cement pastes are presented in Fig. 3.8. As can be observed from Fig. 3.8a, the TG/DTG spectra of the samples hydrated for 7 days shows similar amounts of hydration products for both micronized sand-blended cement paste and limestone-blended cement paste. These results are in agreement with the findings in x-ray diffraction analysis. At the age of 28 days (Fig. 3.8b), the weight loss at approx. 150 °C in limestone-blended cement paste indicates the presence of monocarbonate in minute quantities.

To further investigate the reactivity of limestone powder in cement paste, the amount of limestone in the sample of limestone-blended cement paste was calculated from the TGA tests and compared with theoretical calculations as shown in Table 3.4. Data from TGA tests is rather similar to theoretical calculations, which indicates that the chemical activity of limestone powder is very low during cement hydration. Considering this low chemical activity of limestone in the sample of limestone-blended cement paste, limestone powder is assumed inert.

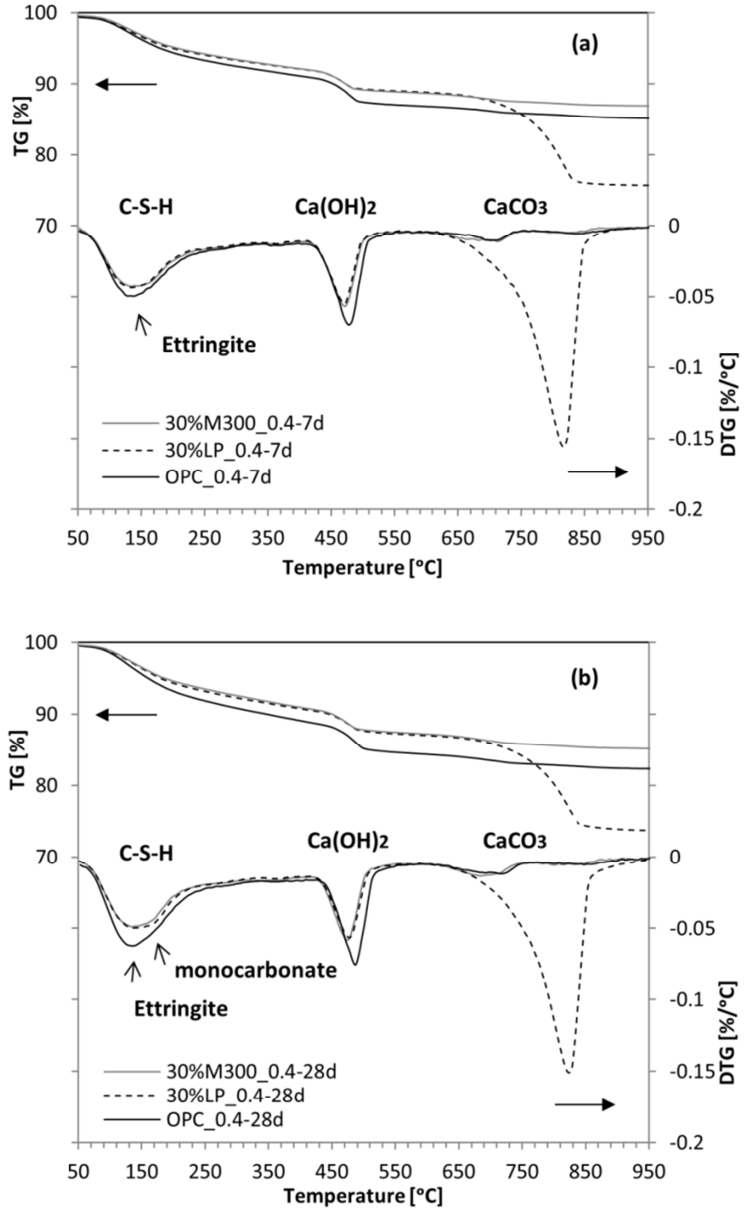

Fig. 3.8 Thermal decomposition of pastes by thermogravimetric analysis (TG) and derivative thermogravimetric analysis (DTG) at the age of 7 days (a) and at the age of 28 days (b).

Table 3.4 Proportion of limestone in the mixtures from TGA and theoretical calculations.

Items	TGA	Theoretical calculations
30%LP_0.4 (7d)	29.56%	30%
30%LP_0.4 (28d)	30.34%	30%

3.4.2 Relationship between measured compressive strength and simulated contact area

The relationship between the measured compressive strength and the calculated specific effective contact area (SECA) of the solid phase of cement pastes were investigated. As indicated in section 3.3.2, the effective contact area (ECA) is a microstructure parameter that can be calculated by HYMOSTRUC3D. The contact area concept is an approach to not only quantify the connection between the solid phases in the microstructure [8], but also evaluate the quality of interparticle bonds between the solid phases. As mentioned in section 3.3.2, there are two types of contact area: CF contact area and CC contact area. Besides CC contact area, marked with CC as shown below, the contact area discussed below refers to the total contact area, which includes both CF contact area and CC contact area. In Portland cement paste there is only CC contact area. In blended cement pastes, both CC contact area and CF contact area appear. The results of four effects on the relationship between the measured compressive strength and the simulated contact area are reported below. It starts with the effect of water-to-binder ratio. Next, the effects of content and size of filler are discussed, respectively. Finally, the effect of filler type is studied.

3.4.2.1 Effect of water-to-binder (w/b) ratio

Fig. 3.9 shows the effect of water-to-binder ratio on the relationship between the measured compressive strength and the calculated specific effective contact area in Portland cement pastes and the blended cement pastes. The compressive strength of cement pastes is determined according to the methods described in section 3.2.2.3 at ages of 1, 3, 7, 14, 28 and 90 days, and shown in Fig. 3.9a. As mentioned previously, the specific effective contact area (SECA) is defined as the contact area per unit volume of the simulated cement paste at a given degree of hydration. The SECA of cement pastes is calculated by HYMOSTRUC3D at ages of 1, 3, 7, 14, 28 and 90 days, and is presented in Fig. 3.9b. Both contact area and compressive strength of cement pastes increase with increasing degree of hydration. The relationship between the SECA and the compressive strength of cement pastes with w/b = 0.3 and 0.4 are presented in Fig. 3.9c. The black dashed line in Fig. 3.9c illustrates the relationship between the compressive strength and the total SECA, which includes CC-SECA and CF-SECA in the cement pastes blended with 30% M300. The relationship between compressive strength and CC-SECA is represented by the red line (Fig. 3.9c).

From Fig. 3.9c it can be seen that when the SECA is 0, all the pastes have the similar compressive strength of about 6 MPa. This can also be seen in Fig. 3.10c, 3.11c and 3.12b. It could be explained that at the stage when the SECA is 0, the particles stay very close to each other and begin to make contact with each other. In this case, the capillary forces and van der Waal forces become strong enough to hold particles together and enable the pastes to obtain a small strength.

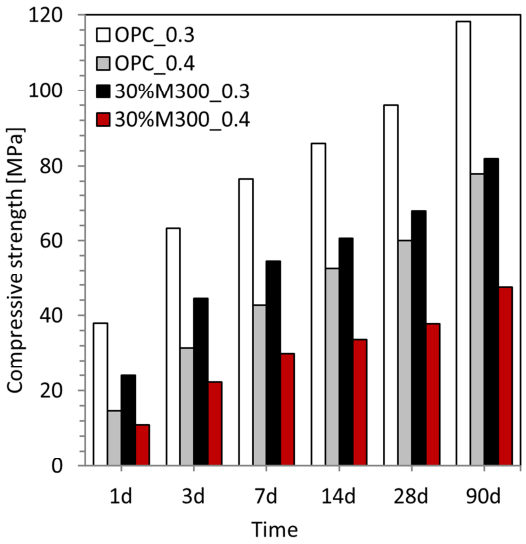

(a) Compressive strength

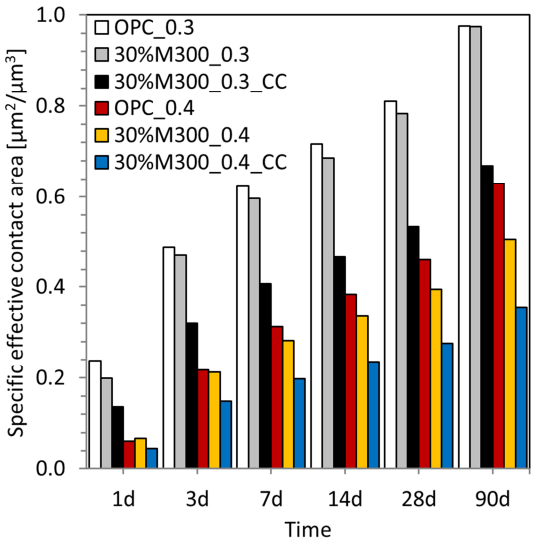

(b) Specific Effective Contact Area

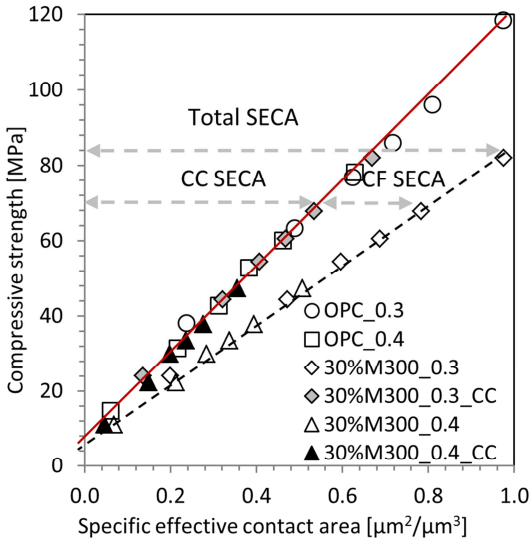

(c) Correlation between Specific Effective Contact Area and compressive strength

Fig. 3.9 Effect of water-to-binder ratio (0.3 and 0.4) on the relationship between the measured compressive strength and the calculated Specific Effective Contact Area (Besides CC SECA which marked with CC as shown in the figure, the rest without marked with CC refers to the total SECA which includes both CF and CC SECA, the same as follows).

It can be seen in Fig. 3.9c that there is a single linear relationship between the measured compressive strength and the calculated SECA. This suggests that the compressive strength of cement paste can be directly related to the quantity of interparticle bonds of the solid phase in cement pastes. Moreover, Fig. 3.9c also shows that the linear relationship (the black dashed line) between compressive strength and SECA in blended cement paste with w/b = 0.3 and that with w/b = 0.4 overlap each other. The same overlap can be found between Portland cement paste with w/b = 0.3

and that with w/b = 0.4 (the red line in Fig. 3.9c). This overlap implies that the linear relationships between compressive strength and SECA are independent of the w/b ratio, no matter for Portland cement paste or for the cement paste blended with 30% M300. Since these relationships are linear, the compressive strength is only related to the magnitude of contact area. It indicates that the interparticle bonds in both Portland cement paste and the cement paste blended with 30% M300 have stable mechanical properties which do not change with either the curing age or w/b ratio.

From Fig. 3.9c it is clear that the red line representing the relationship between CC-SECA and compressive strength has a steeper slope than the black dashed line that represents the relationship between total SECA and compressive strength in the cement paste blended with 30% M300. Moreover, it is noteworthy that the linear relationship between the compressive strength and the CC-SECA in the cement paste blended with 30% M300 coincides with the relationship between compressive strength and CC-SECA in Portland cement paste. It appears that the strength of cement pastes blended with 30% M300 is determined by the CC contact area, and CF contact area does not contribute to the strength. In other words, for any given CC contact area, regardless w/b ratio and curing age, the addition of M300 does not contribute to the compressive strength of cement paste. This finding is in line with an observation made by Termkhajornkit et al. [29]. Their study showed that the fine quartz grains had no noticeable contribution to the compressive strength of cementitious materials.

3.4.2.2 Effect of filler content

Fig. 3.10 demonstrates the influence of the content (0%, 30% and 50%) of filler on the relationship between the measured compressive strength and the calculated SECA of cement pastes. Fig. 3.10a shows the measured compressive strength of cement pastes at ages of 1, 3, 7, 14, 28 and 90 days. The calculated SECA is presented in Fig. 3.10b. The relationships between the calculated SECA and the measured compressive strength of cement pastes with w/b = 0.3 are presented in Fig. 3.10c. As shown in Fig. 3.10c, the same linear relationships between compressive strength and SECA are observed in Portland cement paste and the cement pastes blended with 30% and 50% M300 filler. The relationship between compressive strength and CC-SECA is represented by the red line. The black line indicates the relationship between the compressive strength and the total SECA in cement paste blended with 30% M300. In cement paste blended with 50% M300, the relationship between the compressive strength and the total SECA is illustrated by the black dashed line.

It can be seen in Fig. 3.10c that the linear relationships between the compressive strength and the CC-SECA in Portland cement paste and the cement pastes blended with 30% and 50% M300 can be represented with one single line (the red line). It further illustrates that CF contact area does not contribute to the strength of cement pastes and the strength of cement pastes is determined by CC contact area. As shown in Fig. 3.10c, the compressive strength of cement paste blended with less M300 increases more rapidly as a function of total SECA. This is because the cement paste with a higher M300 content has less CC-SECA (Fig. 3.10b), which determines the compressive strength of cement paste.

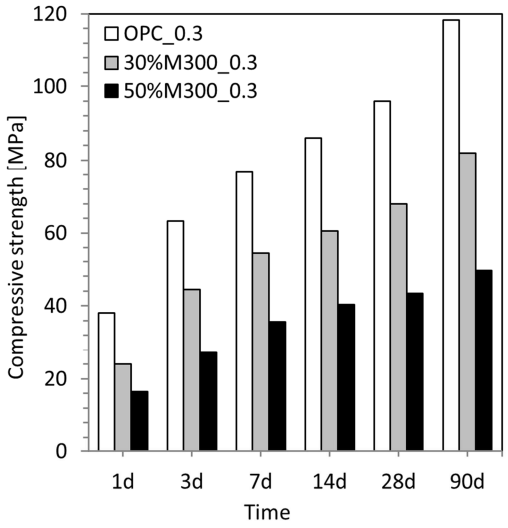

(a) Compressive strength

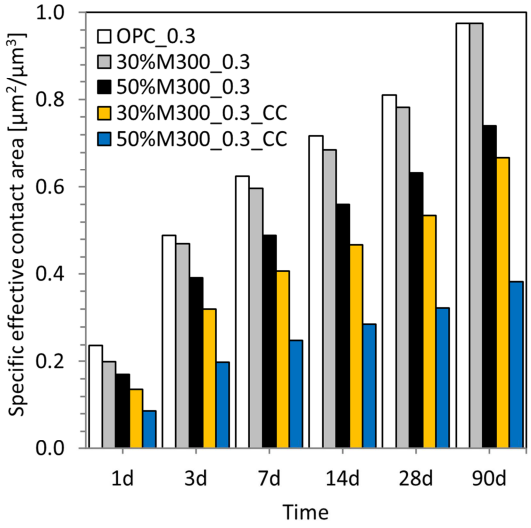

(b) Specific Effective Contact Area

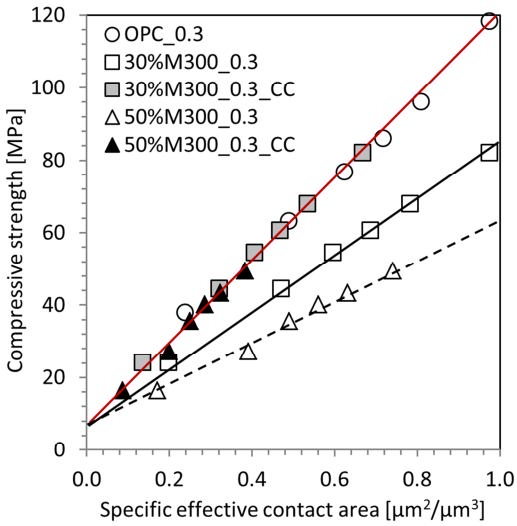

(c) Correlation between Specific Effective Contact Area and compressive strength

Fig. 3.10 Effect of the content (0%, 30% and 50%) of micronized sand on the relationship between the measured compressive strength and the calculated Specific Effective Contact Area (w/b = 0.3).

3.4.2.3 Effect of filler size

Fig. 3.11 shows the effect of the filler size on the relationship between the measured compressive strength and the calculated SECA of cement pastes. Fig. 3.11a shows the measured compressive strength of cement pastes at ages of 1, 3, 7, 14, 28 and 90 days. The calculated SECA is presented in Fig. 3.11b. The relationships between the calculated SECA and the measured compressive strength of cement pastes with w/b = 0.4 are presented in Fig. 3.11c. As shown in Fig. 3.1, M6 is much coarser than both M300 and Portland cement, while M300 is finer than Portland cement. It can be seen in Fig. 3.11c that the relationships between compressive strength and SECA are still linear in Portland cement paste and the cement pastes blended with 30% of M6 or M300 filler. As shown in Fig. 3.11c, the relationship between compressive strength and CC-SECA is represented by the red line. The black line denotes the relationship between the compressive strength and the total SECA in cement paste blended with 30% M6. In the cement paste blended with 30% M300, the relationship between the compressive strength and the total SECA is illustrated by the black dashed line.

It can be seen in Fig. 3.11a that the compressive strength of cement paste with fine filler is higher than that with coarse filler. This can be explained by the fact that the cement paste with fine filler has more CC-SECA (Fig. 3.11b), which determines the compressive strength of cement paste as indicated in previous findings. As can be noted in Fig. 3.11c, the linear relationship between the compressive strength and the CC-SECA in the cement pastes blended with 30% M6 and that with 30% M300, and that in Portland cement paste can be represented with one single line. This fact also illustrates that the compressive strength of cement pastes is determined by CC contact area in both Portland cement paste and the cement paste blended with micronized sand, regardless the particle size of filler.

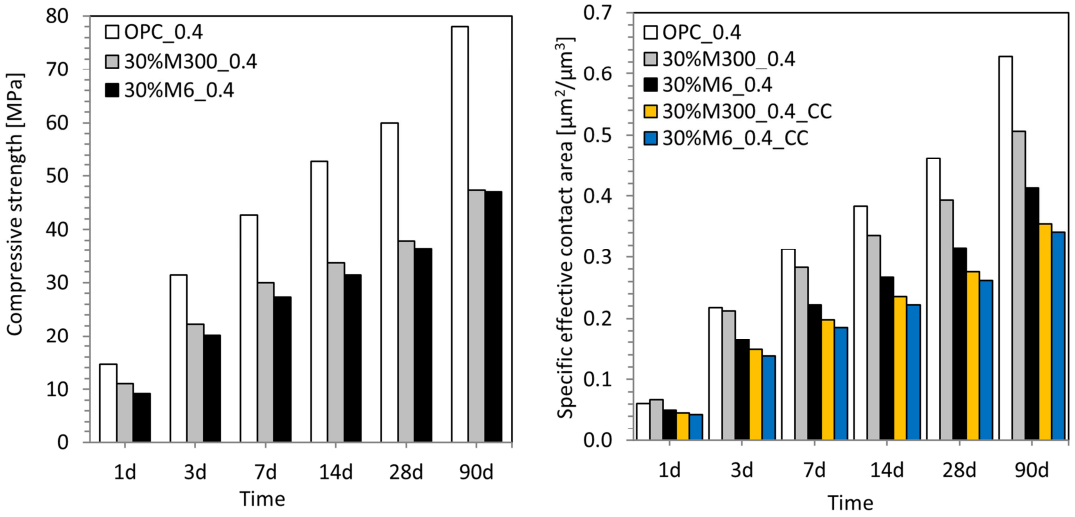

(a) Compressive strength (b) Specific Effective Contact Area

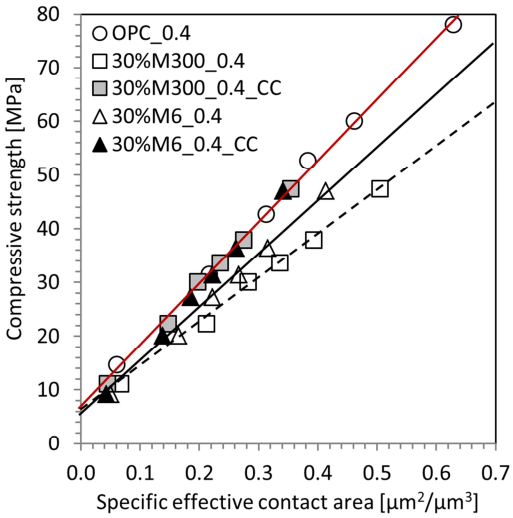

(c) Correlation between Specific Effective Contact Area and compressive strength

Fig. 3.11 Effect of the size of micronized sand on the relationship between the measured compressive strength and the calculated Specific Effective Contact Area (w/b is 0.4 and the content of filler is 30%).

3.4.2.4 Effect of filler type

Fig. 3.12 demonstrates the influence of the filler type on the relationship between the measured compressive strength and the calculated contact area of cement pastes. Two types of filler were chosen: limestone powder(LP) and micronized sand(M300). As highlighted in 3.4.1, both fillers are inert in cement paste. The chemical and physical properties of these fillers can be found in Table 3.1. The linear relationships between compressive strength and the calculated contact area hold for both blended cement pastes, as shown in Fig. 3.12b. Like before, the relationship between compressive strength and the contact area between hydrating cement particles (CC contact area) in

M300-blended cement paste and that in Portland cement paste can be represented with one single line (the red solid line). The relationship between compressive strength and the contact area between hydrating cement particles (CC contact area) in LP-blended cement paste is indicated by the red dashed line. The black line shows the relationship between the compressive strength and the total contact area in cement paste blended with 30% LP. The relationship between the compressive strength and the total contact area in cement paste blended with 30% M300 is represented by the black dashed line.

As indicated by the red solid line and the red dashed line in Fig. 3.12b, the compressive strength of the LP-blended cement paste increases more rapidly as function of CC contact area than that of the M300-blended cement paste. As indicated previously the contact area between hydrating cement particle and filler particle (CF contact area) in M300-blended cement paste does not contribute to the compressive strength. The compressive strength is only related to the contact area between hydrating cement particles (CC contact area). As a result the linear relationship between compressive strength and CC contact area in the M300-blended cement paste and that in Portland cement can be represented with one single line. However, as shown in Fig. 3.12b, LP-blended cement paste has a higher compressive strength compared to the M300-blended cement paste and Portland cement paste for a given CC contact area. It appears that in the LP-blended cement paste not only the contact area between hydrating cement particles (CC contact area), but also the contact area between hydrating cement particle and filler particle (CF contact area) contributes to the compressive strength. The shaded area as shown in the Fig. 3.12b is assumed to indicate the compressive strength contribution of the contact area between hydrating cement particle and filler particle (CF contact area) in LP-blended cement paste.

Fig. 3.12a shows the development of compressive strength of cement pastes. At early ages (1 to 3 days) M300-blended cement paste shows slightly higher compressive strength than LP-blended cement paste. However, it is soon overtaken by LP-blended cement past, even though M300-blended cement paste has more CC contact area than LP-blended cement paste at all curing ages (Fig. 3.12c). The ‘gap’ between the compressive strength of M300-blended cement paste and that of LP-blended cement paste becomes wider with increasing age. To explain this change, we can find the answer in Fig. 3.12d. At early ages (1 to 3 days), the amount of CF contact area in LP-blended cement paste is very low (Fig. 3.12d). So the strength provided by the contact area between hydrating cement particle and filler particle (CF contact area) in LP-blended cement paste cannot bridge the ‘gap’ between the strength offered by the contact area between hydrating cement particles (CC contact area) in M300-blended cement paste and the strength offered by CC contact area in LP-blended cement paste, as shown in Fig 3.12a (for 1 to 3 days). As a result, M300-blended cement paste has higher compressive strength. However, at an age of 7 days LP-blended cement paste shows slightly higher compressive strength (Fig. 3.12a) due to an increase of CF contact area in LP-blended cement paste (Fig. 3.12d). Although the CF contact area in M300-blended cement paste also increases substantially with increasing CF contact area in LP-blended cement paste, this increasing CF contact area makes no change to the strength. At later ages (>7 days), the compressive strength of LP-blended cement paste largely surpasses that of M300-blended cement paste (Fig. 3.12a) as CF contact area in LP-

blended cement paste continues to increase (Fig. 3.12d). These observations further demonstrate that the contact area between hydrating cement particle and filler particle (CF contact area) in LP-blended cement paste contributes to the compressive strength, but that in M300-blended cement paste does not.

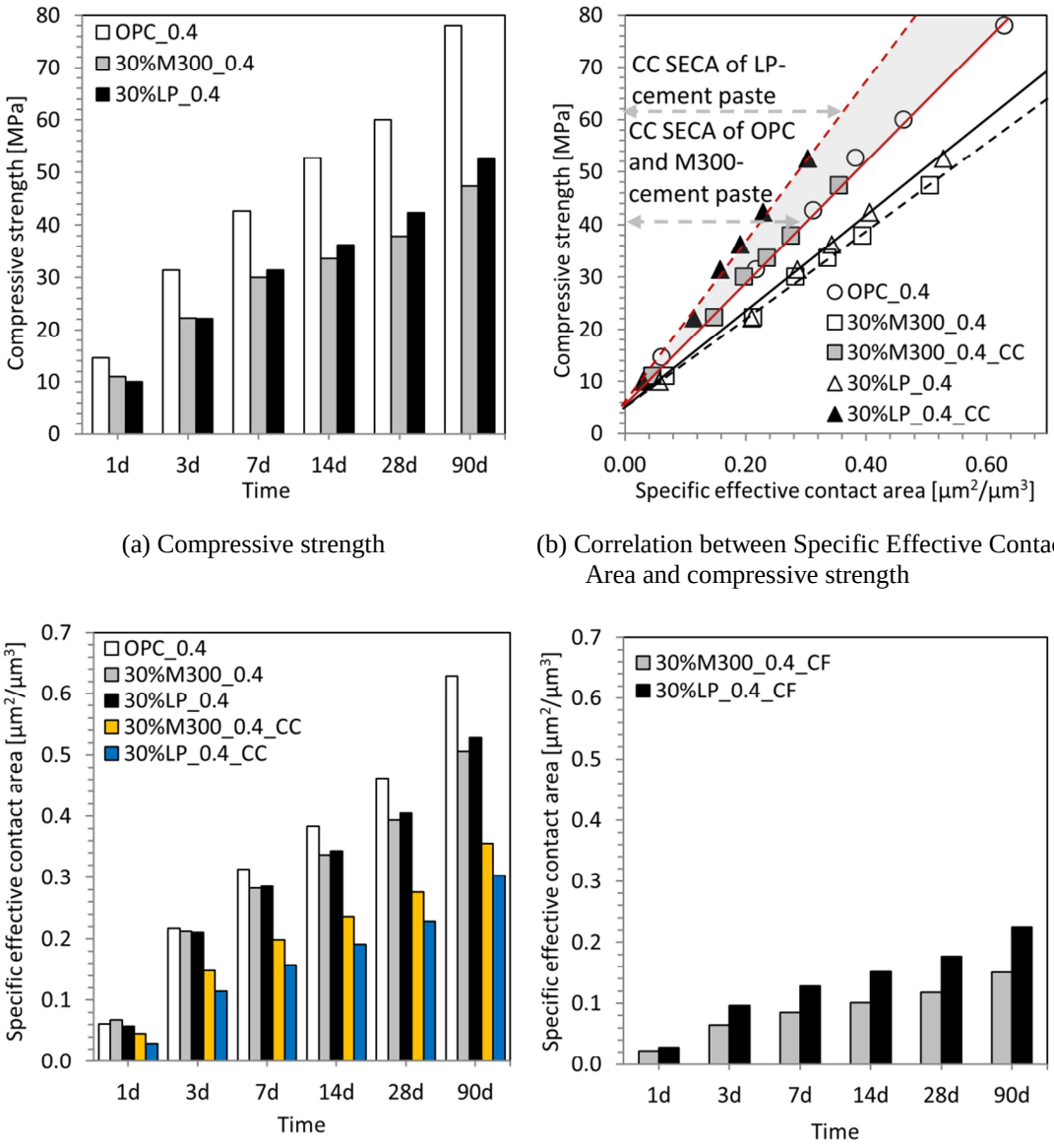

(a) Compressive strength

(b) Correlation between Specific Effective Contact Area and compressive strength

(c) Specific Effective Contact Area

(d) CF Specific Effective Contact Area

Fig. 3.12 Effect of the type of filler on the relationship between the measured compressive strength and the calculated Specific Effective Contact Area (w/b is 0.4 and the content of filler is 30%).

3.4.3 Discussion

The correlations between the measured compressive strength and the calculated specific effective contact area (SECA) of the solid phases in blended cement pastes were investigated. From the evaluation of the experiments and simulations, it is concluded that the contact area between hydrating cement particle and filler particle in cement paste blended with limestone powder has a substantial contribution to the compressive strength, but the contact area between hydrating cement particle and filler particle in cement paste blended with micronized sand has not. A previous study by de Vries [30] showed that the compressive strength of cement paste decreased along with an increasing replacement level of Portland cement by micronized sand (Fig. 3.13). Even the cement paste blended with 10% of very fine micronized sand M600 (the surface area of cement and M600 in this study is 420 m^2/kg and 1300 m^2/kg, respectively [30]), its compressive strength is lower than that of Portland cement paste. By contrast, in the study of Tsivilis et al. [31], it was shown that the addition of 10% limestone did not significantly alter the compressive strength at any age of cement pastes (Binders have fineness up to 340, 380, 410, and 430 m^2/kg, respectively). In a study of Voglis et al. [32], cement paste produced by inter-grinding 15% limestone shows the same compressive strength as the Portland cement paste at the curing age of 28 days. Based on these observations, it is believed that the limestone powder has better adhesion properties than micronized sand.

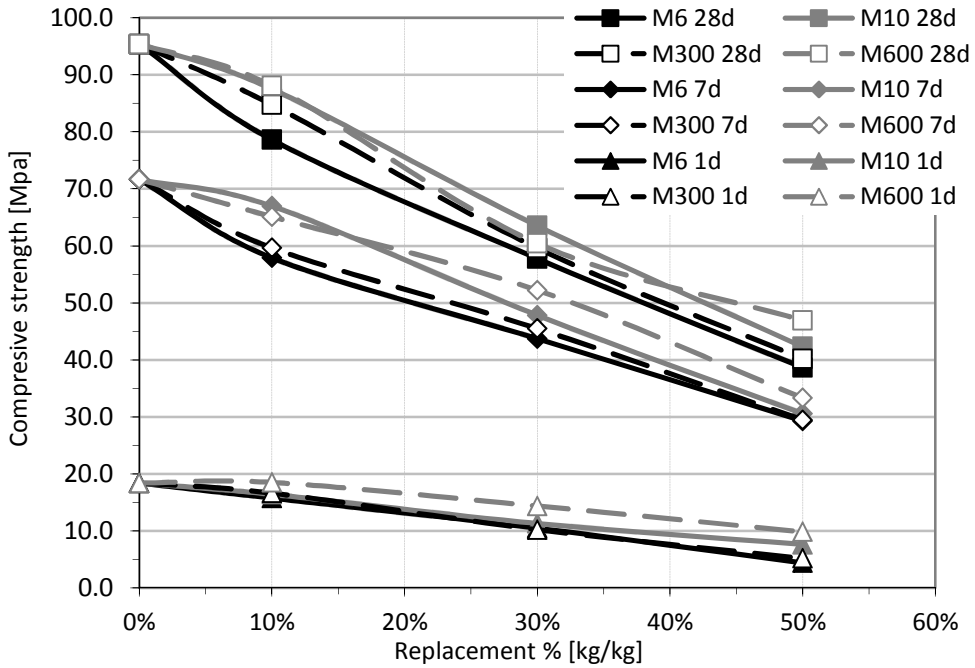

Fig. 3.13 Compressive strength of cement pastes blended with different micronized sand at the curing age of 1, 7 and 28 days, with the water-to-binder ratio of 0.35 [30].

The mechanical properties of cement paste were directly related to microstructure features, more particularly to the simulated contact area in cement paste. The simulated contact area was divided into the contact area between hydrating cement particles (CC contact area) and the contact area between hydrating cement particle and filler particle (CF contact area). Based on this division, the role of the filler-hydrates adhesion properties (the quality of the contact area between filler particles and reaction products) in the strength of blended cement paste was evaluated. In the following chapters, the fundamental explanations for the different performance of limestone powder and micronized sand as replacement of Portland cement will be presented.

3.5 Conclusions

Numerical simulations of the contact area between cement and/or filler particles combined with experimental measurements were used to investigate the filler-hydrates adhesion properties on the strength of blended cement paste. Based on this study, the following conclusions can be drawn:

- The measured compressive strength of Portland cement paste and the cement paste blended with inert fillers can directly be related to the calculated contact area. The relationship between calculated contact area and measured compressive strength was found to be linear.

- In Portland cement paste the linear relationship between the measured compressive strength and the calculated contact area was independent of the water-to-cement ratio. In the cement pastes blended with micronized sand the linear relationship between the measured compressive strength and the calculated CC contact area and that in Portland cement paste can be represented with one single line, regardless the water-to-binder ratio, the particle size and the content of filler.

- In the cement pastes blended with limestone powder, the measured compressive strength increases as a function of the calculated CC contact area more rapidly than that in Portland cement paste and the cement paste blended with micronized sand.

- In the cement pastes blended with micronized sand, the compressive strength was determined by CC contact area. The contact area between hydrating cement particle and filler particle had no contribution to the compressive strength. In contrast, in the cement paste blended with limestone powder the contact area between hydrating cement particle and filler particle had a substantial contribution to the compressive strength. It is believed that limestone powder has much better adhesion properties than micronized sand.

References

1. Moosberg-Bustnes, H., B. Lagerblad, and E. Forssberg, *The function of fillers in concrete.* Materials and Structures, 2004. **37**(2): p. 74-81.
2. Bonavetti, V., et al., *Limestone filler cement in low w/c concrete: A rational use of energy.* Cement and Concrete Research, 2003. **33**(6): p. 865-871.
3. Lawrence, P., M. Cyr, and E. Ringot, *Mineral admixtures in mortars - Effect of inert materials on short-term hydration.* Cement and Concrete Research, 2003. **33**(12): p. 1939-1947.
4. van Breugel, K., *Simulation of hydration and formation of structure in hardening cement-based materials*, 1991, Delft University of Technology: The Netherlands.
5. Koenders, E.A.B., *Simulation of volume changes in hardening cement-based materials*, 1997, Delft University of Technology: The Netherlands.
6. Ye, G., K. van Breugel, and A.L.A. Fraaij, *Three-dimensional microstructure analysis of numerically simulated cementitious materials.* Cement and Concrete Research, 2003. **33**(2): p. 215-222.
7. Ye, G., *Experimental study and numerical simulation of the development of the microstructure and permeability of cementitious materials*, 2003, Delft University of Technology: The Netherlands.
8. Sun, Z.H., G. Ye, and S.P. Shah, *Microstructure and early-age properties of portland cement paste - Effects of connectivity of solid phases.* Aci Materials Journal, 2005. **102**(2): p. 122-129.
9. Taylor, H.F., *Cement chemistry*1997: Thomas Telford.
10. Standard, A., *C305, Standard practice for mechanical mixing of hydraulic cement pastes and mortars of plastic consistency*, in *Annual book of ASTM standards*2006.
11. Standard, A., *C109, Standard test method for compressive strength of hydraulic cement mortars*, in *Annual book of ASTM standards*2006.
12. Fagerlund, G., *CHEMICALLY BOUND WATER AS MEASURE OF DEGREE OF HYDRATION*. Division of Building Materials 2009: p. 25.
13. Copeland, L.E. and J.C. Hayes, *The determination of non-evaporable water in hardened portland cement paste*, 1900.
14. Molina, L., *On predicting the influence of curing conditions on the degree of hydration*1992: Swedish Cement and Concrete Research Institute.
15. Kakali, G., S. Tsivilis, and A. Tsialtas, *Hydration of ordinary portland cements made from raw mix containing transition element oxides.* Cement and Concrete Research, 1998. **28**(3): p. 335-340.
16. Stepkowska, E., et al., *Phase transformation on heating of an aged cement paste.* Thermochimica Acta, 2004. **420**(1): p. 79-87.
17. Lothenbach, B., et al., *Influence of limestone on the hydration of Portland cements.* Cement and Concrete Research, 2008. **38**(6): p. 848-860.
18. Alarcon-Ruiz, L., et al., *The use of thermal analysis in assessing the effect of temperature on a cement paste.* Cement and Concrete Research, 2005. **35**(3): p. 609-613.
19. Liu, X., et al., *Simulation of the microstructure formation in hardening self-compacting cement paste containing limestone powder as filler via computer-based model.* Materials and Structures, 2013. **46**(11): p. 1861-1879.
20. van Breugel, K., *simulation of hydration and formation of structure in harding cement-based materials*, 1991, Delft University: Delft.
21. Collepardi, M. and B. Marchese, *Morphology and surface properties of hydrated tricalcium silicate pastes.* Cement and Concrete Research, 1972. **2**(1): p. 57-65.
22. GRANJU, J. and J. MASO, *LAW OF RESISTANCE IN SIMPLE COMPRESSION OF WATER CURED PORTLAND-CEMENT PASTES.* Cement and Concrete Research, 1980. **10**(5): p. 611-621.
23. Lawrence, F. and J. Young, *Studies on the hydration of tricalcium silicate pastes I. Scanning electron microscopic examination of microstructural features.* Cement and Concrete Research, 1973. **3**(2): p. 149-161.
24. Sun, Z., et al. *Early age properties of Portland cement pastes investigated with ultrasonic shear waves and numerical simulation*. in *Proceedings of the RILEM International Symposium on Advances in Concrete through Science and Engineering*. 2004.

25. Xiaowei Ouyang, Guang Ye, and K.v. Breugel, *Effect of Inert Additives on Compressive Strength of Cement Paste:Results from Numerical Analysis of Connectivity of Solid Phases*, in *The 14th International Congress on the Chemistry of Cement (ICCC 2015)* 2015: Beijing, China.
26. Kumar, A., J. Reed, and G. Sant, *Vertical Scanning Interferometry: A New Method to Measure the Dissolution Dynamics of Cementitious Minerals.* Journal of the American Ceramic Society, 2013. **96**(9): p. 2766-2778.
27. Luz, A.P. and V.C. Pandolfelli, *CaCO3 addition effect on the hydration and mechanical strength evolution of calcium aluminate cement for endodontic applications.* Ceramics International, 2012. **38**(2): p. 1417-1425.
28. Mindess, S. and S. Diamond, *SEM investigations of fracture surfaces using stereo pairs: II. Fracture surfaces of rock-cement paste composite specimens.* Cement and Concrete Research, 1992. **22**(4): p. 678-688.
29. Termkhajornkit, P., R. Barbarulo, and G. Chanvillard, *Microstructurally-designed cement pastes: A mimic strategy to determine the relationships between microstructure and properties at any hydration degree.* Cement and Concrete Research, 2015. **71**: p. 66-77.
30. De Vries, W., *the use of micronized sand as cement replacement*, 2008, Delft University of technology: Delft.
31. Tsivilis, S., et al., *A study on the parameters affecting the properties of Portland limestone cements.* Cement & Concrete Composites, 1999. **21**(2): p. 107-116.
32. Voglis, N., et al., *Portland-limestone cements. Their properties and hydration compared to those of other composite cements.* Cement & Concrete Composites, 2005. **27**(2): p. 191-196.

4

Evaluation of Filler-hydrates Adhesion Properties*

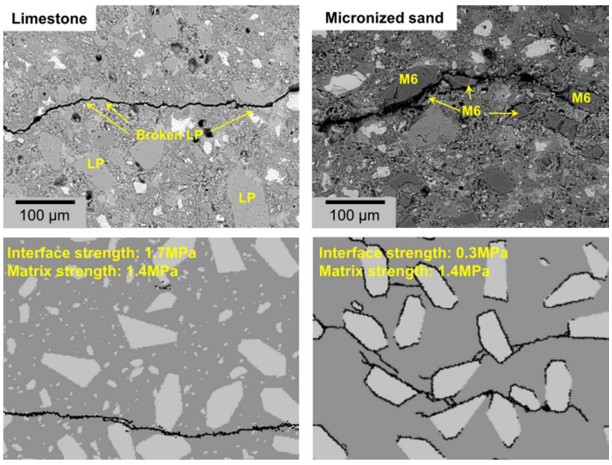

The interface between filler particles and hydration products can have a significant effect on the mechanical properties of the cement paste system. SEM observation and mechanical modelling can be used to study the mechanical properties of the interface. The fillers used in this study are limestone powder and micronized sand. Crack paths and fracture surfaces of loaded cement pastes were investigated by SEM observation. The influence of the mechanical properties of the interface on crack propagation, tensile strength and fracture energy was studied numerically by using a lattice model. Based on the SEM observations and simulation results, the mechanical properties of the interface between filler particles and hydration products were evaluated. Limestone powder exhibited superior bond characteristics with hydration products compared to micronized sand. This study provides a validation of the contact area concept and justifies the findings presented in chapter 3. Meanwhile, this study provides insight into adhesion mechanisms between filler particles and hydration products. The further study of the adhesion mechanisms will be presented in chapter 5.

* This chapter based on:

1. Xiaowei Ouyang, Guang Ye, Klass van Breugel. Experimental and numerical evaluation of mechanical properties of interface between filler and hydration products. *Construction and Building Materials*, 2017. 135: p. 538-549.

2. Xiaowei Ouyang, Guang Ye, Klaas van Breugel. Characterization of Crack in Cement Paste Incorporating Inert Fillers under Compressive Loading. *The 3rd International Conferences on Microstructure Related Durability of Cementitious Composites (Microdurability2016)*. Nanjing, China 2016.

4.1 Introduction

The mechanical properties of the interface between filler particles and hydration products have a significant influence on the development of the fracture process in blended cement pastes. Improvement of the effect of fillers in cementitious materials, especially the effect on the mechanical properties of the interface between filler particles and hydration products, is a big issue and a challenge today. So far not many attempts are known to quantify the mechanical properties of the interface between filler and hydration products in cement paste. To evaluate the mechanical properties of this interface, a surface analysis technique, i.e., scanning electron microscopy (SEM) observation, was used. Scanning electron microscopy is known as an appropriate method to characterize the crack paths and the fracture surfaces in cementitious materials [1-5]. The mechanical properties of the interface have a strong relationship with the resistance to crack propagation. Cracks preferentially propagate along weak interfaces [5].

In order to predict the effect of the mechanical properties of the interface on the fracture process and the strength of blended cement pastes, a numerical model was applied. This model, called lattice fracture model, was proposed by Schlangen and Van Mier in the 1990s and has been further developed by many others [6-8]. In the lattice fracture model, the material is represented by a lattice of beam elements. Subsequently, the microstructure of the material can be mapped onto these beam elements by assigning different properties to them, depending on whether the beam element represents a grain, the interface or the matrix. The lattice model has been used extensively in the past decades both for mesoscale and, more recently, also microscale modelling of concrete and cement paste [8-13]. The numerical results showed that the model can reproduce the fracture processes observed in experiments. In this chapter, the lattice fracture model was used to study the influence of interface properties on crack propagation, strength and fracture energy. The results from a simulated direct tension test were compared to experimental results and were used to simulate the micromechanical properties of the interface.

4.2 Materials and experimental methods

4.2.1 Sample preparation

The cement used in this study is Portland cement (OPC). The fillers used are limestone powder (LP) and micronized sand (M6). The chemical composition and physical characteristics of these materials were presented in Table 3.1. The mineral composition of OPC was presented in Table 3.2. The particle size distribution (PSD) data of OPC, LP and M6 was shown in Fig. 3.1. Two series of specimens were prepared, denoted as M01 and L01. The percentage of filler and w/b ratio are given in Table 4.1.

Table 4.1 Mixture compositions of blended cement pastes.

Mixtures	OPC*(%)	M6*(%)	LP*(%)	w/b
M01	70	30	-	0.4
L01	70	-	30	0.4

* Percentage of the total mass of binder by weight.

4.2.2 Experimental methods

4.2.2.1 Experimental procedures

The mixtures were prepared in a Hobart mixer according to the standard procedure described in ASTM C305 [14]. After mixing and casting, cement pastes were covered with a plastic sheet and stored at 20 ± 2°C. After 24 hours all the specimens were demolded and then stored in the curing room with a constant temperature of 20 ± 2°C and a relative humidity of 95 ± 5% until the designated testing age.

4.2.2.2 SEM analysis

The scanning electron microscope (SEM) equipped with energy dispersive spectroscopy (EDS) with a working voltage of 20 kV was used to observe the fracture surface between filler particles and hydration products and the propagation of cracks in the loaded cement pastes. Sample preparations for these SEM analyses are as follows:

i) The samples for observation of the fracture surface between filler particles and hydration products were loaded in compression at 90% of the peak load. After loading, the specimens were crushed into small pieces. Then, crushed samples with different sizes were collected. In order to stop the hydration process of the specimens, they were submerged in 100% ethanol for 72 hours and placed in a 35 °C oven during 24 hours. These samples were kept in a desiccator until testing. SE mode was adopted for high magnification (20000×) observations. The samples for SE observation were coated with carbon.
ii) After stopping hydration a part of the samples was selected for observation of the propagation of cracks. These samples were submerged in an epoxy resin. Afterward the samples were grinded and polished. Again, these samples were stored in a desiccator until testing.

4.3 Numerical simulation

4.3.1 Build-up of lattice structure

In the lattice approach blended cement paste is considered a material made only of three components: the matrix phase, the fillers and interface. The unhydrated cement, hydration products and other components are assumed to be part of the matrix phase. For the mesh generation the microstructure of the blended cement paste is represented

by a pixel-based structure, as shown in Fig. 4.1a. After the generation of a network of pixels, a sub-pixel can be defined within each pixels (Fig. 4.1b). A node is randomly placed in every sub-pixel of size s in a regular grid with size α, as shown in Fig. 4.1b. In order to set a proper pixel size (cell size of mesh, α), its effect on the simulation results was analysed and presented in section 4.5.1. The ratio s/α is defined as randomness of a lattice. The reason for assigning certain randomness to the lattice mesh is to describe the material more realistically. Here randomness is set to be 0.5. To connect the nodes, lattice elements are generated using Delaunay triangulation, as shown in Fig. 4.1c. The different types of beam are identified by material overlap procedures. Element properties depend on the two nodes assigned to an element. If the two element nodes are located within filler, the filler element can be identified. If one element node is located in the matrix and another element node in filler, the element is called an interface element. In Fig. 4.1d, identification of different elements is illustrated. In this model, we generated a square specimen with a size of 100 × 100 × 1 μm^3 for a 3D lattice model.

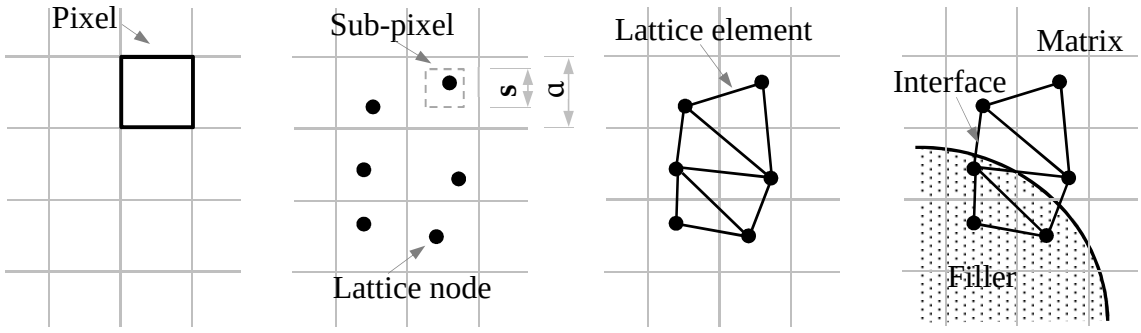

(a) Pixel generation (b) Node placement (c) Element generation (d) Overlay procedure

Fig. 4.1 Schematics of the generation of microstructure of the cement paste blended with filler.

4.3.2 Fracture processes simulation

4.3.2.1 Numerical approach

In the lattice approach the cement paste is discretized as a set of lattice beam elements. A lattice beam element is a straight bar of uniform cross-section and can transmit axial forces, shear forces, bending moments and torsional moments, as shown in Fig. 4.2. The 3D lattice beam element has two nodes and each node has six degrees of freedom including three translational and three rotational degrees of freedom, as shown in Fig. 4.3. The displacement u^e of the nodes of the beam (Fig. 4.3) in the local domain is:

$$u^e = [u_1 \quad u_2 \quad u_3 \quad u_4 \quad u_5 \quad u_6 \quad u_7 \quad u_8 \quad u_9 \quad u_{10} \quad u_{11} \quad u_{12}]^T \tag{4.1}$$

The local force vector f^e caused by local displacement u^e can be computed with the following equation:

$$f^e = k^e u^e \tag{4.2}$$

where k^e is the element stiffness matrix in the local domain. The formulation of a lattice beam element stiffness matrix is based on the Timoshenko beam theory. It can be formulated by assembling an axial component, a torsional component, and bending and shear components in the planes *x*O*y* and *x*O*z* (see Fig. 4.3) and given by:

$$k^e = \begin{bmatrix}
\frac{EA}{l} & 0 & 0 & 0 & 0 & 0 & -\frac{EA}{l} & 0 & 0 & 0 & 0 & 0 \\
 & \frac{12EI_z}{l^3(1+\Phi_1)} & 0 & 0 & 0 & \frac{6EI_z}{l^2(1+\Phi_1)} & 0 & -\frac{12EI_z}{l^3(1+\Phi_1)} & 0 & 0 & 0 & \frac{6EI_z}{l^2(1+\Phi_1)} \\
 & & \frac{12EI_y}{l^3(1+\Phi_1)} & 0 & -\frac{6EI_y}{l^2(1+\Phi_2)} & 0 & 0 & 0 & -\frac{12EI_y}{l^3(1+\Phi_2)} & 0 & -\frac{6EI_y}{l^2(1+\Phi_2)} & 0 \\
 & & & \frac{GJ}{l} & 0 & 0 & 0 & 0 & 0 & -\frac{GJ}{l} & 0 & 0 \\
 & & & & \frac{(4+\Phi_2)EI_y}{l(1+\Phi_2)} & 0 & 0 & 0 & \frac{6EI_y}{l^2(1+\Phi_2)} & 0 & \frac{(2-\Phi_2)EI_y}{l(1+\Phi_2)} & 0 \\
 & & & & & \frac{(4+\Phi_1)EI_z}{l(1+\Phi_1)} & 0 & -\frac{6EI_z}{l^2(1+\Phi_1)} & 0 & 0 & 0 & \frac{(2-\Phi_2)EI_z}{l(1+\Phi_1)} \\
 & & & & & & \frac{EA}{l} & 0 & 0 & 0 & 0 & 0 \\
 & & & & & & & \frac{12EI_z}{l^3(1+\Phi_2)} & 0 & 0 & 0 & -\frac{6EI_z}{l^2(1+\Phi_1)} \\
 & & & & & & & & \frac{12EI_y}{l^3(1+\Phi_2)} & 0 & \frac{6EI_y}{l^2(1+\Phi_2)} & 0 \\
 & & & & & & & & & \frac{GJ}{l} & 0 & 0 \\
 & & & & & & & & & & \frac{(4+\Phi_2)EI_y}{l(1+\Phi_2)} & 0 \\
 & & & & & & & & & & & \frac{(4+\Phi_1)EI_z}{l(1+\Phi_1)}
\end{bmatrix} \tag{4.3}$$

where *E* is the elastic modulus, G is the shear modulus, *A* is the cross-sectional area of the element, *l* is the length of the element, I_z and I_y are the moments of inertia about the z-axis and the y-axis respectively, J is the polar moment of inertia about the x-axis, Φ_1 and Φ_2 are the shear effect adjustment factors in the plane *x*O*y* and *x*O*z*, respectively, and can computed by:

$$\Phi_1 = \frac{12EI_z}{GA_s l^2}$$
$$\Phi_2 = \frac{12EI_y}{GA_s l^2} \tag{4.4}$$

in which A_s is the shear cross-sectional area and is given by:

$$A_s = \frac{A}{\mathrm{K}} \tag{4.5}$$

where K is the shear correction factor. A more detailed description of the numerical approach can be found in [6].

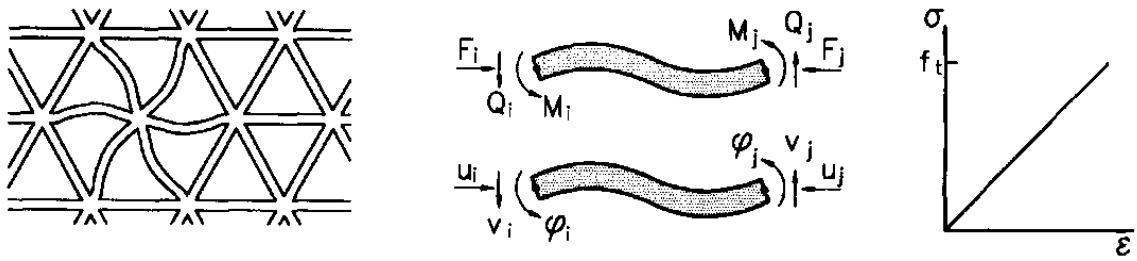

(a) (b) (c)

Fig. 4.2 Lattice of beam elements (a), definition of forces and degrees of freedom (b), stress-strain relation of the beam element (c) [15].

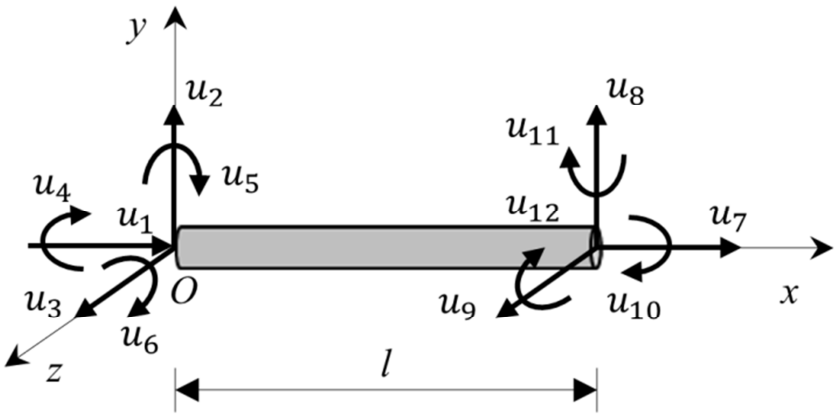

Fig. 4.3 The displacement of a 3D lattice beam element.

4.3.2.2 Geometry and boundary conditions

A uniaxial tensile test can be conjured by fixing all the nodes on the bottom surface of the specimen and imposing a uniform surface load on the top surface, as shown in Fig. 4.4. In the lattice network construction, all the layers close to the surfaces are forced to be regularly meshed, irrespective of the material randomness setting, as irregular geometry on the boundaries might create some extra stresses, which may have negative effect on the fracture processes simulation. In addition all the lattice elements involved in the bottom and top layers are not allowed to break, even if the stress in such an element has exceeded its strength, as the external loads need a path to be transferred into the specimen. In other words, it is assumed that all the restraint elements on the boundaries have infinite strength.

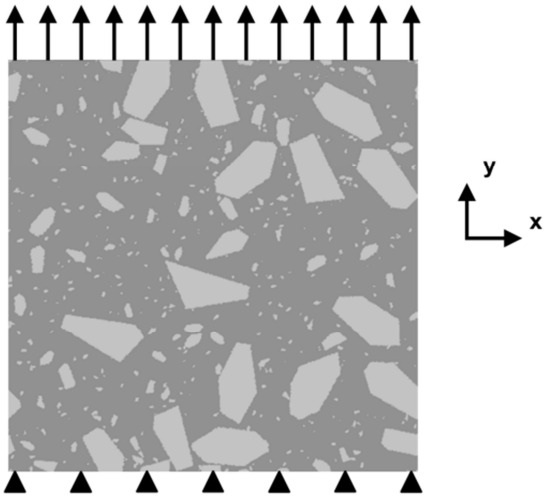

Fig. 4.4 Uniaxial tensile test setup.

4.3.2.3 Fracture law

In lattice fracture analysis, a linear elastic analysis of the lattice is performed in each loading step. An element in which a prescribed fracture criterion is exceeded is removed from the mesh. This analysis is subsequently repeated in a step-wise manner, removing a single element in which a prescribed fracture criterion is exceeded in each step. Multiple analysis steps are performed until the system fails. The step-by-step removal of critical lattice elements simulates the microcrack evolution in the specimen.

In this model, a fracture criterion based on the tensile stress in beams is adopted, and can be described as:

$$\sigma_t = \alpha_N \frac{N}{A} + \alpha_M \frac{\max(M_i, M_j)}{w} \leq f_{t,k} \tag{4.6}$$

where σ_t [kPa] is the maximum tensile stress in the beam, N [kN] is the normal force acting on the beam element, M_i [kN·m] and M_j [kN·m] are the bending moments in two nodes at each end of the element, w [m^3] is the cross sectional moment of resistance. α_N is the normal force influence factor. α_M is the bending influence factor. Details about the underlying elastic equations and the full computational procedure of the lattice model can be found in [6, 8].

4.3.3 Model parameters

Specific material parameters are assigned to the lattice beams. In particular, fracture properties of the three types of beam elements are needed, including properties of the filler, the matrix and the filler-matrix interface. The value of these parameters has significant influence on the microscopic mechanical behaviour. In particular, the strength of the filler-matrix interface directly affects the final results, i.e. crack patterns,

stress-strain curve, Young's modulus and fracture energy of the simulated specimen [15, 16]. In Table 4.2 a summary of the mechanical parameters of chosen fillers and matrix is given. The Young's modulus of limestone powder (LP), micronized sand (M6) and matrix were measured using nanoindentation, and their measured average values are 65.5, 76.2 and 22.0 GPa, respectively. The Young's modulus of LP is slightly lower compared with that of M6, but much higher than that of the matrix. A single value of 71 GPa (the mean value of LP and M6) is used here for the elastic properties of both of LP and M6. The tensile strength of these materials is considered proportional to the measured microhardness [6]. No data could be found for the ratio between hardness and tensile strength of these materials. Therefore, the tensile strengths are inferred from nanoindentation tests. As LP and M6 are much stronger than the matrix, their influence on the fracture process is very small compared to that of the matrix and the interface. As can be seen in Table 4.2 cases that the interface strength is higher and lower than that of the matrix will be considered. The material constants of interfaces and the matrix used in the analysis enable us to gain insight into fracture properties of the virtual pastes.

Table 4.2 Mechanical properties of filler, matrix and the interface of mature paste.

Material properties	Young's modulus E [GPa]	Tensile strength f_t [MPa]	ν
Filler (both for LP, M6)	71	2.1	0.2
Matrix	22	1.4	0.2
Interface 1	17	2.1	0.2
Interface 2	17	1.7	0.2
Interface 3	17	1.4	0.2
Interface 4	17	1.1	0.2
Interface 5	17	0.8	0.2
Interface 6	17	0.5	0.2
Interface 7	17	0.4	0.2
Interface 8	17	0.3	0.2
Interface 9	17	0.2	0.2
Interface 10	17	0.1	0.2

4.3.4 Measure of damage

From the simulation results of the load-displacement response, the crack pattern in the final failure state can be obtained. The load-displacement response can be converted to a stress-strain diagram and a stress-crack opening diagram. From the stress-strain diagram, the tensile strength can be inferred. Fracture energy can be calculated from the post peak part of the stress-crack opening diagram. It represents the area under the curve. A more detailed description of the measure of damage can be found in [17].

4.4 Experimental results

4.4.1 Crack propagation

The crack propagation in the cement paste blended with LP and M6 subjected to compressive loading is illustrated in Fig. 4.5. Fig. 4.5a shows cracks in cement paste blended with 30% LP. Crack patterns in cement paste blended with 30% M6 are shown in Fig. 4.5b. As can be observed in Fig. 4.5a, the cracks tend to propagate in the matrix and avoid to propagate through the interface between LP particles and hydration products. The crack that propagated through LP particles can be seen in Fig. 4.5a. On the contrary, tortuous cracks that have a tendency to propagate around the M6 particles are observed in the cement paste blended with 30% M6 (Fig. 4.5b). Furthermore, also cracks encircling the M6 particles can easily be observed in Fig. 4.5b.

Parallel with the SEM observations of the crack propagation, the morphology of the surface of cracks in cement paste blended with 30% LP and 30% M6 is investigated and shown in Fig. 4.6. The locations of SEM images were randomly selected. It is hard to find LP particles with clear surface at the fracture surface in the cement paste blended with 30% LP (Fig. 4.6a). In the cement paste blended with 30% M6, however, M6 particles with a clear surface can easily be distinguished, as shown in Fig. 4.6b.

These differences in crack propagation and morphology of the surface of the cracks originate from properties of the interface between filler particles and hydration products. According to the previous studies [17, 18], the microcracks are governed by local stress distribution and weak links in the system. The weak interfaces have the highest probability of breaking. These observations suggest that the interface between LP particles and hydration products is much stronger than that between M6 particles and hydration products.

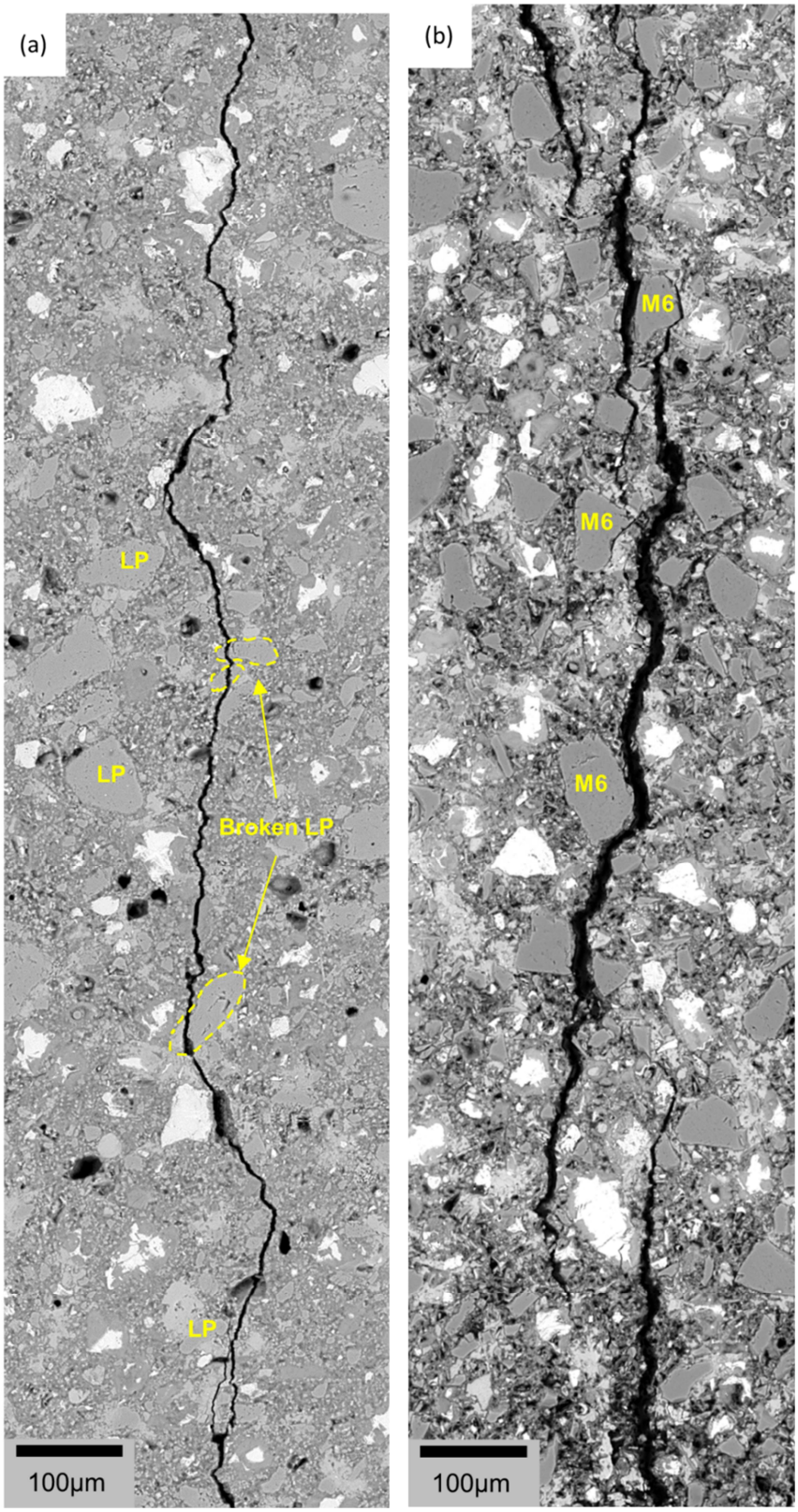

Fig. 4.5 Cracks in the cement paste blended with 30% LP (a) and the cement paste blended with 30% M6 (b) at the curing age of 28 days, at the w/b ratio of 0.4.

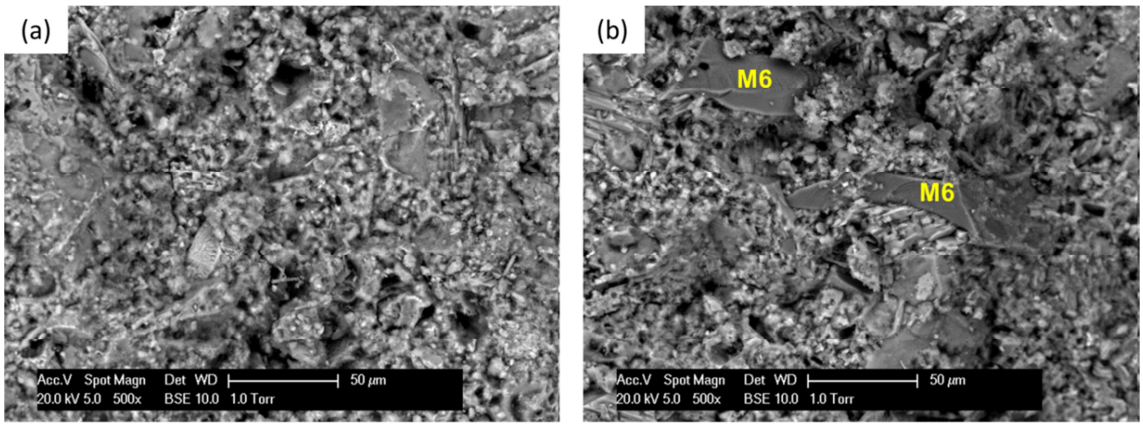

Fig. 4.6 Morphology of the crack surface in the cement paste blended with 30% LP (a) and the cement paste blended with 30% M6 (b) at the curing age of 28 days, at the w/b ratio of 0.4.

4.4.2 Fracture surface

Fig. 4.7 presents the fracture surface between filler particles and hydration products in the cement paste blended with limestone powder (LP) and coarse micronized sand (M6). Fig. 4.7a shows that there are hydration product residues left on the surface of LP particle, which indicate that failure of the cement paste system occurs to a large extent in the hydrations products. Moreover, there is no interfacial gap between the LP particle and surrounding hydration products. This indicates that the bond between LP particle and surrounding hydration products is relatively strong.

As shown in Fig. 4.7b, an interfacial gap between a M6 particle and surrounding hydration products can easily be observed in the micrograph. A similar observation was reported earlier by Wang [19]. The M6 particle has a very clear and smooth fracture surface. Few hydration products can be found on the M6 surface. These observations demonstrate that the bond between LP surfaces and hydration products is stronger than that between M6 surfaces and hydration products.

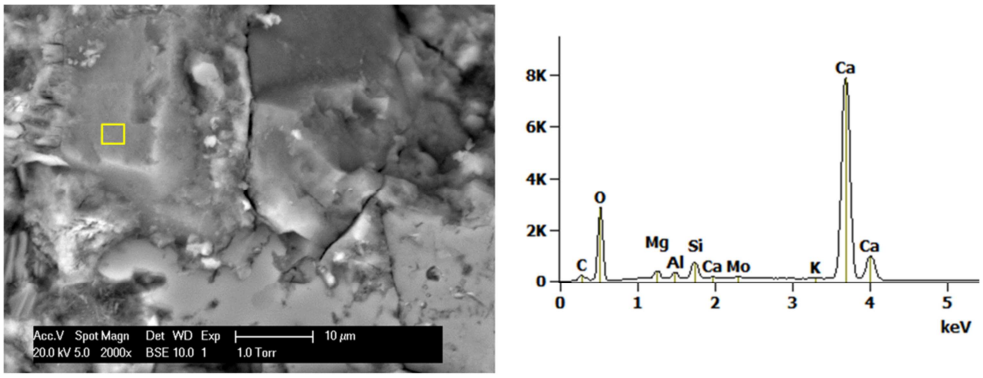

(a) Limestone powder-hydrates interface

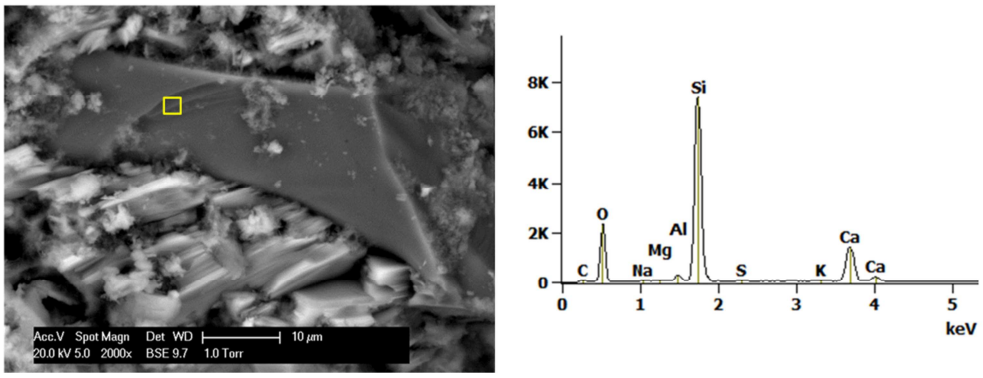

(b) Micronized sand-hydrates interface

Fig. 4.7 SEM micrograph with EDS pattern of products in filler-hydrates interface of the cement paste blended with 30% filler at the curing age of 28 days, with the w/b ratio of 0.4.

To further study the filler-hydrates interface, SEM observations of the fracture surface were made with different magnifications. Fig. 4.8a shows the fracture surface between an LP particle and hydration products at comparatively low magnification (2000×). SE micrographs of the fracture surface at high magnification (20000×) are presented in Fig. 4.8b and c, respectively. Fig. 4.8b shows that there are no typical residuals of hydration products on the fracture surface. Obviously, it is the fracture surface of a broken LP particle. Fig. 4.8c shows that the surface of the LP particle is fully covered with broken hydration products, especially C-S-H, and there is no interfacial gap between the LP particle and broken hydration products. It indicates a strong bond between hydration products and the surface of the LP particle.

Fig. 4.9a presents the fracture surface between a M6 particle and hydration products at comparatively low magnification (2000×). High magnification (20000×) SE micrographs of the fracture surface are shown in Fig. 4.9b and c, respectively. As can be seen in Fig. 4.9b and c there are a few residuals of hydration products present on the surface of M6 particles. Fig. 4.9c shows that the fracture surface is partially covered with loose residuals of hydration products. These observations offer further support to previous findings that the bond between LP surface and hydration products (mainly, C-S-H) is much stronger than that between M6 surface and hydration products.

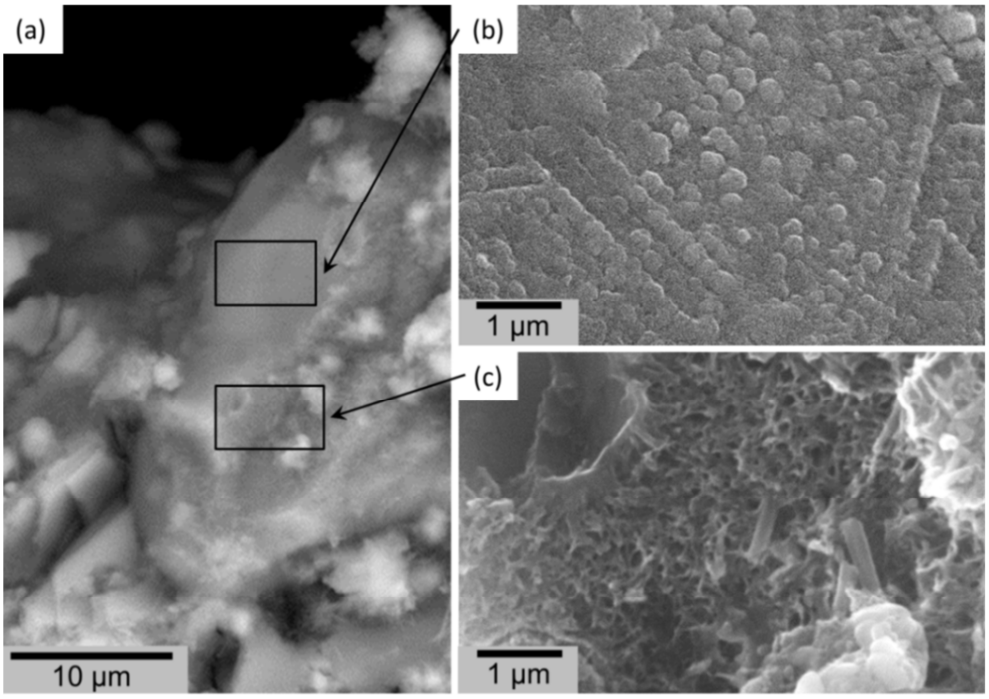

Fig. 4.8 SEM photographs with a relatively low magnification (2000×) (a) and a relatively high magnification (20000×) (b) and (c) show the LP-hydrates interface in the cement paste blended with 30% LP at the curing age of 28 days, with the w/b ratio of 0.4.

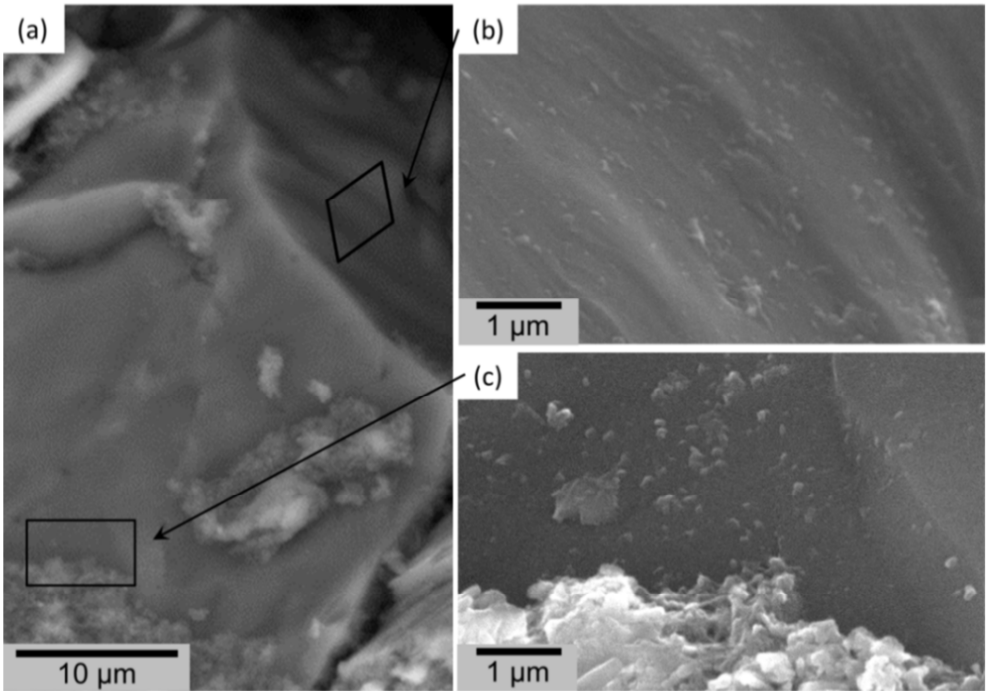

Fig. 4.9 SEM photographs with a relatively low magnification (2000×) (a) and a relatively high magnification (20000×) (b) and (c) show the M6-hydrates interface in the cement paste blended with 30% M6 at the curing age of 28 days, with the w/b ratio of 0.4.

4.5 Simulation results

4.5.1 Effect of mesh size

Simulation results provide insight into the fracture properties of the interface, how the local micromechanical properties govern fracture propagation through the weak locations and how this determines the response of the blended cement paste system. In order to get a more precise estimation of the mechanical properties of the interface, the mesh size should be chosen with care since the adopted mesh size may cause some variations in the simulation results, such as crack pattern and strength of the specimen. In order to estimate the influence of the mesh size, four meshes with the cell size α of 0.25, 0.4, 0.5 and 1.0 µm were generated (see Fig. 4.1). A series of numerical tests was carried out with these meshes. An interface strength of 1.4 MPa is adopted. Damage patterns obtained for different meshes are presented in the Fig. 4.10. It appears that the location of the crack remains the same for all simulations. However, in the case of a coarse mesh (cell size is equal to 1.0 µm), the crack propagation starts to branch. For the fine meshes (cell size is equal to 0.25, 0.4 or 0.5 µm), similar crack patterns are observed.

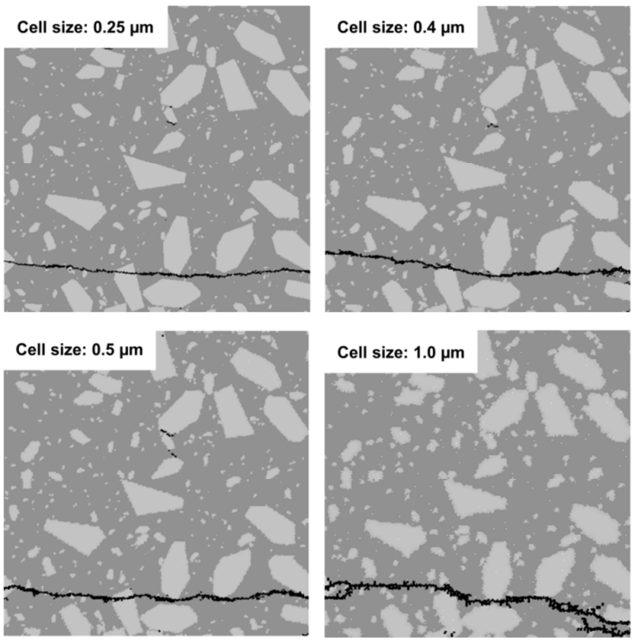

Fig. 4.10 Simulated crack pattern calculated with meshes with different cell size in the cement pastes blended with 30% LP at the curing age of 28 days, with the w/b ratio of 0.4 (the cell size is indicated in the figures).

For the sample with different cell size the tensile stress-strain curves and the peak strengths are shown in Fig. 4.11a and b, respectively. It can be seen in Fig. 4.11a that tensile stress-strain curves start to converge with decreasing cell size. For samples with

cell sizes of 0.4 and 0.25 µm, a similar stress-strain curve is observed. In Fig. 4.11b, it is noted that the peak strength of the sample with cell size of 0.4 µm is also close to that of 0.25 µm. Therefore, to save some computational time, the cell size for the simulations presented in this study is set to 0.4 µm.

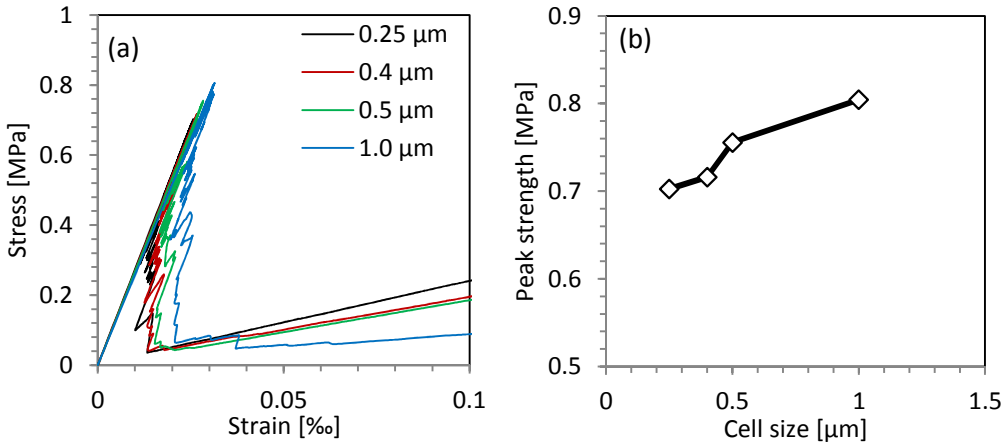

Fig. 4.11 Simulated tensile stress-strain curves (a) and peak strength versus cell size (b) of 4 different meshes in the cement pastes blended with 30% LP at the curing age of 28 days, with the w/b ratio of 0.4.

4.5.2 Effect of mechanical properties of the interface

Simulated cracks in the cement paste blended with a filler with the PSD taken from Fig. 3.1 are shown in Fig. 4.12 and 4.13, respectively. As indicated in in chapter 3, LP shows a continuous particle size distribution from very fine particles to very big particles, while M6 consists mainly of big particles. As indicated in Fig. 4.12 and 4.13, although there is a significant difference in the particle size distribution between LP and M6, the damage patterns do not show a big difference between LP and M6 specimens.

From Fig. 4.12 and 4.13 it can be inferred that when the tensile strength of the interface (2.1, 1.7 and 1.4 MPa) is equal to or higher than that of matrix (1.4 MP), the simulated crack patterns are similar to the crack patterns of cement paste blended with LP from experimental results. From this observation it is concluded that the strength of the interface between LP particles and hydration products is equal to or even higher than that of hydration products. When the tensile strength of the interface (1.1, 0.8, 0.5, 0.4, 0.3, 0.2 and 0.1 MPa) is lower than that of the matrix (1.4 MP), the presence of filler particles has a significant impact on the crack pattern. There is a tendency for cracks to propagate along the filler particle and this tendency becomes more obvious with decreasing tensile strength of the interface. When the tensile strength of the interface is lower than 0.5 MPa, the cracks begin to propagate around the filler particle. Compared with experimental results, cement paste blended with M6 has similar crack patterns as the numerical specimens with an interface strength below 0.5 MPa. From this observation it is concluded that the strength of the interface between M6 particle and hydration products is much lower than that of hydration products.

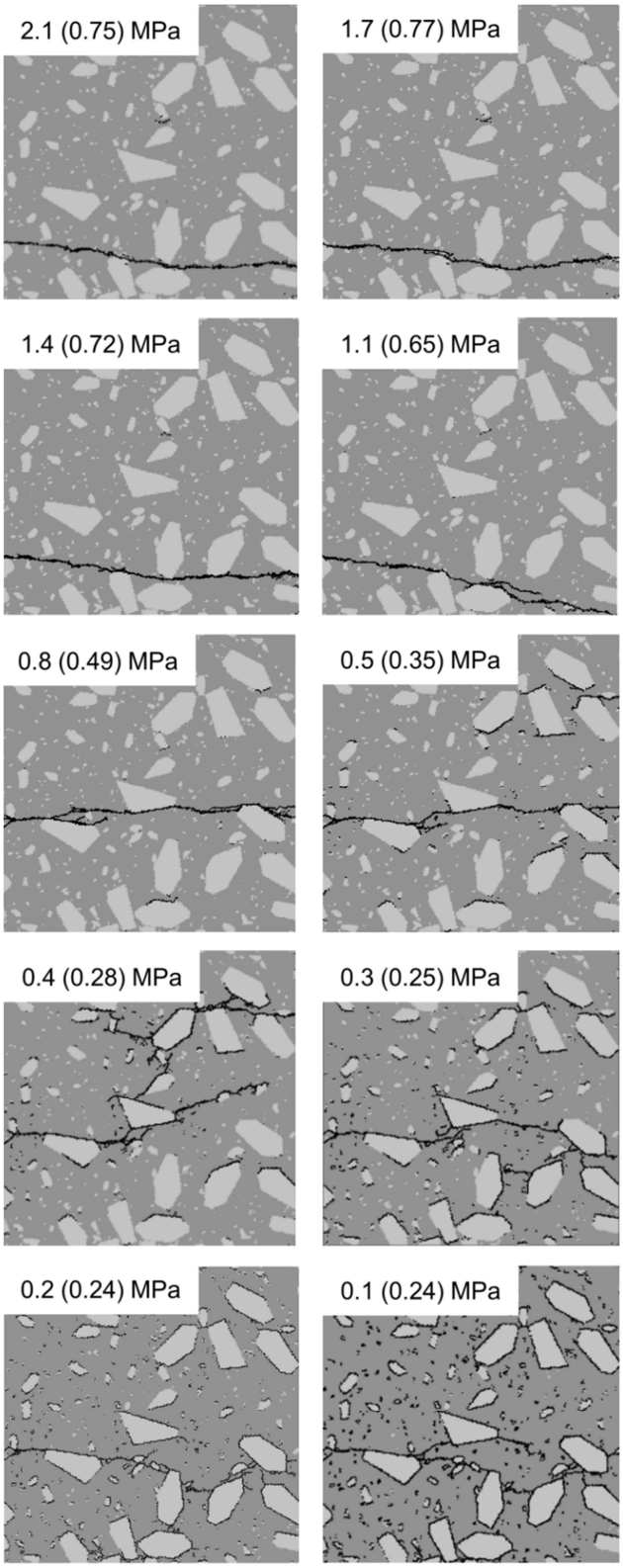

Fig. 4.12 Simulated effect of mechanical properties of the interface on the damage pattern in the cement pastes blended with 30% LP at the curing age of 28 days, with the w/b ratio of 0.4 (the interface strength is indicated in the figures, the value inside parentheses refers to the tensile strength of the specimen).

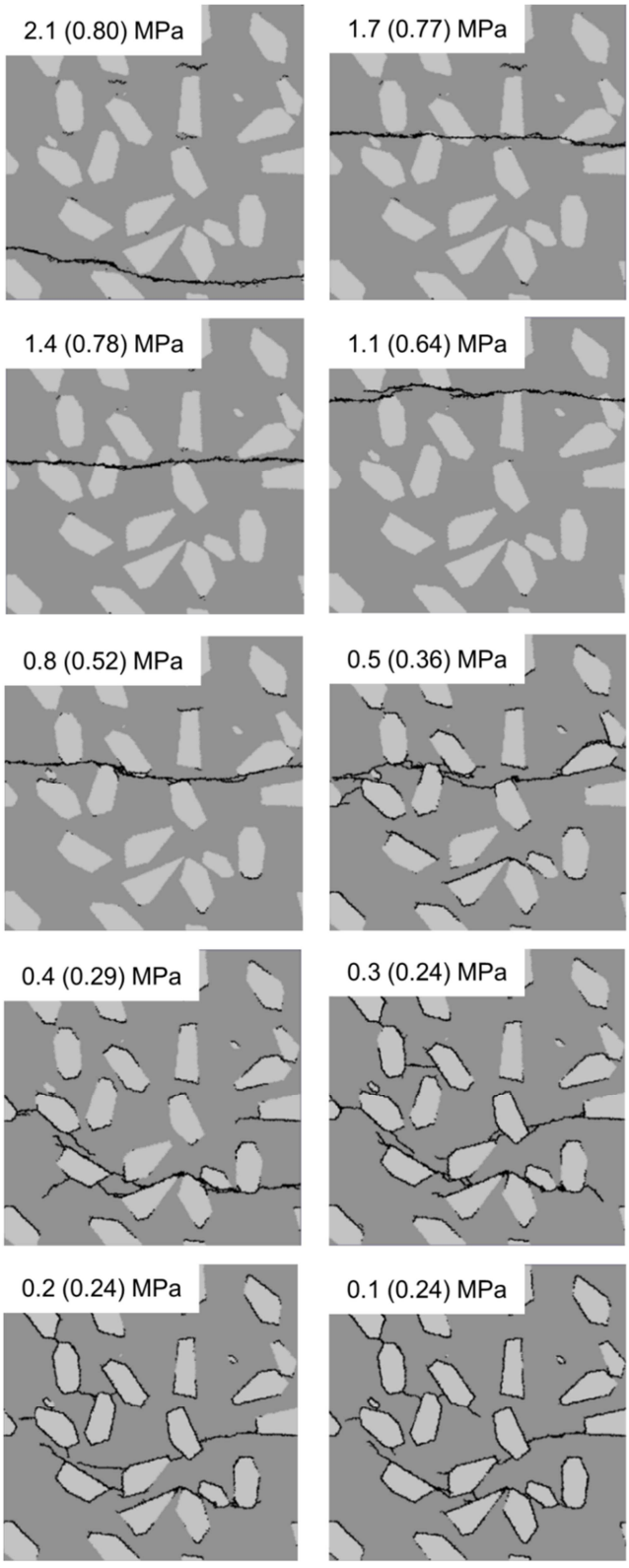

Fig. 4.13 Simulated effect of mechanical properties of the interface on the damage pattern in the cement pastes blended with 30% M6 at the curing age of 28 days, with the w/b ratio of 0.4 (the interface strength is indicated in the figures, the value inside parentheses refers to the tensile strength of the specimen).

The effect of the strength of the interface on the stress-strain diagram of specimens with a filler with the PSD taken from Fig. 3.1 is shown in Fig. 4.14a and b, respectively. Tensile strength and fracture energy can be obtained from the stress-strain diagrams of Fig. 4.15a and b, respectively. Fig. 4.15 shows that the particle size distribution (see Fig. 3.1) of the filler does not have a significant influence on tensile strength and fracture energy.

Fig. 4.15a shows the influence of interface strength on the resulting strength of the specimen. When the tensile strength of the interface is between 0.4 MPa and 1.4 MPa, the strength of specimens has a linear relationship with the strength of the interface. However, when the tensile strength of the interface is lower than 0.4 MPa or higher than 1.4 MPa, the strength of the specimen is constant, regardless the strength of the interface. It means that there is no contribution to the strength of the specimen when the tensile strength of interface under 0.4 MPa. As mentioned before, the strength of the interface between M6 particles and hydration products is lower than 0.5 MPa. Therefore, the interface between M6 particles and hydration products is supposed to have little or even no contribution to the strength of the specimen.

As mentioned previously, when the tensile strength of the interface is over 1.4 MPa, the strength of the specimens remains almost the same regardless the interface strength. Since 1.4 MPa is the strength of the matrix, it seems that the effect of the strength of the interface on the strength of the specimen hits a limit when the strength of the interface is equal to or higher than that of the matrix. As analysed previously, the strength of the interface between LP particles and hydration products is believed to be equal to or higher than that of the matrix. Therefore, the contribution of LP to the strength of the specimen is very significant.

Fig. 4.15b presents the influence of the strength of the interface on the fracture energy in specimens with the filler which has the same PSD as LP and M6. The effect of the particle size distribution of fillers is not distinct. It is known that propagation of more cracks consumes more energy, and less energy is needed to form cracks located at a weaker interface. Since more cracks develop with decreasing interface strength, the total fracture energy does not change much. As mentioned in section 4.4.1, the strength of the interface between M6 particles and hydration products is much lower than that between LP particles and hydration products. This weak interface causes more and wider cracks. These findings are supported by the observation in Fig. 4.5, which shows that the cement paste blended with M6 has more and wider cracks than that with LP.

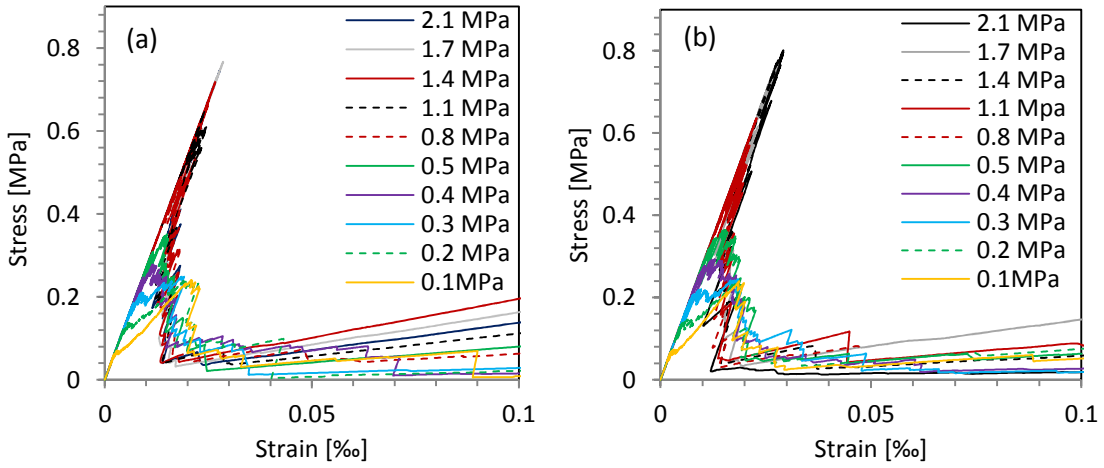

Fig. 4.14 Simulated tensile stress-strain diagram of the specimens with the filler that has the same PSD as LP (a) and that with the filler that has the same PSD as M6 (b) at different interface strength.

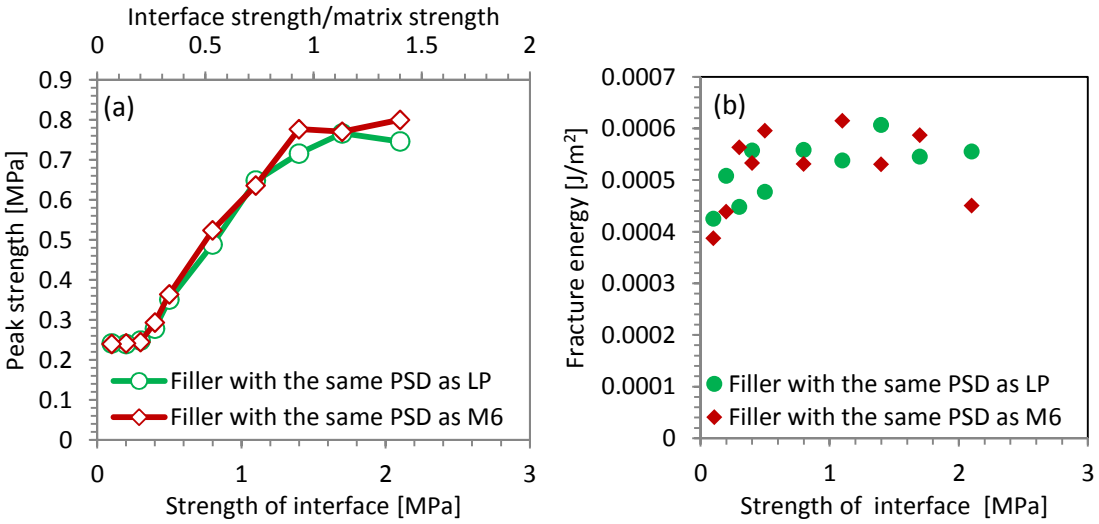

Fig. 4.15 Simulated influences of the strength of the interface on the strength (a) and fracture energy (b) of specimens.

4.6 Discussion

A combined experimental and numerical study was performed on the mechanical properties of the interface between filler particles and hydration products. The crack patterns and the fracture surfaces in the loaded cement pastes blended with different fillers were investigated by SEM observations. It could be confirmed that the interface between LP particles and hydration products is much stronger than that between M6 particles and hydration products. Furthermore, it appears that the interfaces between LP

particles and hydration products are superior in strength compared to the hydration products themselves.

To further investigate the mechanical properties of the interface, the effects of the interface strength on crack propagation, tensile strength and fracture energy were investigated numerically using a lattice model. From a comparison of the experimental results with simulations it could be inferred that the strength of the interface between M6 particles and hydration products is so low that the interface has almost no contribution to the strength of the specimen. This finding is in agreement with previous observations in chapter 3 that the interface between M6 does not contribute to the strength of cement paste. Termkhajornkit et al. [20] also claimed that fine quartz grains have no significant contribution to compressive strength of cementitious materials. On the other hand, from the observations it is believed that the strength of the interface between LP particles and hydration products is equal to or higher than that of the matrix.

It is well known that there is an interfacial transition zone (ITZ) between the aggregate particles and cement paste in concrete because of a ‘wall effect’, which arises due to the packing of cement grains against the larger aggregate particles [21]. In case of cement paste blended with fillers, there is no such a ‘wall effect’ as fillers have similar grains size as Portland cement. The bonds between filler particles and hydration products are the key to understand the differences between the mechanical properties of the interface between LP particles and hydration products and that between M6 particles and hydration products. Among hydration products, C-S-H is the most important component and the main binding phase in the cement paste, and its presence is critical for the development of strength of cement paste [22].

In previous sections, it was found that the bond between limestone particles and hydration products is stronger than the bond between micronized sand particles and hydration products. However, what type of bond prevails and how the chemistry and surface characteristics of fillers affect the bond are still not very clear. From molecular simulation studies and direct-force measurements by atomic-force microscopy (AFM), it has been inferred that short- and medium-range surface forces, which are caused by partially or totally hydrated calcium ions between C-S-H particles, are essential components of cement strength, with additional contributions from van der Waals and capillary forces [23-25]. Since the surface forces are responsible for the strength of hydration products, mainly C-S-H, the surface forces including the van der Waals force, the electrostatic force and the ionic-covalent force (see section 2.3.2) are suggested to contribute to the bond strength between the surface of filler particles and C-S-H. A more detailed study of the bond between the surface of filler particles and C-S-H will be presented in the following chapter.

4.7 Conclusions and outlook

To evaluate the mechanical properties of the interface between filler particles and hydration products, a combined experimental and numerical investigation was carried out. The crack patterns and the fracture surfaces of loaded cement pastes blended with fillers were investigated by SEM. Parallel with the SEM observations, the influence of the interface strength on crack propagation, tensile strength and fracture energy was investigated numerically by using a lattice model. Furthermore, interfacial bonds between the surface of the filler particle and hydration products were discussed. Based on the study, the following conclusions can be drawn:

- Experimental observations demonstrate that in the cement paste with LP the cracks tend to propagate through the matrix and avoid to propagate through the interface between LP particles and hydration products. The fracture surface between LP particles and hydration products is rough. There are hydration product residues left on the surface of LP particles. This indicates that failure occurs to a greater extent in the hydrations products. It is inferred that the bond between LP particle and surrounding hydration products is relatively strong.

- In the cement paste with M6 the cracks have a tendency to propagate through the interface between M6 particles and hydration products. The M6 particles have a smooth fracture surface. Few hydration product residues can be found on the M6 surfaces, which indicate that failure occurs to a greater extent at the interface region. It is inferred that the bond between LP particles and hydration products is much stronger than that between M6 particles and hydration products.

- Numerical simulations suggest that the strength of the interface between M6 particles and hydration products is so low that it has little contribution to the strength of the cement paste. This is in agreement with the experimental results from literature [26, 27]. By contrast, the strength of the interface between LP particles and hydration products is suggested to be equal to or higher than that of the matrix.

- The findings in this chapter bear out that the observations presented in chapter 3 that the limestone has better adhesion properties than micronized sand. These findings can be considered as a validation for contact area concept for strength development which was discussed in chapter 3. Meanwhile, the study also provides insight into adhesion mechanisms between filler particles and hydration products. The further study of the adhesion mechanisms will be presented in chapter 5.

References

1. Pan, Z., et al., *Mechanical properties and microstructure of a graphene oxide–cement composite.* Cement and Concrete Composites, 2015. **58**: p. 140-147.
2. Xu, F., et al., *Mechanical performance evaluation of polyester fiber and SBR latex compound-modified cement concrete road overlay material.* Construction and Building Materials, 2014. **63**: p. 142-149.
3. Lee, W.K.W. and J.S.J. van Deventer, *The interface between natural siliceous aggregates and geopolymers.* Cement and Concrete Research, 2004. **34**(2): p. 195-206.
4. Mindess, S. and S. Diamond, *SEM investigations of fracture surfaces using stereo pairs: II. Fracture surfaces of rock-cement paste composite specimens.* Cement and Concrete Research, 1992. **22**(4): p. 678-688.
5. Mindess, S. and S. Diamond, *The cracking and fracture of mortar.* Matériaux et Construction, 1982. **15**(2): p. 107-113.
6. Qian, Z., *multiscale modeling of fracture processes in cementitious materials*, 2012, Delft University of Technology: Delft.
7. Schlangen, E. and J. Van Mier, *Experimental and numerical analysis of micromechanisms of fracture of cement-based composites.* Cement and Concrete Composites, 1992. **14**(2): p. 105-118.
8. E., S., *Experimental and numerical analysis of fracture processes in concrete*, 1993, Delft University of Technology.
9. Qian, Z., et al., *Prediction of mechanical properties of cement paste at microscale.* Materiales De Construccion, 2010. **60**(297): p. 7-18.
10. Van Vliet, M.R.A., *Size effect in tensile fracture of concrete and rock*2000: TU Delft, Delft University of Technology.
11. Lilliu, G. and J.G.M. van Mier, *3D lattice type fracture model for concrete.* Engineering Fracture Mechanics, 2003. **70**(7–8): p. 927-941.
12. Vervuurt, A.H.J.M., *Interface fracture in concrete*1997: Delft University of Technology.
13. Luković, M., et al., *Micromechanical study of the interface properties in concrete repair systems.* Journal of Advanced Concrete Technology, 2014. **12**: p. 320-339.
14. Standard, A., *C305, Standard practice for mechanical mixing of hydraulic cement pastes and mortars of plastic consistency*, in *Annual book of ASTM standards*2006.
15. Schlangen, E. and E.J. Garboczi, *Fracture simulations of concrete using lattice models: Computational aspects.* Engineering Fracture Mechanics, 1997. **57**(2–3): p. 319-332.
16. Luković, M., *Influence of interface and strain hardening cementitious composite (SHCC) properties on the performance of concrete repairs*, 2016, Delft University of Technology.
17. Luković, M., E. Schlangen, and G. Ye, *Combined experimental and numerical study of fracture behaviour of cement paste at the microlevel.* Cement and Concrete Research, 2015. **73**(0): p. 123-135.
18. van Mier, J.M., *Multi-scale interaction potentials (F − r) for describing fracture of brittle disordered materials like cement and concrete.* International Journal of Fracture, 2007. **143**(1): p. 41-78.
19. Wang, Y., *Performance Assessment of cement-based materials blended with micronized sand: microstructure, durability and sustainability*, 2013, Delft University of Technology: Delft.
20. Termkhajornkit, P., R. Barbarulo, and G. Chanvillard, *Microstructurally-designed cement pastes: A mimic strategy to determine the relationships between microstructure and properties at any hydration degree.* Cement and Concrete Research, 2015. **71**: p. 66-77.
21. Scrivener, K.L., A.K. Crumbie, and P. Laugesen, *The Interfacial Transition Zone (ITZ) Between Cement Paste and Aggregate in Concrete.* Interface Science, 2004. **12**(4): p. 411-421.
22. Chiang, W.-S., et al., *Microstructure determination of calcium-silicate-hydrate globules by small-angle neutron scattering.* The Journal of Physical Chemistry C, 2012. **116**(8): p. 5055-5061.
23. Pellenq, R.J.M. and H. Van Damme, *Why does concrete set?: The nature of cohesion forces in hardened cement-based materials.* Mrs Bulletin, 2004. **29**(5): p. 319-323.
24. Plassard, C., et al., *Nanoscale experimental investigation of particle interactions at the origin of the cohesion of cement.* Langmuir, 2005. **21**(16): p. 7263-7270.

25. Lesko, S., et al., *Investigation by atomic force microscopy of forces at the origin of cement cohesion.* Ultramicroscopy, 2001. **86**(1-2): p. 11-21.
26. French, C.W. and A. Mokhtarzadeh, *High strength concrete: Effects of materials, curing and test procedures on short-term compressive strength.* PCI Journal, 1993. **38**(3): p. 76-87.
27. Bentz, D.P., et al., *Multi-scale investigation of the performance of limestone in concrete.* Construction and Building Materials, 2015. **75**: p. 1-10.

5

Filler-hydrates Adhesion Mechanisms*

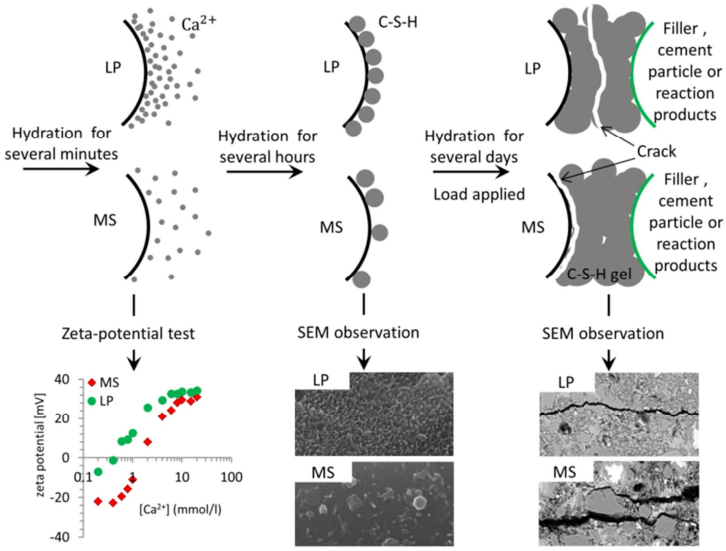

In the previous chapter, it was concluded that the interface between LP particles and hydration products is much stronger than that between MS particles and hydration products, and even stronger than the hydration products themselves. This is due to the different adhesion mechanisms between filler particles and hydration products. In this chapter, the affinity of filler surfaces to ions in the pore solution of cement paste is reported from the viewpoint of the governing mechanisms. The various interactions between the filler surfaces and ions are illustrated by results from zeta-potential measurements, and further illustrated by microscopic observations of the morphology and distribution of hydrates on the filler surfaces. The C-S-H/filler adhesion appears to depend on the interactions between a filler surface and calcium ions. In the case of calcite, the interactions between a filler surface and calcium ions are predominantly determined by acid-base interactions, which lead to the formation of a strong bond (most likely ionic-covalent bond). In the case of silica, the adhesion is found to be governed by an attractive ion-ion correlation force.

.

* This chapter based on:

1. Xiaowei Ouyang, D. A. Koleva, Guang Ye, and K. van Breugel. Understanding the Adhesion Mechanisms between C-S-H and Fillers. *Cement and Concrete Research* 100 (2017): 275-283.

2. Xiaowei. Ouyang, D. A. Koleva, Guang Ye, and K. van Breugel. Insights into the Mechanisms of Nucleation and Growth of C-S-H on Fillers. *Materials and Structures*, 50 (2017) 213.

5.1 Introduction

In the previous chapter the interface between LP particles and hydration products was found to be much stronger than the interface between MS particles and hydration products, and even stronger than the hydration products themselves. Mehta and Monteiro [1], French and Mokhtarzadeh [2] and Bentz et al. [3] also found that limestone exhibited superior bond interactions characteristics with hydrates, if compared to those of silica. This result was discussed to be due to the favourable physical and chemical properties of the limestone surfaces. However, the effect of the filler chemical properties on interfacial bond was not fundamentally approached or substantiated. Justification of the exact nature of the effect of fillers in a cement-based matrix, and improvement of these (positive) effects are still challenges. This is especially the case when mechanical properties of the interfaces between filler particles and hydration products are of concern or interest.

Understanding the cohesion between C-S-H particles is an initial step to study the adhesion mechanisms between C-S-H particles and filler particles. The cohesion forces in hardened cement-based materials were investigated previously by many researchers [4-9]. The results indicate that the inter-layer calcium ions are linked to the tobermoritic C-S-H lamellae by a strong ionic-covalent bond. C-S-H lamellae are compactly stacked due to this ionic-covalent bond, forming a C-S-H particle with typical dimensions of 60 × 30 × 5nm^3. The cohesion between these C-S-H nanoparticles is a consequence of ion-ion interactions. As mentioned in section 2.3.3.4, these ion-ion interactions are caused by the very high negative charge density of the C-S-H particles and the presence of divalent counterions, e.g. Ca^{2+}.

This chapter reports on the effects of surface properties and related ionic charge interactions of filler particles on adhesion between C-S-H particles and filler particles. Two types of filler are considered: micronized sand and limestone powder. The nature of the various interactions (mainly, the interaction between calcium ions and filler surface) is studied via zeta potential measurements in model solutions, simulating the pore solution of cement paste. Microscopic observations of the nucleation and growth of C-S-H on the surface of these filler particles are performed by scanning electron microscopy (SEM) in order to further elucidate these interactions. The influence of the chemical properties of the fillers on the strength of the bond between C-S-H and filler particles is discussed based on these zeta potential measurements and microscopic observations. This discussion provides a deeper insight into the adhesion mechanisms between C-S-H and filler particles.

5.2 Materials and experimental methods

5.2.1 Materials and mixture

Portland cement (OPC) was used for the study in this Chapter. The fillers used were limestone powder (LP) and micronized sand (MS). The chemical composition and

physical characteristics of these materials were reported in Table 3.1. The mineral composition of OPC was presented in Table 3.2. In order to get more accurate zeta potential measurements, the fillers used for the zeta potential test were ground. After grinding, the LP particles have an average size of 9 µm, while the MS particles have a size of 13 µm. To maintain nucleation and growth of C-S-H on the surface of both filler particles in constant solution and identical conditions, only one specimen was prepared for microscopic observations of the morphology of hydration products on filler surfaces by mixing OPC, LP, MS and water. This mixture was denoted as OLM (OPC+LP+MS). The percentage of different filler and the water-to-binder (w/b) ratio are given in Table 5.1. This mixture was prepared in a Hobart mixer according to the standard procedures described in ASTM C305 [10].

Table 5.1 Mixture compositions of blended cement paste.

Mixture	OPC*(%)	Limestone powder *(%)	Micronized sand *(%)	w/b
OLM	60	20	20	0.4

* Percentage of the total mass of binder by weight.

5.2.2 Cement paste filtrate analysis

A VARIAN Vista 720 ICP-OES was used to analyse the elemental concentrations in OLM paste filtrates. The filtrates of the fresh OLM paste were collected at each required time by vacuum filtration using 0.22 µm filter paper. The OLM paste filtrates were then stored in sealed 20 ml plastic vials until used.

5.2.3 Zeta potential test

5.2.3.1 Technical background and considerations

The zeta potential is a measure of the charge of particles suspended in a solution. As shown in Fig. 5.1, a charged particle surface attracts a layer (Stern layer [11]) of counter-ions (ions of opposite charge). In this layer, the strongly adsorbed counter-ions do not fully offset the surface charge. A second layer (diffuse layer) of more loosely attracted counter-ions forms subsequently. At a certain distance from the particle surface, the surface charge will be fully balanced by counter-ions. Within the diffuse layer, there is a notional boundary (the shear plane in Fig. 5.1) where ions and particles form a stable entity. The ions beyond the boundary remain in the bulk dispersant. When the net electrical charge contained within the boundary is positive or negative, particles will migrate towards the oppositely-charged electrode. The higher the net electrical charge, the faster the particles will migrate. The potential at the location of this shear plane is the zeta potential, which is related to the surface charge of the particle.

Two important concepts are related to the concept and manner of executing zeta potential measurements. One is the point of zero charge (PZC). It corresponds to

conditions in which the surface charge of the solid is equal to zero. The PZC does not necessarily correspond to a zeta potential ζ=0. Another one is the iso-electric point (IEP). It corresponds to a zeta potential ζ=0, and hence to a zero electrophoretic mobility, but not necessarily to a zero surface charge [12, 13].

The surface charge of particles in a solution is also influenced by the adsorption of ions from the solution onto their surfaces. Furthermore, processes such as dissolution of mineral phases, precipitation (heterogeneous nucleation and crystal growth) and ion exchange are influenced by adsorption [14]. There are mainly two mechanisms of adsorption. One is the chemical adsorption of solutes onto the surfaces, by formation of coordinative bonds[†]. The other one concerns electrical adsorption of solutes onto the surfaces, such as electrostatics interactions and polarization interactions [16]. With regard to the work in this chapter, the following needs to be considered: C-S-H is formed by dissolution-precipitation process during the hydration of cement. The presence of fillers affects the process of the heterogeneous nucleation and crystal growth of C-S-H. Additionally, the molecular (atomic) interface structures are also affected by the adsorption of ions on the surface of filler particles. Adsorption of ions, in turn, affects the surface charge of these fillers. In other words, the adsorptions mechanisms are linked to alterations of surface charge and consequently related to nucleation and growth of hydration products and the properties of the interface between C-S-H and filler particles.

5.2.3.2 Zeta potential measurements

The surface charge, or zeta-potential, is determined based on the particle velocity, induced by a potential difference applied across a capillary cell containing the sample (and particles respectively), as schematically illustrated in Fig. 5.1. Appling a controlled electric field by means of electrodes immersed in the sample suspension, the charged particles will move towards the electrode of opposite charge. From the known applied electric field and measured particle velocity, the particle mobility is determined. Based on the particle mobility, the zeta-potential, which is related to the surface charge of the particle, can be calculated by using the Smoluchowski model [17].

The zeta potential of fillers in the model solutions (see section 5.2.3.3) was measured by Malvern Zetasizer Nano (Z-ZS-ZSP) (Malvern instruments Ltd., UK). The suspension in the capillary cell (Fig. 5.1) was prepared by dispersing about 0.1 g filler in 100 mL of the model solution. Five runs were conducted for each sample, with the average value being taken as the final result. This technique is appropriate, but also has limitations which restrict the range of ions concentrations in the electrolyte. If these concentrations are too high, the electrical conductivity of the electrolyte increases and erroneous results can be obtained. In this work, the upper electrolyte concentration limit was maintained at roughly 50 mmol/L for the solutions.

[†] Coordinative bond is a type of bond in which the shared pair of electrons are supplied by one of the reacting molecules. The molecule which donates the electron is called the donor and the one that accepts it is called the acceptor [15].

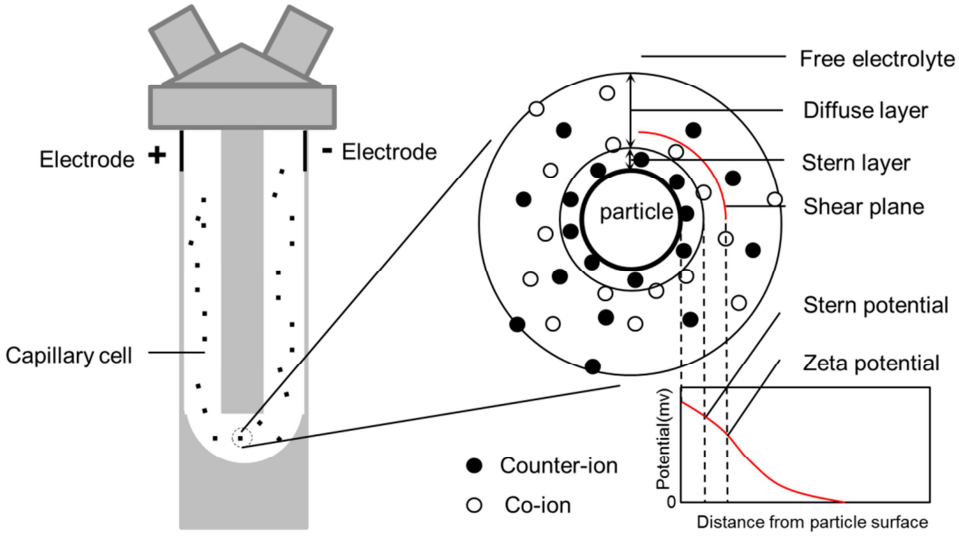

Fig. 5.1 Schematic illustration of the electrical double layer and principle of a zeta potential test.

5.2.3.3 Preparation of suspensions

The zeta potential tests for the various particles in this study were performed in five series of model solutions. The detailed chemical composition of the five model solutions is shown in Table 5.2. The zeta potential of MS and LP particles was initially measured in aqueous NaOH solutions with different concentrations, where the pH of the NaOH solutions was 8, 9, 10, 11 and 12, respectively. In order to evaluate the effect of different concentrations of Ca^{2+}, Na^{+}, K^{+} and SO_4^{2-} ions on the surface charge of the filler particles, the zeta potential measurements were also performed separately for the MS and LP particles suspended in solutions with different concentrations of $Ca(OH)_2$, and in mixture solutions of $Ca(OH)_2$ + NaOH, $Ca(OH)_2$ + KOH and $Ca(OH)_2$ + K_2SO_4 (Table 5.2).

Table 5.2 Preparation of model solutions (concentrations are shown in mmol/l units).

Solution 1		Solution 2		Solution 3		Solution 4		Solution 5	
NaOH	pH	$Ca(OH)_2$	pH	$Ca(OH)_2$	NaOH	$Ca(OH)_2$	KOH	$Ca(OH)_2$	K_2SO_4
-	8	0.2	9.2	0.1	10	0.1	10	0.1	10
-	9	0.4	9.3	0.4	10	0.4	10	0.4	10
-	10	0.6	9.6	1	10	1	10	1	10
-	11	0.8	10.1	4	10	4	10	4	10
-	12	1	10.5	8	10	8	10	8	10
-	-	2	10.8	0.1	50	0.1	50	10	10
-	-	4	10.9	0.4	50	0.4	50	15	10
-	-	6	11.0	1	50	1	50	19.6	10
-	-	8	11.9	4	50	4	50	0.1	50
-	-	10	12.0	8	50	8	50	0.4	50
-	-	15	12.2	-	-	-	-	1	50
-	-	20	12.3	-	-	-	-	4	50
-	-	-	-	-	-	-	-	8	50
-	-	-	-	-	-	-	-	10	50
-	-	-	-	-	-	-	-	15	50
-	-	-	-	-	-	-	-	18	50

5.2.4 SEM analysis

ESEM Philips XL 30 was used for morphological investigation of the hydration products on the surface of filler and cement particles. The sample preparation for SEM analysis was performed according the procedures reported by Berodier and Scrivener [18], as follows: at each required time interval, about 1 g of the OLM paste was taken to stop hydration by solvent exchange with isopropanol; after stopping cement hydration and removing the isopropanol, the paste collapsed to a dried powder; the dried powder was then collected and stored under vacuum in a desiccator until used. SEM observations were performed on the dried powder coated by carbon. SE mode was used.

5.3 Results

5.3.1 Chemical composition of cement paste filtrate

Table 5.3 lists the chemical composition of the filtrates of the OLM paste. It shows that upon contact with water ions go into solution quickly. Within 10 minutes, the concentration of Na^+, K^+, SO_4^{2-} and Ca^{2+} ions increases significantly. The silicate concentration is very low and the aluminate concentration is even lower. This is in accordance with reported pore solution composition [19]. Since the liquid phase of cement paste at early stage mainly consists of Na^+, K^+, SO_4^{2-} and Ca^{2+} ions, lime, alkali hydroxides, or alkali sulfate solutions were used as the liquid phase to measure the zeta potential of MS and LP particles.

Table 5.3 Elemental concentrations for cement paste filtrates

Time	Na (mM)	K (mM)	S (mM)	Si (µM)	Al (µM)	Ca (mM)
10 min	79.0	180.8	81.3	46.4	< 37.0	11.8
30 min	79.1	175.5	70.9	39.3	< 37.0	15.7
1 h	80.1	180.6	65.7	39.3	< 37.0	16.6
3 h	94.2	200.7	77.5	142.9	< 37.0	16.1

5.3.2 Zeta potential

5.3.2.1 Effect of pH

The evolution of the zeta potential of MS and LP particles as a function of pH was determined in a series of model solutions (Table 5.2). The results for NaOH solution (solution 1, as shown in Table 5.2) are presented in Fig. 5.2. The measurements in NaOH solution were performed in the pH range from 8 to 12, in order to obtain an overall information on the zeta potential values of MS and LP particles from close to neutral (pH 7) to an alkaline medium. In an acidic medium, LP particles could dissolve and generate CO_2. Therefore, no measurements were performed in a solution with the pH lower than 8.

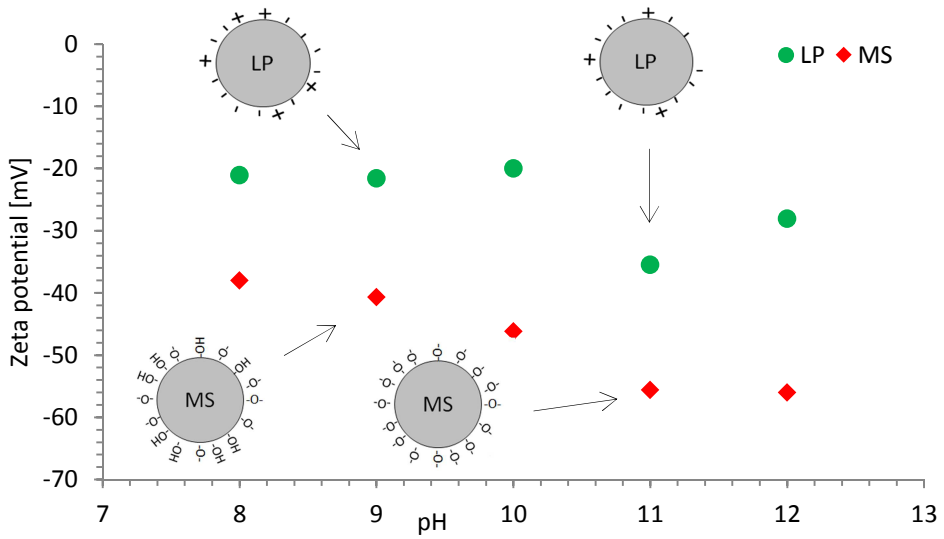

Fig. 5.2 Evolution of the zeta potential of MS and LP particles as a function of pH in NaOH solution (higher pH → more negative for zeta potential).

As can be seen in Fig. 5.2, in the pH range of 8 to 11 the zeta potential of both MS and LP particles ranges from -20 to -56 mV. The zeta potential values for LP are stable and around -20 mV. The zeta potential for the MS particles reaches -60 mV at pH 11. The potential for LP particles remains less negative than that for the MS particles in the

full pH range of this test. The values recorded at pH 12 are slightly different from those at pH 11: less negative for LP and similar to pH 11 for MS. Since these values could have been affected by interferences within the measurement itself (mainly due to a normally observed abrupt increase of the ionic strength/conductivity of the solution in ranges of pH below 2 and higher than 11.5), the results at pH 12 are considered as indicative, rather than as absolute values.

With regard to MS particles, the main cause of surface charge generation at the silicate-solution interface is due to dissociation of the silanol groups at this interface. The dissociation is related to gain or loss of a proton, which depends on the pH value of the aqueous phase [20, 21]. The silanol groups in pure water dissociate through the following reactions [14, 22]:

$$\equiv SiOH + H^+ \rightleftharpoons \equiv SiOH_2^+ \quad (6.1)$$

$$\equiv SiOH + OH^- \rightleftharpoons \equiv SiO^- + H_2O \quad (6.2)$$

The H^+ and OH^- ions are the potential determining ions for silica. With an increase of pH, more silanol groups are ionized and the surface charge of silica hence becomes more negative (Fig. 5.2).

Different from the generation of surface charge on silica, which corresponds to ionization of surface silanol groups, the surface charge of calcite is associated with surface defects. There are three main groups of surface defects [12]: (1) Structural defects of the crystal lattice; (2) Defects due to ion exchange, involving ions in the crystal lattice and ions in solution; (3) Defects caused by surface chemical reactions with constitutive ions or adsorption on the surface. The principal mechanism of charge development at the calcite-water interface is assumed to be a preferential hydrolysis of surface calcium and carbonate ions, followed by the adsorption of the resulting complexes at the surface [23]. Additionally, previous studies [12, 24, 25] showed that the zeta potential determining ions for calcite are Ca^{2+} and CO_3^{2-}, i.e. the crystal-constituting species, whereas the pH seems to be a second-order controlling parameter through its influence on the CO_3^{2-}/HCO_3^- and $Ca^{2+}/CaOH^+$ speciation, both in the solution, as well as at the calcite/water interface. Therefore, H^+ and OH^- are generally not considered as zeta potential determining ions for calcite [26].

As can be seen in Fig. 5.2, the zeta potential of calcite (LP particles) did not significantly vary in the range from pH = 8 to pH = 10, while a gradually increasing negative charge for the MS particles in identical solutions was observed. Other authors have reported a similar result for LP [27]. The variation of zeta potential as a function of pH for the LP particles is probably caused by the equilibrium of the dissolution of calcium and carbonate ions, and the adsorption of the complexes formed at the calcite/water interface.

5.3.2.2 Effect of Ca^{2+} concentration

The zeta potential of LP and MS particles in solutions of $Ca(OH)_2$ (solution 2, as shown in Table 5.2) was measured as a function of Ca^{2+} concentration and compared to the zeta potential of OPC particles measured by Nachbaur et al. [28] and C-S-H particles

measured by Helene et al. [29] and Nachbaur et al. [28], respectively. The results of the measured zeta potential are depicted in Fig. 5.3. The figure shows that for OPC, MS and C-S-H particles a similar iso-electric point (IEP) was recorded, which was reached at a Ca^{2+} concentration of about 2 mmol/L. This because OPC, MS and C-S-H particles are very rich in silicate, as reported by Nachbaur et al. [28]. At very low Ca^{2+} concentrations, the silica layers are partially ionized as SiO^- groups, leading to an overall negative zeta potential if no counter ions are specifically adsorbed. As outlined in section 5.2.3.1, adsorption plays an important role in the surface charge. At higher Ca^{2+} concentrations (but still lower than 2 mmol/L) adsorption of Ca^{2+} ions on the surfaces of OPC, MS and C-S-H particles partially compensates for this negative charge, resulting in lower absolute values of the zeta potential. When the Ca^{2+} concentrations are higher than 2 mmol/L, the adsorption of the Ca^{2+} gradually compensates the negative charge on the surface, leading to a 'reversal' of the zeta potential (to positive values). Hence, the zeta potential of the MS particles, was positive for Ca^{2+} concentration higher than 2 mmol/L.

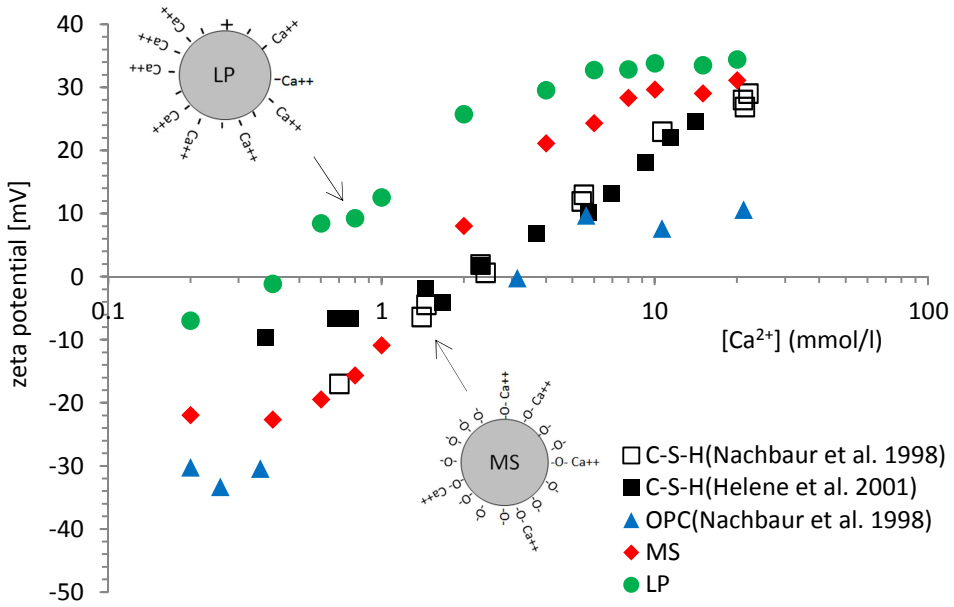

Fig. 5.3 Evolution of the zeta potential of OPC, MS, C-S-H and LP particles as a function of Ca^{2+} concentration in $Ca(OH)_2$ Solution (pH of 9.2 to 12.3).

For LP particles the evolution of zeta potential versus Ca^{2+} concentration shows a different trend compared to OPC, MS and C-S-H particles. A much lower Ca^{2+} concentration of ca. 0.4 mmol/L was needed for the LP particles to reach the iso-electric point (IEP). Compared to the zeta potential of LP particles in NaOH solution at pH of 9, 10, 11 and 12 (Fig. 5.2), the zeta potential in $Ca(OH)_2$ has a higher positive value for the same pH. According to the reported mechanisms of charge development at the calcite/solution interface [12, 23-25], in NaOH solution of pH > 8, the zeta potential of the LP particles was dominated by hydrolysis of calcium ions on the particles surface, leading to an overall negative zeta potential (Fig. 5.2). In other words, at a pH of about

9 and very low Ca^{2+} concentrations (< 0.4 mmol/L for the $Ca(OH)_2$ solution and 0 mmol/L for the NaOH solution), the hydrolysis of surface calcium ions dominated the zeta potential. Upon increase of the Ca^{2+} concentration, the zeta potential shifted to more positive values as a result of Ca^{2+} adsorption on the particles surface (Fig. 5.3). At higher Ca^{2+} concentrations (> 0.4 mmol/L), adsorption of external Ca^{2+} ions, rather than hydrolysis of surface Ca^{2+} ions dominated the surface charge, leading to a 'reversal' (from negative to positive values after IEP) of the zeta potential. As the Ca^{2+} concentration increased from 0.4 to about 6 mmol/L, the amount of Ca^{2+} ions adsorbed onto the LP surface would gradually increase, which was reflected by an increase in the zeta potential (Fig. 5.3). The plateau region at concentrations higher than 6.0 mmol/l, as shown in Fig. 5.3, indicates stabilization of the zeta potential and independence of further increase of the calcium ions concentration. This reflects a stage at which a saturation condition was reached for the LP surface.

At a given Ca^{2+} concentration, the zeta potential for LP particles appeared to be more positive compared to the recorded values for OPC, MS and C-S-H particles. These results indicate that the surface of LP particles has more affinity for Ca^{2+} compared with the surface of OPC, MS and C-S-H particles. This point will be discussed in more detail in section 5.4.1.

5.3.2.3 Effect of Na^+ and K^+ concentration

The evolution of the zeta potential of MS, C-S-H and LP particles in NaOH and KOH solutions (solution 3 and 4, as shown in Table 5.2) as a function of calcium content is presented in Fig. 5.4 and 5.5, respectively.

In 10 mmol/L NaOH and KOH solutions, the development of zeta potential for the MS, C-S-H and LP particles as a function of Ca^{2+} concentration (Fig. 5.4 and 5.5) are similar to those, measured in the Na^+ and K^+ - free $Ca(OH)_2$ solutions (Fig. 5.3). For the MS and C-S-H particles a similar IEP was recorded, which was reached at a Ca^{2+} concentration of about 2 mmol/L in both NaOH and KOH solutions (Fig. 5.4 and 5.5). The IEP for the LP particles was again found at a Ca^{2+} concentration of ca. 0.4 mmol/L in both NaOH and KOH solutions (Fig. 5.4 and 5.5).

In 50 mmol/L NaOH and KOH solutions, the IEP for MS, C-S-H and LP particles shifted slightly towards higher Ca^{2+} concentrations compared to the IEPs recorded in 10 mmol/L NaOH and KOH solutions. This result confirms previously reported observations from similar experiments, together with the fact that sodium and potassium are considered as 'indifferent' ions[‡] [28]. The zeta potential of LP and MS particles varies almost linearly with the log of Ca^{2+} concentration near the IEP, and shifted to higher Ca^{2+} concentration for the MS particles. This indicates that as the Ca^{2+} concentration increased, the amount of Ca^{2+} ions, adsorbed on the MS and LP surface, increased gradually, accompanied by an increase in the zeta potential. Furthermore, these changes suggest that the surface of LP particles have a larger affinity for Ca^{2+} compared to the surface of MS particles, as also mentioned in section 5.3.2.2. This point will be discussed in more detail in section 5.4.1.

[‡]The 'indifferent' ions are the ions which have no or very little effect on the zeta potential of tested particle.

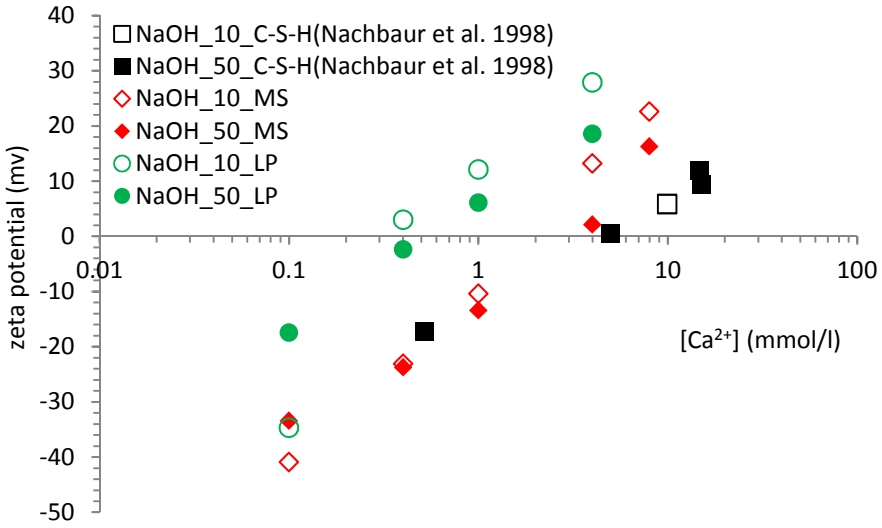

Fig. 5.4 Evolution of the zeta potential of MS, C-S-H and LP particles as a function of Ca^{2+} concentration in 10 mmol/L and 50 mmol/L NaOH solutions.

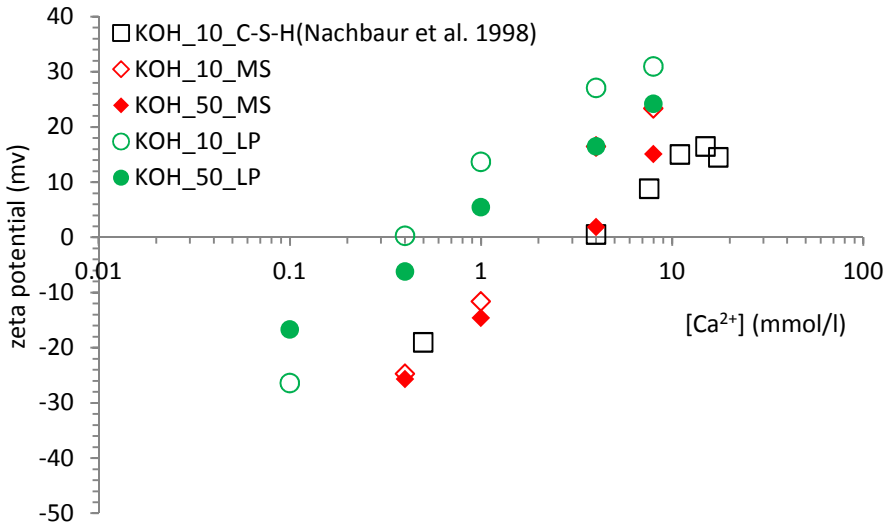

Fig. 5.5 Evolution of the zeta potential of MS, C-S-H and LP particles as a function of Ca^{2+} concentration in 10 mmol/L and 50 mmol/L KOH solutions.

5.3.2.4 *Effect of SO_4^{2-} concentration*

The evolution of the zeta potential of MS, C-S-H and LP particles as a function of Ca^{2+} concentration in potassium sulfate solutions (solution 5, Table 5.2) is illustrated in Fig. 5.6. The figure shows that there is almost no difference between the behaviour of MS and C-S-H particles. This is because the MS and C-S-H particles are very rich in silicate, as previously mentioned. The zeta potential of MS and C-S-H particles varied linearly with the log of Ca^{2+} concentration and shifted to higher Ca^{2+} concentration with increasing sulfate concentration. With an increase of the sulfate concentration of the solution, the IEP for MS and C-S-H particles also shifted to higher Ca^{2+} concentration. It is interesting to note that when the sulfate concentration is 10 mmol/L, the IEP for MS and C-S-H is also at a Ca^{2+} concentration of about 10 mmol/L. This means that SO_4^{2-} and Ca^{2+} are equally adsorbed on MS and C-S-H surfaces. The observed linear relation of zeta potential/log Ca^{2+} concentration and the simultaneously occurring shift to higher Ca^{2+} concentration as the sulfate concentration increased, confirm that the adsorption of SO_4^{2-} and Ca^{2+} onto MS and C-S-H surfaces are similar.

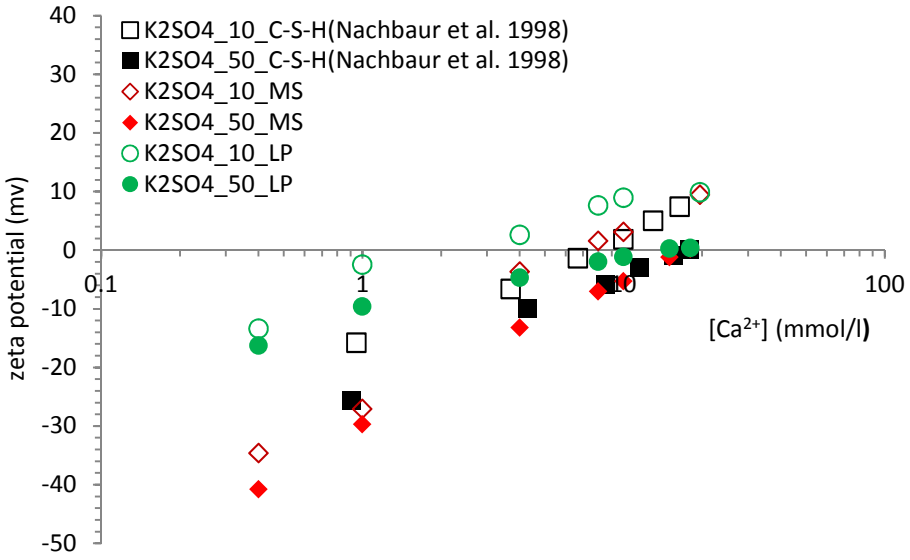

Fig. 5.6 Evolution of the zeta potential of MS, C-S-H and LP particles as a function of Ca^{2+} concentration in 10 mmol/L and 50 mmol/L K_2SO_4 solutions.

By contrast, in the case of LP particles, the zeta potential varied non-linearly with the log of Ca^{2+} concentration. As shown in Fig. 5.6, the zeta-potential values for LP slightly changed with an increase of Ca^{2+} concentration and stabilises around zero in the 50 mmol/L K_2SO_4 solution with high Ca^{2+} concentration (>10 mmol/L). This is due to the Langmuir type of adsorption of ions on the calcite surface, as previously discussed and reported by Huang et al. [24]. The basic idea of the Langmuir type of adsorption is the coverage of the surface by a monomolecularic layer. The adsorption only occurs on distinct sites capable of binding the adsorbate.

Furthermore, different from the MS and C-S-H particles, for which the IEP was reached at equal SO_4^{2-} and Ca^{2+} concentration, when the sulfate concentration is 10 mmol/L, the IEP for LP particles is at a Ca^{2+} concentration of about 2 mmol/L. This is attributed to the fact that calcite surfaces have a higher affinity for Ca^{2+} ions than for SO_4^{2-} ions. This has also been reported by Pourchet et al. [31], who conducted a study of adsorption of SO_4^{2-} and Ca^{2+} ions on calcite. The results of their study showed that when both SO_4^{2-} and Ca^{2+} ions adsorption on calcite reached a saturation point, the amount of adsorbed Ca^{2+} ions much higher than the total adsorbed SO_4^{2-} ions.

Since the adsorption of Ca^{2+} and SO_4^{2-} ions onto MS and C-S-H surfaces is similar, while LP surfaces have a higher affinity for Ca^{2+} ions than SO_4^{2-} ions, it is concluded that calcite surfaces have a much higher affinity for Ca^{2+} ions than MS and C-S-H surfaces. This point will be discussed in more detail in section 5.4.1.

5.3.3 Morphology of hydration products on surface of cement and filler particles

In order to further elucidate the interactions between the filler surfaces and ions, microscopic observations of the nucleation and growth of hydration products (mainly, C-S-H) on the surface of Portland cement (OPC), micronized sand (MS) and limestone (LP) particles were performed by scanning electron microscopy (SEM). Fig. 5.7 shows the presence of hydrates on the surface of these particles.

From the topography of the studied surfaces in the OLM paste, on both MS and OPC surfaces hydrates formed in a similar way. There is no evidence for a different state or behaviour of the cement and MS surfaces with respect to C-S-H nucleation. Fig. 5.7a and b show the surface of MS and OPC after 1 h 30 min of hydration. Small particles can be seen on both surfaces. The particles seem to be tiny blobs, or clusters of, most likely, C-S-H nuclei. The presence of randomly distributed nuclei on micronized sand and Portland cement surfaces confirms that these surfaces act as a substrate for the heterogeneous nucleation of the hydrates. After 4 h, some of the C-S-H nuclei started to grow, presenting a needle shape morphology and several calcium hydroxide particles (hexagonal plates) can be identified, as shown in Fig. 5. 7d and e. After hydration for 7 h and 30 min (Fig. 5.7g and h) the C-S-H crystals were well defined as needles which varied in growth orientation. As can be observed clearly, the nucleation and growth of C-S-H on micronized sand grains were very similar to that on Portland cement grains.

The micrographs in Fig. 5.7c, f and i clearly show that limestone had a different effect on the nucleation and growth of C-S-H compared to micronized sand and Portland cement. After 1.5 h hydration, the limestone surface was covered with a large amount and uniform layer of C-S-H nuclei (Fig. 5.7c). In contrast, at equal hydration period of 1.5 h, the surfaces of micronized sand and Portland cement presented only a few dispersed nuclei (Fig.7a and b). This microstructural observation indicates that C-S-H nucleates preferentially on the limestone surface. Fig. 5.7f shows a limestone grain after 4 h of hydration. C-S-H needles were grown densely perpendicular to the surface, while the C-S-H crystals on the Portland cement and micronized sand grains were irregular (Fig. 5.7d and e). After hydration for 7 h 30 min (Fig. 5.7i) the C-S-H needles were already larger. The size and length of the C-S-H particles on the surface of

Portland cement, micronized sand and limestone grains seemed similar with prolonged hydration. However, the layer of hydration products on the LP surface (Fig. 5.7i) appeared to be higher amount and more uniformly distributed of the crystallites, compared to these in the case of MS and OPC (Fig. 5.7g and h). Similar observations were reported by Berodier and Scrivener [18].

This difference of the nucleation and growth of C-S-H phase on silica and calcite surface seems consistent with the difference of the surface charge properties between silica and calcite. The relationship between the surface charge properties and the nucleation and growth of C-S-H phase on fillers will be discussed more in detail in the section 5.4.2.

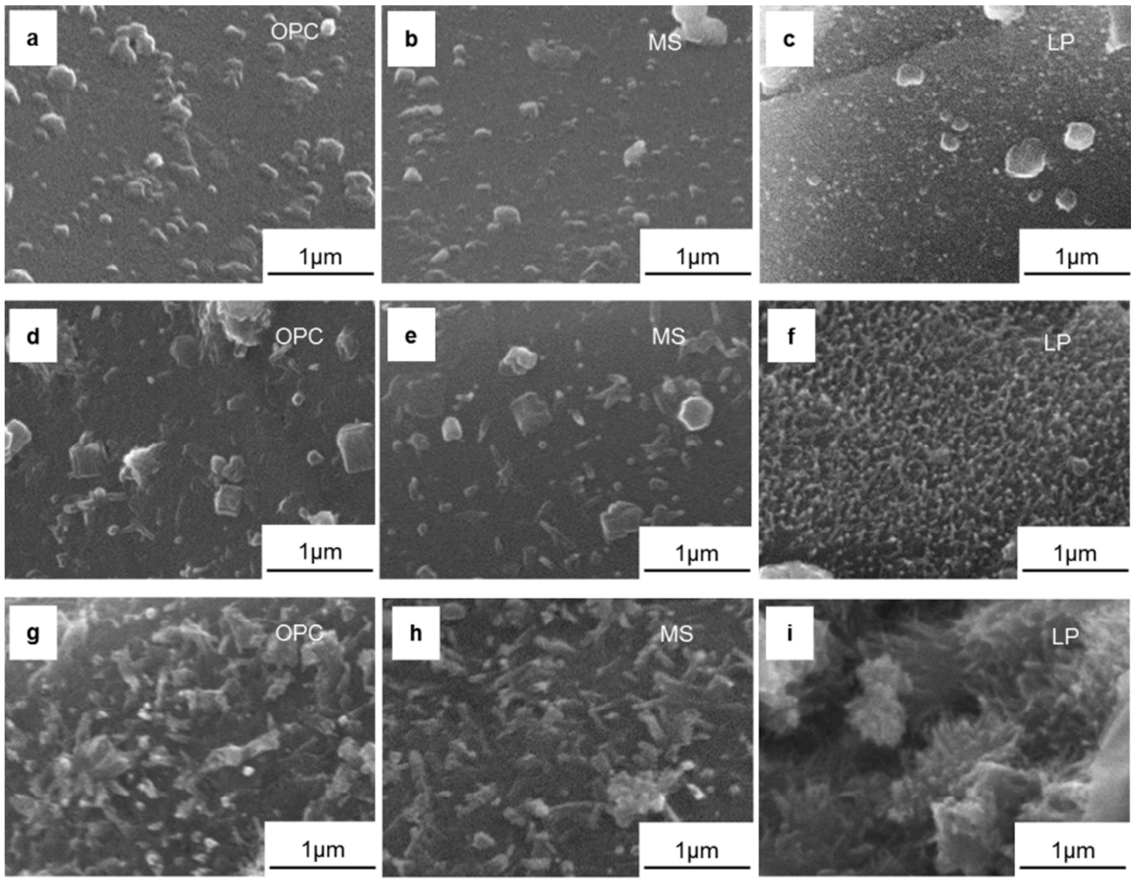

Fig. 5.7 Morphology of hydration products on surface of Portland cement grain at (a) 1 h 30 min (d) 4 h (g) 7 h 30 min, micronized sand grain at (b) 1 h 30 min (e) 4 h (h) 7 h 30 min and limestone grain at (c) 1 h 30 min (f) 4 h (i) 7h 30 min.

5.4 Discussion

5.4.1 Zeta potential and surface chemical properties

The molecular (atomic) interface structures which relate to the strength of the interface is affected by the adsorption of ions on the surface of filler particles. Adsorption of ions, in turn, affects the surface charge of these fillers which relates to zeta potential. Therefore, zeta potential measurements are important to understand the interactions between the filler surfaces and ions, and filler-hydrates adhesion mechanisms.

5.4.1.1 Interaction between ions and calcite surface

In section 5.3.2, it was found that LP particle surfaces have a much higher affinity for Ca^{2+} ions than MS and C-S-H particle surfaces. This can be explained by the different surface chemist of fillers. In the case of LP, it is believed that the adsorption driving force is entirely enthalpy-governed, and the adsorption of Ca^{2+} ions onto LP surfaces is due to a strong acid-base (donor-acceptor) interaction between the adsorbing Ca^{2+} ion and the active surface site [24]. This chemical interaction results in a strong adsorption of calcium ions onto calcite surfaces as previously discussed by Pourchet et al. [31]. As a result, a more positive zeta potential is expected and was as observed (Fig. 5.3, 5.4, 5.5 and 5.6).

5.4.1.2 Interaction between ions and silica surface

The adsorption of Ca^{2+} ions onto the silica surface is caused by electrostatic and non-Coulombic interactions [32]. In fact, as already suggested by Jonsson et al. [6] and Jang and Fuerstenau [33], electrostatic interaction is the main driving force for adsorption of Ca^{2+} on the surface of silica particles. This relatively weak interaction leads to a weak adsorption of Ca^{2+} and SO_4^{2-} ions onto MS and C-S-H surfaces. As a result, fewer calcium ions are adsorbed onto the MS particle surfaces compared to LP particle surface, which cause a lower positive zeta potential.

These interactions also play an important role in the nucleation and growth of C-S-H phases, since the liquid phase of cement paste before setting contains a high concentration of Ca^{2+} and SO_4^{2-} ions. Although the concentration of K^+ and Na^+ ions is even higher, these ions are ‘indifferent’ ions. The silicate concentration is very low and the aluminate concentration is even lower, as shown in Table 5.2. This will be discussed in more detail in the following section.

5.4.2 Nucleation and growth of C-S-H on fillers

The difference of surface charge properties between silica (MS) and calcite (LP), i.e. zeta potential values as depicted in Fig. 5.3, 5.4, 5.5 and 5.6, is consistent with the difference in nucleation and growth of C-S-H on the silica and calcite surfaces (Fig. 5.7). This indicates the strong relationship between the surface charge properties of fillers and the mechanisms of C-S-H nucleation and growth.

Two types of nucleation are generally known: homogeneous and heterogeneous nucleation. Homogeneous nucleation occurs when there are no foreign constituents in a phase. Homogeneous nucleation is initiated by the saturation of the solution. In the case that foreign constituents are present in a phase, they promote the nucleation process and thereby increase the nucleation rate. In this situation the nucleation is called heterogeneous [34]. The nucleation of C-S-H on the surface of fillers is heterogeneous.

The adsorption of nucleus constituents onto the surface of the substrate affects heterogeneous nucleation [14]. The overall kinetics of heterogeneous nucleation and crystal growth consists of a series of consecutive steps [14]:

i) Adsorption: adsorption (physical or chemical adsorption) of constituent ions onto the substrate;
ii) Surface nucleation: diffusion of adsorbed ions from the substrate to solution; partial dehydration; formation of a two-dimensional nucleus; growth to three-dimensional nucleus;
iii) Crystal growth: each one of these sequential processes consists of more than one reaction step.

In this study, when OPC, LP, MS particles and water are mixed, the cement grains start to dissolve. The solution soon contains a variety of anions and cations, and ionic strength increases. The surfaces of OPC, LP and MS particles are soon charged. The cations and anions compete with each other to absorb on these charged surfaces. As mentioned before, the concentration of Na^+, K^+, SO_4^{2-} and Ca^{2+} ions soon reaches concentrations of approximately 0.08, 0.2, 0.08 and 0.015 mol/L (Table 5.2), respectively. The concentration of K^+ and Na^+ ions is very high, but these ions are "indifferent" ions. The silicate concentration is very low and the aluminate concentration is even lower. The high density divalent ions, such as Ca^{2+} and SO_4^{2-} ions, dominate in this competition. The Ca^{2+} ions, well known to be the most important factor determining the kinetic, morphological and structural features of C-S-H, also control the heterogeneous C-S-H nucleation [35].

As previously discussed in section 5.4.1, the surface of LP particles possesses a much higher affinity for Ca^{2+} ions than that of MS particles. This is due to the fact that the driving force for the adsorption of Ca^{2+} ions onto LP particle surfaces is entirely enthalpy-governed. This adsorption is caused by a strong acid-base (donor-acceptor) interaction. Because of this chemical bonding of Ca^{2+} ions (nucleus constituents) to the surface of the LP particle, much more calcium ions are adsorbed onto the LP particle surfaces and thereby more positive zeta potential are expected. The results of zeta potential measurements, as shown in Fig. 5.3, 5.4, 5.5 and 5.6, confirmed it. Besides, this chemical interaction enhances the adsorption of calcium ions onto calcite surfaces and reduces the mobility of these adsorbed Ca^{2+} ions, which result in facilitating the formation of a 'stable nuclei'. This 'stable nuclei', subsequently, grows to form macroscopic particles. As a result, a high density of C-S-H nuclei is generated on the LP particle surfaces, which are supported by microscopic observations of morphology and distribution of hydration products on the LP particle surfaces, as shown in Fig. 5.7. Furthermore, the C-S-H growth orientation is uniform and perpendicular to the LP

particle surfaces (Fig. 5.7). This is likely due to the strong chemical interaction, which is able to stabilize the C-S-H crystal phase.

MS, OPC and C-S-H with similar surface properties, have no affinity for Ca^{2+} ions. The adsorption of Ca^{2+} and SO_4^{2-} ions onto MS, OPC and C-S-H particles surfaces is similar, which was confirmed by zeta potential measurements, as shown in Fig. 5.6. The adsorption is mainly driven by electrostatic interaction. This relatively weak interaction leads to a weak adsorption of Ca^{2+} and SO_4^{2-} ions onto MS, OPC and C-S-H particle surfaces and high mobility of these adsorbed Ca^{2+}, which make these adsorbed ions to diffuse into the solution again easily. As a result, less calcium ions are adsorbed onto the MS, OPC and C-S-H particle surfaces, which cause less positive zeta-potential. These were confirmed by the zeta potential measurements, as shown in Fig. 5.3, 5.4, 5.5 and 5.6. This relatively weak interaction is unfavourable for the formation of the 'stable nuclei'. Consequently, only a few dispersed nuclei were generated on the MS and OPC particle surfaces, which are confirmed by microscopic observations of morphology and distribution of hydration products on their surfaces, as shown in Fig. 5.7. Moreover, the variation of the C-S-H growth orientation (Fig. 5.7) on MS and OPC particle surfaces is probably due to the weak electrostatic interaction, which makes the C-S-H crystal phase attached to MS and OPC particle surface insecure.

5.4.3 Filler-hydrates adhesion mechanisms

In the previous chapter, we found that the bond between LP particles and hydration products is much stronger than that between MS particles and hydration products, and even stronger than that between hydration products themselves. To understand the strength of the bond between filler particles and hydration products, adhesion mechanisms between filler particles and C-S-H are the key. As previously outlined (section 5.2.3.1), the interactions between ions in the pore solution of cement paste and filler surfaces affect the molecular (atomic) interface structures and hence the strength of C-S-H/filler bond. The relation between these interactions and the strength of C-S-H/filler bond is discussed in what follows, emphasizing on the adhesion mechanisms between C-S-H and filler particles.

5.4.3.1 Adhesion between C-S-H and silicate

Since the C-S-H and silicate particles have similar surface charge properties, the electric interaction between C-S-H surface and silicate surface is similar to that between C-S-H surfaces. From direct-force measurements [7, 36] and simulation studies [4, 6, 37, 38], it has been inferred that the cohesion between C-S-H particles is a consequence of ion-ion correlation forces. The van der Waals force has only a marginal contribution to the strength of C-S-H [5-7, 9, 39]. The existence of the attractive ion-ion correlation force between silica particles was also confirmed by Franks [40]. These cohesion mechanisms between C-S-H particles and between silicate particles can also be applied to the adhesion between C-S-H and silicate particle since the C-S-H and silicate particles have the similar surface charge properties.

As shown in Fig. 5.8, a dielectric continuum water and ions are in between C-S-H surface and silicate surface. In these two surfaces with an intervening electrolyte solution, the overwhelming majority of instantaneous ionic configurations lead to polarizations of the ionic clouds. For example, the excess of Ca^{2+} ions in the right of the mid-plane leads to a deficit in the left, which results in an overall positive charge in the right side, and an overall negative charge in the left side (Fig. 5.8). This charge separation gives rise to an attractive ion-ion correlation force, acting in the same way as if a correlations between fluctuating electronic dipoles would give rise to the London dispersion force. This force mainly depends on the surface charge density and the valence of the counterions. More details about ion-ion correlation force can be found in section 2.3.3.4.

However, it seems contrary to the finding that the adhesion between C-S-H particle and micronized sand (silicate) particle is very weak. This can be explained by the fact that C-S-H have a much larger surface area than micronized sand. The surface area of the C-S-H particle is quite variable, with a conservative value of 200 m^2/g [41], while the specific surface area of the micronized sand (silica) particle is roughly around 1 m^2/g (Table 3.1). As a consequence, there are a few contact points between the micronized sand (silica) particle and C-S-H particle. This leads to a weak adhesion between the micronized sand (silica) particle and C-S-H particle, even though the adhesion force between the micronized sand (silica) particle and C-S-H particle is similar as the cohesion force between C-S-H particles.

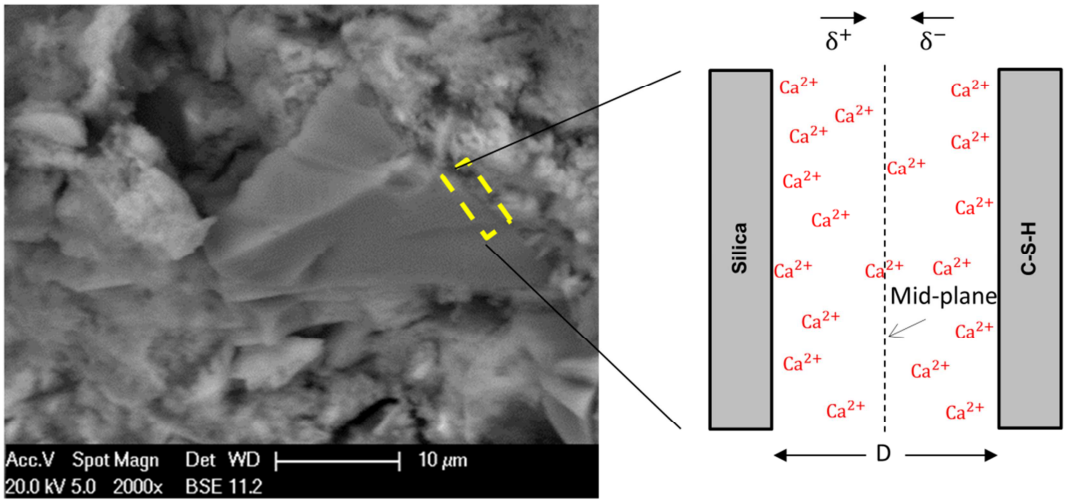

Fig. 5.8 Schematic representation of two surfaces (silica surface and C-S-H surface) and Ca^{2+} counterions. The two surfaces are separated by a dielectric continuum in which Ca^{2+} ions are free to move. Additional salt pairs have been left out for clarity. In the overwhelming majority of possible configurations, the distribution of ions is neither symmetrical with respect to the mid-plane nor homogeneous along the vertical axis. The excess of ions in some places leads to a deficit in other places. This generates an attractive ion-ion correlation force. D is the interlayer separation.

5.4.3.2 Adhesion between C-S-H and calcite

As mentioned, the surface area of the C-S-H gel is very large, i.e., a conservative value of 200 m^2/g [41]. The specific surface area of LP particles is roughly less than 1 m^2/g (Table 3.1). It is obvious that the contact points between the LP particle and C-S-H particle are much less than those between C-S-H particles and would be similar to MS/C-S-H interactions if only surface area is considered. In spite of this, the adhesion between LP particle and hydration products is even stronger than that between the hydration products. There should be a much stronger bond between C-S-H particle and calcite particle compared to the bond between C-S-H particle and silicate particle.

As discussed in section 5.4.1, the surface of LP particles has a much higher affinity for calcium ions than for sulfate ions due to the fact that the driving force for the adsorption of Ca^{2+} ions onto LP surfaces is entirely enthalpy-governed. This adsorption is caused by a strong acid-base (donor-acceptor) interaction. Because of this chemical bonding of Ca^{2+} ions (nucleus constituents), much more calcium ions are adsorbed onto the LP surfaces. A more positive zeta potential for LP particles can be expected. These results from zeta potential measurements, as shown in Fig. 5.3, 5.4, 5.5 and 5.6, confirmed it. Besides, a high density of the C-S-H nuclei generated on the LP surfaces (Fig. 5.7) is an additional supportive evidence.

This very strong bond between C-S-H and LP particles is very likely caused by the strong adsorption of calcium ions onto calcite surfaces. It most probably is an ionic-covalent bond, as schematically illustrated in Fig. 5.9. This mechanism of chemically adsorbed Ca^{2+} ions on calcite surface is similar to the one of inter-layer calcium ions linking to the tobermoritic C-S-H lamellae by a strong ionic-covalent bond. More details about ionic-covalent bond and the tobermoritic C-S-H lamellae can be found in section 2.3.2. The chemically adsorbed Ca^{2+} ions 'connect' the C-S-H lamellae and calcite surface by similar ionic-covalent bonds, resulting in an interlayer separation (D, Fig. 5.9) at a subnano level. This is probably the reason why the interface between hydrates and limestone particles has very high resistance to crack propagation, as shown in Fig. 4.5.

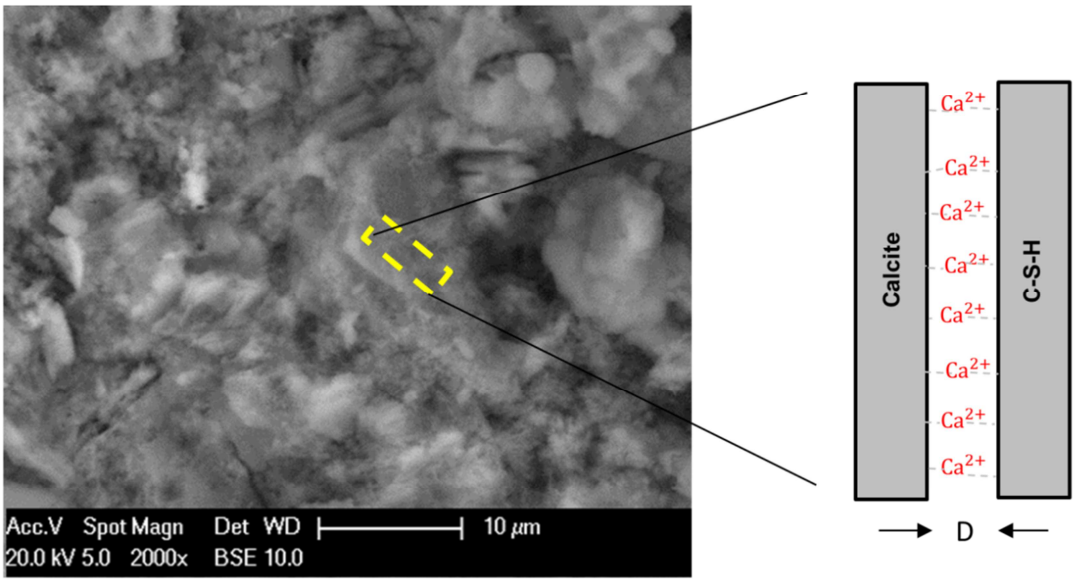

Fig. 5.9 Schematic representation of calcite surface and C-S-H surface, and Ca^{2+} ions in the between. The two surfaces are separated by a dielectric continuum in which Ca^{2+} ions have low mobility. Additional salt pairs have been left out for clarity. The strong chemical bonding of calcium ions to limestone surface results in a very strong filler/C-S-H bond (most likely ionic-covalent bond). D is the interlayer separation.

In summary, the strength of the bonds between the filler particles and hydration products, and the cement hydration process itself, are strongly affected by the adsorption of calcium ions onto the filler surfaces. This adsorption depends on the chemical properties of fillers. Fig. 5.10 shows an overview of the influence of the chemical properties of fillers on the adsorption of calcium ions, the heterogeneous C-S-H nucleation and crystal growth, and strength development of the interface between the filler surface and hydration products.

i) As shown in Fig. 5.10a, at the beginning of the hydration process, much more calcium ions are adsorbed on LP surfaces than on MS surfaces, which were supported by results from zeta-potential tests. This is attributed to the fact that the adsorption driving force is a chemical interaction for LP but it is a relatively weak electrostatic interaction for MS.
ii) As shown in Fig. 5.10b, with the on-going hydration process, a high density of adsorbed calcium ions caused a high amount of C-S-H nuclei on LP surfaces. By contrast, a relatively low density of adsorbed calcium ions resulted in only a few dispersed nuclei on the MS surfaces. This was visualised by SEM observations.
iii) As shown in Fig. 5.10c, with enhanced hydration and increased amount of hydration products (mainly, C-S-H), the cement and filler grains become interconnected i.e. bridged by the C-S-H gels, leading to setting and strength development. Chemically adsorbed Ca^{2+} ions onto LP surfaces led to the formation of a strong bond (most likely, ionic-covalent bond) and thereby

resulted in a strong link between LP particles and C-S-H. By contrast, a relatively weak, electrostatically adsorbed Ca^{2+} ions onto MS surfaces resulted in an attractive ion-ion correlation forces and hence a relatively weak connection between the MS particles and C-S-H. The SEM observations of the crack paths and fracture surfaces of cement pastes after applying a mechanical load indicated the strength of the bond between filler particles and C-S-H.

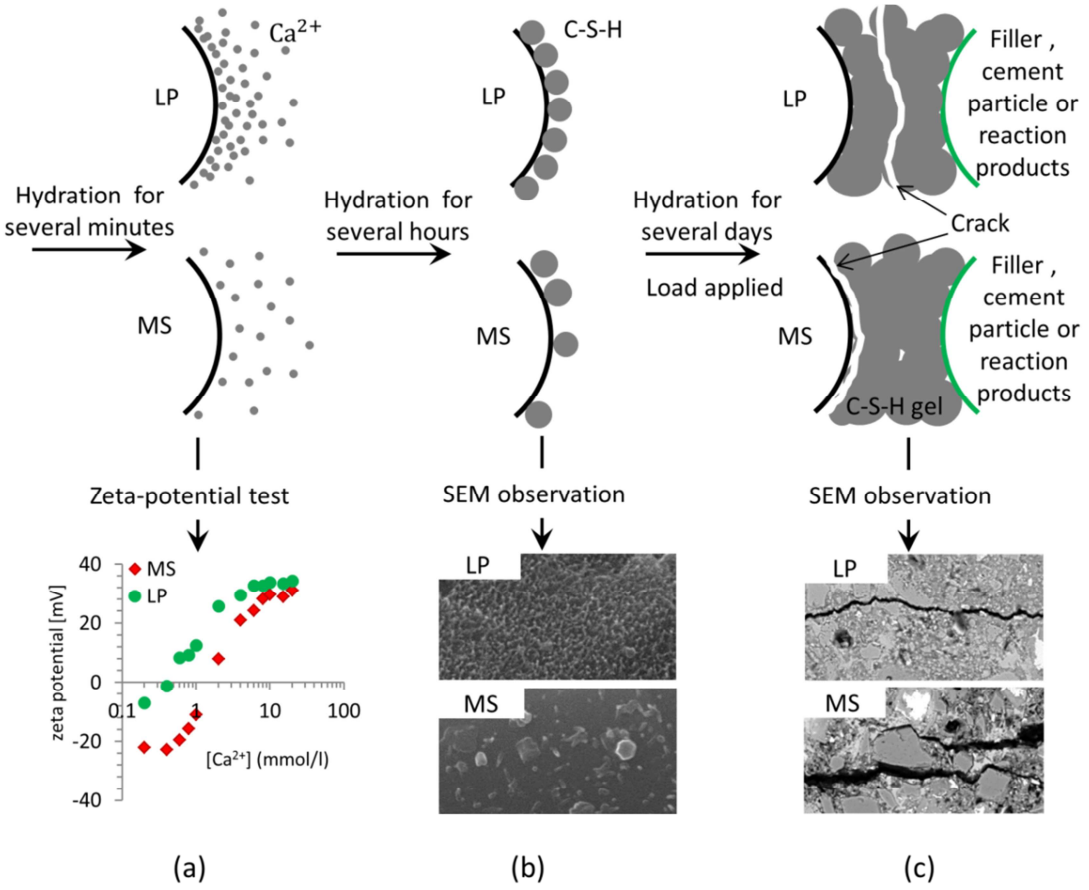

Fig. 5.10 Schematic diagram of the influence of chemical properties of fillers on the processes, such as adsorption of calcium ions (a), heterogeneous nucleation and crystal growth (b), and strength development of interface between the filler particles and hydration products (c).

5.5 Conclusions

This chapter discussed the adhesion mechanisms between C-S-H and the surface of two different filler particles (micronized sand and limestone powder). The surface charge properties of the two different fillers were studied using zeta-potential measurements. Microscopical observations of nucleation and growth of C-S-H on particle surfaces were carried out by SEM. The relation between the surface properties of filler particles and the strength of the C-S-H/filler bond was discussed. Based on this study, the following conclusions can be drawn:

1. The zeta-potential measurements showed that micronized sand, cement and C-S-H particles have similar surface properties due to the fact that they are rich in silicate. Micronized sand and C-S-H have low affinity for Ca^{2+} ions. This was confirmed by the fact that the adsorption of Ca^{2+} and SO_4^{2-} ions onto micronized sand and C-S-H surfaces is similar. The adsorption of Ca^{2+} ions onto micronized sand and C-S-H surfaces is mainly driven by relatively weak electrostatic interaction.
2. Compared to micronized sand and C-S-H, the surface of a limestone particle has a higher affinity for Ca^{2+} ions due to a moderately strong acid-base (donor-acceptor) interaction between the adsorbing Ca^{2+} ion and the active surface site. This is supported by the fact that LP surfaces have a much higher affinity for Ca^{2+} ions than SO_4^{2-} ions, which was confirmed by the zeta-potential measurement.
3. Microscopic observations showed that limestone has a different effect on the nucleation and growth of C-S-H compared to micronized sand. On the surface of limestone, a much higher amount of C-S-H nuclei were generated, whereas only a few dispersed nuclei were observed on micronized sand surfaces. These observations confirmed the difference of the interaction between the adsorbing Ca^{2+} ions and filler surfaces.
4. The results showed a strong relation between surface chemical properties and the strength of the C-S-H/filler bond. This relation can be explained by the fact that the surface chemical properties of fillers govern the adsorption reaction of calcium ions on their surfaces. Chemically adsorbed calcium ions onto a limestone surface led to the formation of a relatively strong bond (most likely ionic-covalent bond) between a limestone particle and C-S-H. By contrast, a relatively weak electrostatically adsorbed Ca^{2+} ions onto micronized sand surface resulted in an attractive ion-ion correlation force and hence a relatively weak bond between a micronized sand particle and C-S-H.

References

1. Mehta, P. and P.J.M. Monteiro, *Concrete: Microstructure, Properties, and Materials*2006: McGraw-Hill Education.
2. French, C.W. and A. Mokhtarzadeh, *High strength concrete: Effects of materials, curing and test procedures on short-term compressive strength.* PCI Journal, 1993. **38**(3): p. 76-87.
3. Bentz, D.P., et al., *Multi-scale investigation of the performance of limestone in concrete.* Construction and Building Materials, 2015. **75**: p. 1-10.
4. Jonsson, B., et al., *Onset of cohesion in cement paste.* Langmuir, 2004. **20**(16): p. 6702-6709.
5. Gmira, A., et al., *Microscopic physical basis of the poromechanical behavior of cement-based materials.* Materials and Structures, 2004. **37**(265): p. 3-14.
6. Jonsson, B., et al., *Controlling the cohesion of cement paste.* Langmuir, 2005. **21**(20): p. 9211-9221.
7. Plassard, C., et al., *Nanoscale experimental investigation of particle interactions at the origin of the cohesion of cement.* Langmuir, 2005. **21**(16): p. 7263-7270.
8. Pellenq, R.J.M., N. Lequeux, and H. van Damme, *Engineering the bonding scheme in C-S-H: The iono-covalent framework.* Cement and Concrete Research, 2008. **38**(2): p. 159-174.
9. Pellenq, R.J.M. and H. Van Damme, *Why does concrete set?: The nature of cohesion forces in hardened cement-based materials.* Mrs Bulletin, 2004. **29**(5): p. 319-323.
10. Standard, A., *C305, Standard practice for mechanical mixing of hydraulic cement pastes and mortars of plastic consistency*, in *Annual book of ASTM standards*2006.
11. Stern, O., *The theory of the electrolytic double-layer.* Z. Elektrochem, 1924. **30**(508): p. 1014-1020.
12. Moulin, P. and H. Roques, *Zeta potential measurement of calcium carbonate.* Journal of Colloid and Interface Science, 2003. **261**(1): p. 115-126.
13. Douglas, H. and R. Walker, *The electrokinetic behaviour of Iceland Spar against aqueous electrolyte solutions.* Transactions of the Faraday Society, 1950. **46**: p. 559-568.
14. Stumm, W., *Chemistry of the solid-water interface*, 1992, Wiley, New York.
15. Moore, J.W. and C.L. Stanitski, *Chemistry: The molecular science*2014: Cengage Learning.
16. Westall, J., *Adsorption mechanisms in aquatic surface chemistry.* IN: Aquatic Surface Chemistry: Chemical Processes at the Particle-Water Interface. John Wiley and Sons, New York. 1987. p 3-32, 10 fig, 6 tab, 28 ref. DOE Contract, 1987.
17. Hunter, R., *Zeta Potential in Colloid ScienceAcademic Press.* New York, 1981.
18. Berodier, E. and K. Scrivener, *Understanding the Filler Effect on the Nucleation and Growth of C-S-H.* Journal of the American Ceramic Society, 2014: p. n/a-n/a.
19. Rothstein, D., et al., *Solubility behavior of Ca-, S-, Al-, and Si-bearing solid phases in Portland cement pore solutions as a function of hydration time.* Cement and Concrete Research, 2002. **32**(10): p. 1663-1671.
20. Leroy, P., et al., *Influence of surface conductivity on the apparent zeta potential of amorphous silica nanoparticles.* Journal of Colloid and Interface Science, 2013. **410**: p. 81-93.
21. Iller, R., *The chemistry of Silica Jon Wiley & Sons.* New York, 1979.
22. Anderson, N. and A.J. Rubin, *Adsorption of inorganics at solid-liquid interfaces*1981: Ann Arbor Science Publishers, Inc.
23. Somasundaran, P. and G.E. Agar, *The zero point of charge of calcite.* Journal of Colloid and Interface Science, 1967. **24**(4): p. 433-440.
24. Huang, Y.C., et al., *Adsorption of Calcium-Ions from Calcium-Chloride Solutions onto Calcium-Carbonate Particles.* Langmuir, 1991. **7**(8): p. 1742-1748.
25. Eriksson, R., J. Merta, and J.B. Rosenholm, *The calcite/water interface: I. Surface charge in indifferent electrolyte media and the influence of low-molecular-weight polyelectrolyte.* Journal of Colloid and Interface Science, 2007. **313**(1): p. 184-193.
26. Thompson, D.W. and P.G. Pownall, *Surface Electrical-Properties of Calcite.* Journal of Colloid and Interface Science, 1989. **131**(1): p. 74-82.
27. Foxall, T., et al., *Charge determination at calcium salt/aqueous solution interface.* Journal of the Chemical Society, Faraday Transactions 1: Physical Chemistry in Condensed Phases, 1979. **75**(0): p. 1034-1039.

28. Nachbaur, L., et al., *Electrokinetic properties which control the coagulation of silicate cement suspensions during early age hydration.* Journal of Colloid and Interface Science, 1998. **202**(2): p. 261-268.
29. Viallis-Terrisse, H., A. Nonat, and J.-C. Petit, *Zeta-Potential Study of Calcium Silicate Hydrates Interacting with Alkaline Cations.* Journal of Colloid and Interface Science, 2001. **244**(1): p. 58-65.
30. Masel, R.I., *Principles of adsorption and reaction on solid surfaces*. Vol. 3. 1996: John Wiley & Sons.
31. Pourchet, S., et al., *Chemistry of the calcite/water interface: Influence of sulfate ions and consequences in terms of cohesion forces.* Cement and Concrete Research, 2013. **52**: p. 22-30.
32. Papirer, E., *Adsorption on silica surfaces*. Vol. 90. 2000: CRC Press.
33. Jang, H.M. and D.W. Fuerstenau, *The nature of simple monovalent cation-silica interaction as reflected in the spin-lattice relaxation time of sodium-23.* Langmuir, 1987. **3**(6): p. 1114-1118.
34. Kalb, J.A., *Crystallization kinetics*, in *Phase Change Materials*2009, Springer. p. 125-148.
35. Garrault-Gauffinet, S. and A. Nonat, *Experimental investigation of calcium silicate hydrate (C-S-H) nucleation.* Journal of Crystal Growth, 1999. **200**(3–4): p. 565-574.
36. Lesko, S., et al., *Investigation by atomic force microscopy of forces at the origin of cement cohesion.* Ultramicroscopy, 2001. **86**(1): p. 11-21.
37. Pellenq, R.-M., J. Caillol, and A. Delville, *Electrostatic attraction between two charged surfaces: A (N, V, T) Monte Carlo simulation.* The Journal of Physical Chemistry B, 1997. **101**(42): p. 8584-8594.
38. Pellenq, R.-M., A. Delville, and H. Van Damme, *Cohesive and swelling behaviour of charged interfaces: a (NVT) Monte-Carlo study.* SPECIAL PUBLICATION-ROYAL SOCIETY OF CHEMISTRY, 1997. **213**(1): p. 596-603.
39. Lesko, S., et al., *Investigation by atomic force microscopy of forces at the origin of cement cohesion.* Ultramicroscopy, 2001. **86**(1-2): p. 11-21.
40. Franks, G.V., *Zeta Potentials and Yield Stresses of Silica Suspensions in Concentrated Monovalent Electrolytes: Isoelectric Point Shift and Additional Attraction.* Journal of Colloid and Interface Science, 2002. **249**(1): p. 44-51.
41. Thomas, J.J., H.M. Jennings, and A.J. Allen, *The surface area of hardened cement paste as measured by various techniques.* Concr. Sci. Eng, 1999. **1**(1): p. 45-64.

6

Fracture Behaviour of Cement Paste with Different Filler-hydrates Adhesion Properties

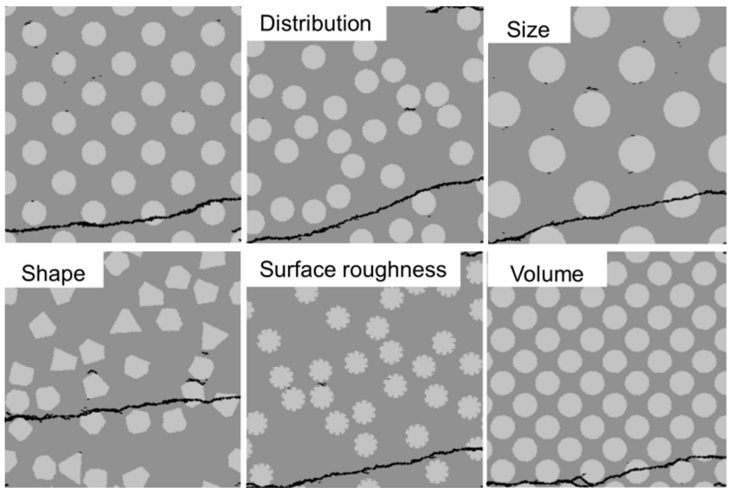

In the previous chapters we have seen that limestone powder has much better adhesion properties than micronized sand. With different adhesion properties, the effect of microstructural features (size, shape, surface roughness), particle size distribution and volume fraction of filler on the fracture behaviour of blended cement paste is supposed to be different as well. In order to understand the effect of the microstructural features, particle size distribution and volume fraction of filler on the fracture behaviour of blended cement paste with either strong or weak filler-matrix interface, microscale simulations with a lattice model are carried out. The results show that the strength of the filler-matrix interface, rather than the microstructural features, particle size distribution and volume fraction of filler, plays a dominant role in the crack propagation and the strength of blended cement paste. The knowledge acquired here provides a clue, or direction, for improving the performance of existing fillers. To improve the performance of fillers in cement paste in terms of strength, priority should be given to improving the bond strength between filler particles and matrix, not to modifying the microstructural features (i.e., shape and surface roughness) of filler.

6.1 Introduction

In previous chapters, it was found that the strength of the interface between micronized sand particles and hydration products was so low that it has no noticeable contribution to the strength of the paste. By contrast, the strength of the interface between limestone particles and hydration products was suggested to be equal to or higher than that of the matrix itself. This is because the limestone has better adhesion properties than micronized sand.

Besides adhesion properties, the microstructural features (size, shape, surface roughness), particle size distribution and volume fraction of filler may also play an important role in the strength and the fracture behaviour of blended cement paste. These roles are not easy to measure experimentally. With the lattice fracture model (see chapter 4), one can effectively simulate the micro-mechanical behaviour of blended cement paste in order to get insight into the effect of microstructural features, particle size distribution and volume fraction of filler on the strength and the fracture behaviour of blended cement paste. The results of these simulations will enable us to get a better understanding of the role of filler-hydrates adhesion properties and its influence on the strength of blended cement paste.

In this chapter microscale simulations with the lattice model are presented. The effect of microstructural features, particle size distribution and volume fraction of filler on fracture behaviour of blended cement paste with weak and strong filler-matrix interfaces will be studied. The strong filler-matrix interface simulates the interface between limestone particles and hydration products, whereas the weak interface simulates the interface between micronized sand particles and hydration products.

6.2 Numerical simulation approach

The effect of the following features of filler will be investigated here.

- Size
- Shape
- Surface roughness
- Particle size distribution
- Volume fraction

The lattice model was used. The numerical simulation approach was described in section 4.3. In this lattice model, all specimens are of a size of 100 × 100 × 1 μm^3. A uniaxial tensile test is conjured by fixing all the nodes on the bottom surface of the specimen and imposing a uniform surface load on the top surface, as shown in Fig. 4.4. The mechanical properties of the interfaces between filler particles and hydration products, together with filler and matrix, are given in Table 6.1.

Table 6.1 Mechanical properties of filler, matrix and the interfaces of mature paste.

Material properties	Young's modulus E [GPa]	Tensile strength f_t [MPa]	ν
Filler	71	2.1	0.2
Matrix	22	1.4	0.2
Strong interface (SI)	17	1.4	0.2
Weak interface (WI)	17	0.4	0.2

6.3 Results

6.3.1 Effect of filler distribution

The concentration of the filler particles in a localized region may have an effect on the strength of cement paste. In this section, five different distributions of filler particles are considered and divided into two groups, as shown in Fig. 6.1. The left column in Fig. 6.1 represents the group with strong interface (SI); The right column is that with weak interface (WI). The filler particles in the specimen of Fig. 6.1a and b are uniformly distributed. The filler particles in the rest of the specimens are randomly distributed. The diameter of filler particles is 10 μm. The filler volume fraction is 25%.

The micro-crack patterns for the different cement paste specimens with strong interface (SI) and weak interface (WI) are shown in Fig. 6.1. Those figures show that in the same group (left or right), the crack patterns are similar. This indicates that the filler particle distribution has little influence on the crack patterns. However, a big difference between the left and right can be observed. A large number of branched and tortuous cracks can be seen in the specimens with weak interface (WI). Only one single crack occurs in the specimens with strong interface (SI), and the crack pattern does not change, regardless the distribution of filler particles. This indicates that the strength of the interface has a significant effect on the crack pattern.

Fig. 6.2 plots the stress-strain relations and variation of the strength and the strain at peak stress for different filler particle distributions with strong interface (SI) and weak interface (WI). From these graphs it can be inferred that the strength of specimens with weak interface (WI) is always much lower compared with that of specimens with strong interface (SI). The specimens with the uniformly distributed filler particles have the highest strength because stresses are uniformly distributed across the cross section of these specimens. However, in practice, it is impossible to achieve such a uniform distribution. For the specimens with randomly distributed filler particles, the influence of the filler distribution on the strength of the specimens with strong interface (SI) is much smaller compared with that with weak interface (WI). The specimen with weak interface (WI) and the filler particle distribution 4 has the lowest strength, as shown in Fig. 6.2b. This is due to the fact that many filler particles in this specimen are concentrated in a small region and very close to each other in the horizontal direction, as shown Fig. 6.1h. This facilitates the initiation of cracks and the further propagation of cracks leading to lower strength. However, for the specimen with strong interface (SI), the initiation of cracks can be stopped due to high local cohesive strength.

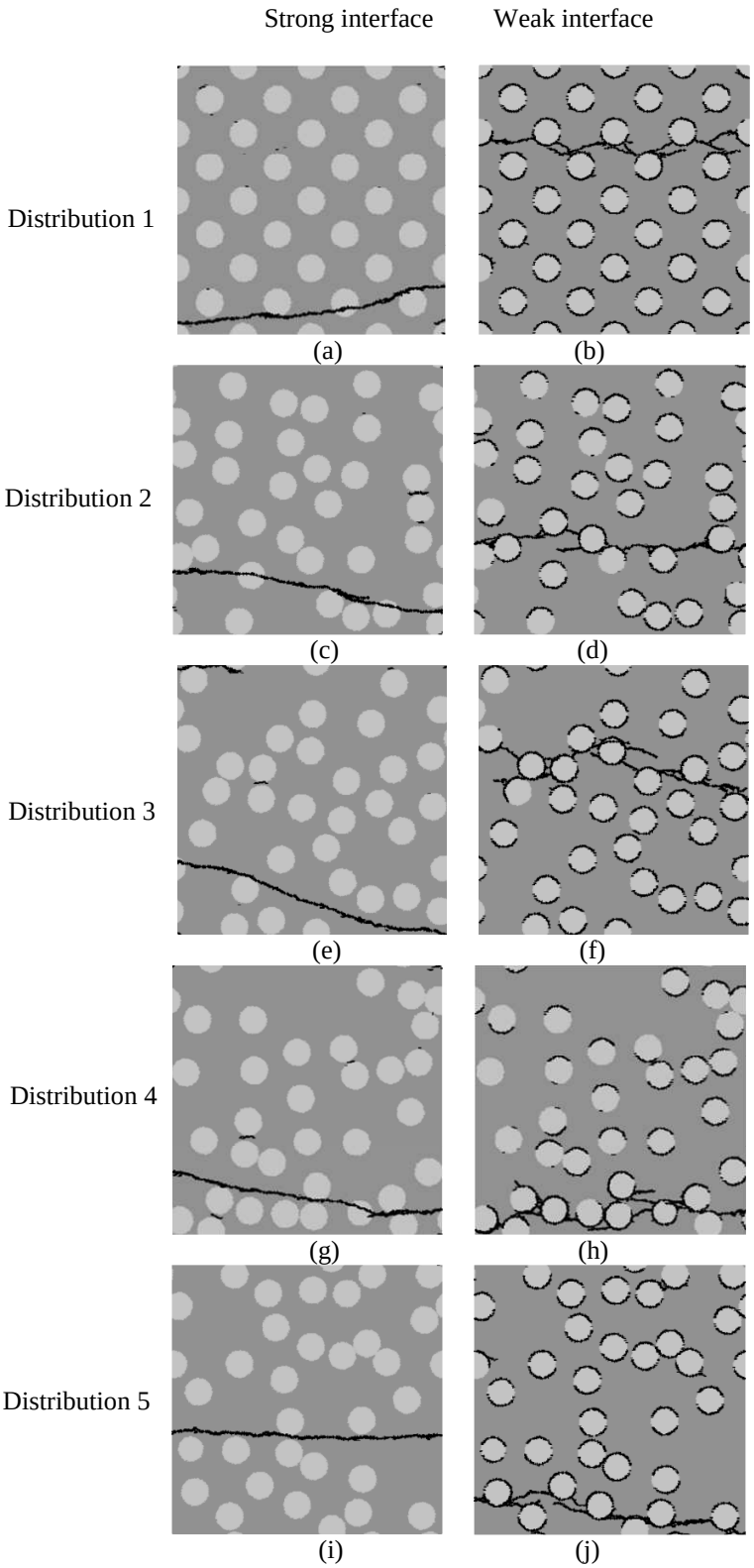

Fig. 6.1 Micro-crack patterns of specimens with strong interface (SI) and that of specimens with weak interface (WI) for different filler particle distribution (for SI and WI, see Table 6.1).

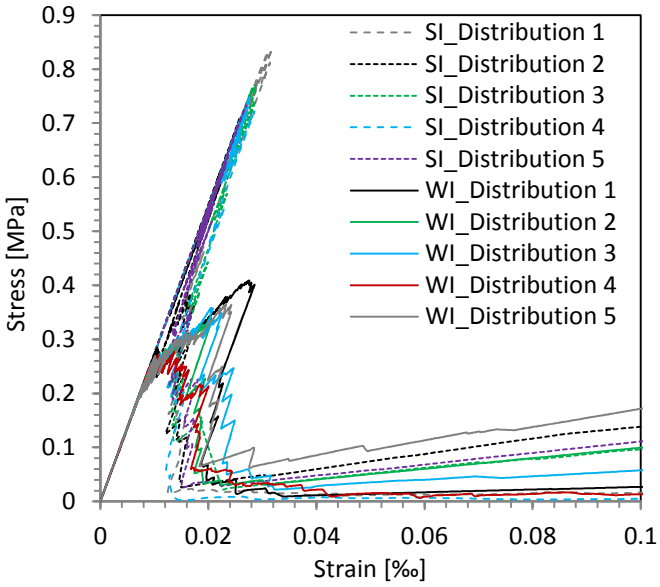

(a) Stress-strain relation for specimens with strong interface (SI) and that with weak interface (WI)

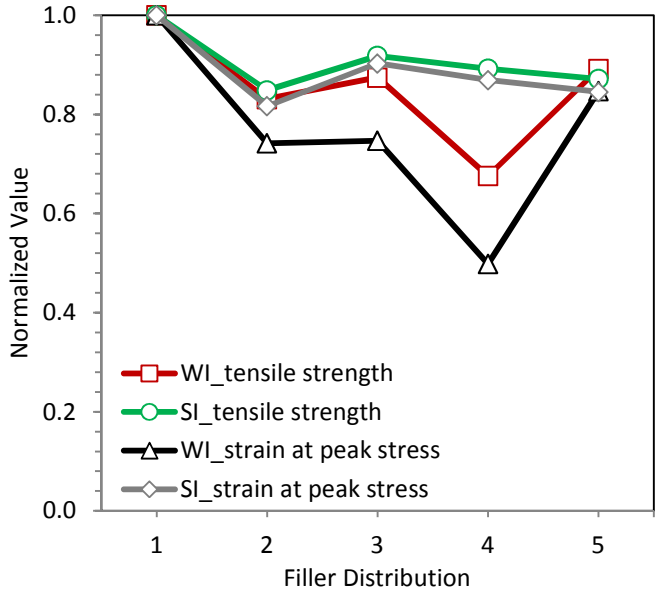

(b) Variation of the strength and the strain at peak stress

Fig. 6.2 Simulated results of the filler distribution effect analyses for specimens with strong interface (SI) and that with weak interface (WI) (for SI and WI, see Table 6.1).

6.3.2 Effect of filler size

In this section the effect of the filler particle size on the strength and the fracture behaviour of blended cement paste is analysed. Four different particle sizes (5, 10, 15 and 20 µm) are considered. They are divided into two groups as indicated in Fig. 6.3 and Fig. 6.4: on the left is the group with strong interface (SI); on the right is that with weak interface (WI). The filler volume fraction is kept constant at 25%. With increasing particle size, the number of filler particle decreases. The filler particles in Fig. 6.3 are randomly distributed. As reference the filler particles presented in Fig. 6.4 are uniformly distributed.

Fig. 6.3 and Fig. 6.4 show the micro-crack patterns for the different cement paste specimens with strong filler-matrix interface (SI) and weak filler-matrix interface (WI). From these graphs, it can be inferred that the distribution of filler particles has little effect on the crack patterns.

Within the same group (left or right group), the micro-crack patterns are similar regardless the particle distribution. This indicates that the particle size has a negligible effect on the micro-crack pattern. However, there is a big difference between the micro-crack patterns of the left and right group. This indicates that the strength of the interface plays a more important role in crack propagation than the effect of the particle size of the filler.

Fig. 6.5 plots the stress-strain relations, the strength and the strain at peak stress for different filler particle sizes with strong filler-matrix interface (SI) and weak filler-matrix interface (WI). Fig. 6.5c shows that for the cement paste specimens with strong filler-matrix interface (SI) the influence of the particle size on strength of specimen is insignificant in the case of uniform distribution of filler particles, whereas in the case of random distribution of filler particles the strength of the specimen decrease with increasing particle size. This may be caused by the increasing stress concentration due to increasing filler size. This stress concentration facilitates the initiation of cracks and the further propagation of cracks leading to lower strength. For the specimens with weak filler-matrix interface (WI) the effect of particle size on the strength of specimen is not apparent regardless the spatial distribution of filler particles.

It can be seen in Fig. 6.5a and b that the strength of specimens with weak filler-matrix interface (WI) is always much lower compared with that of specimens with strong interface (SI). This indicates that the effect of the particle size on the strength is much smaller than the effect of the interface strength on the strength of cement paste specimen.

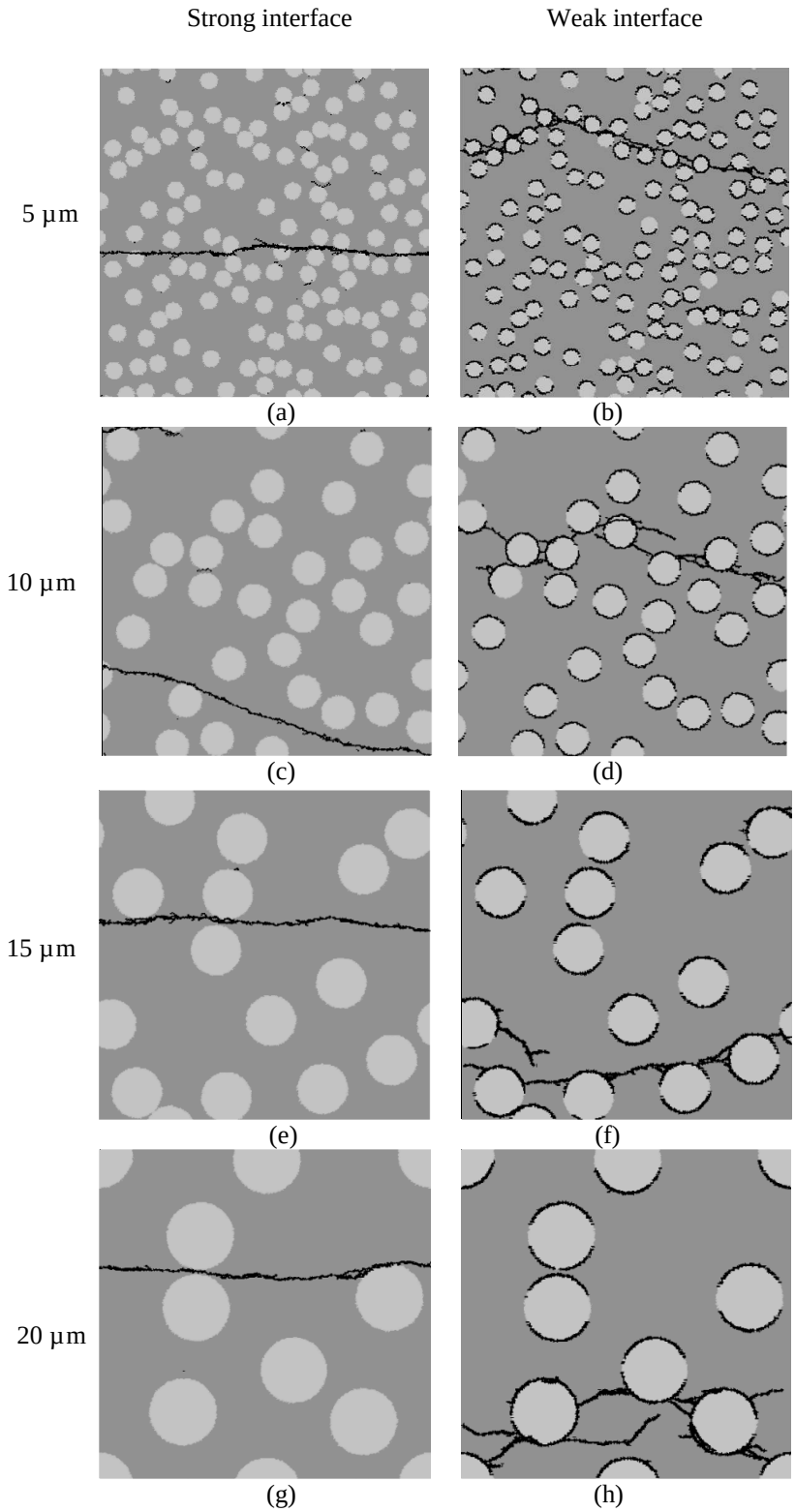

Fig. 6.3 Micro-crack patterns of specimens with randomly distributed filler particles and different filler particle sizes.

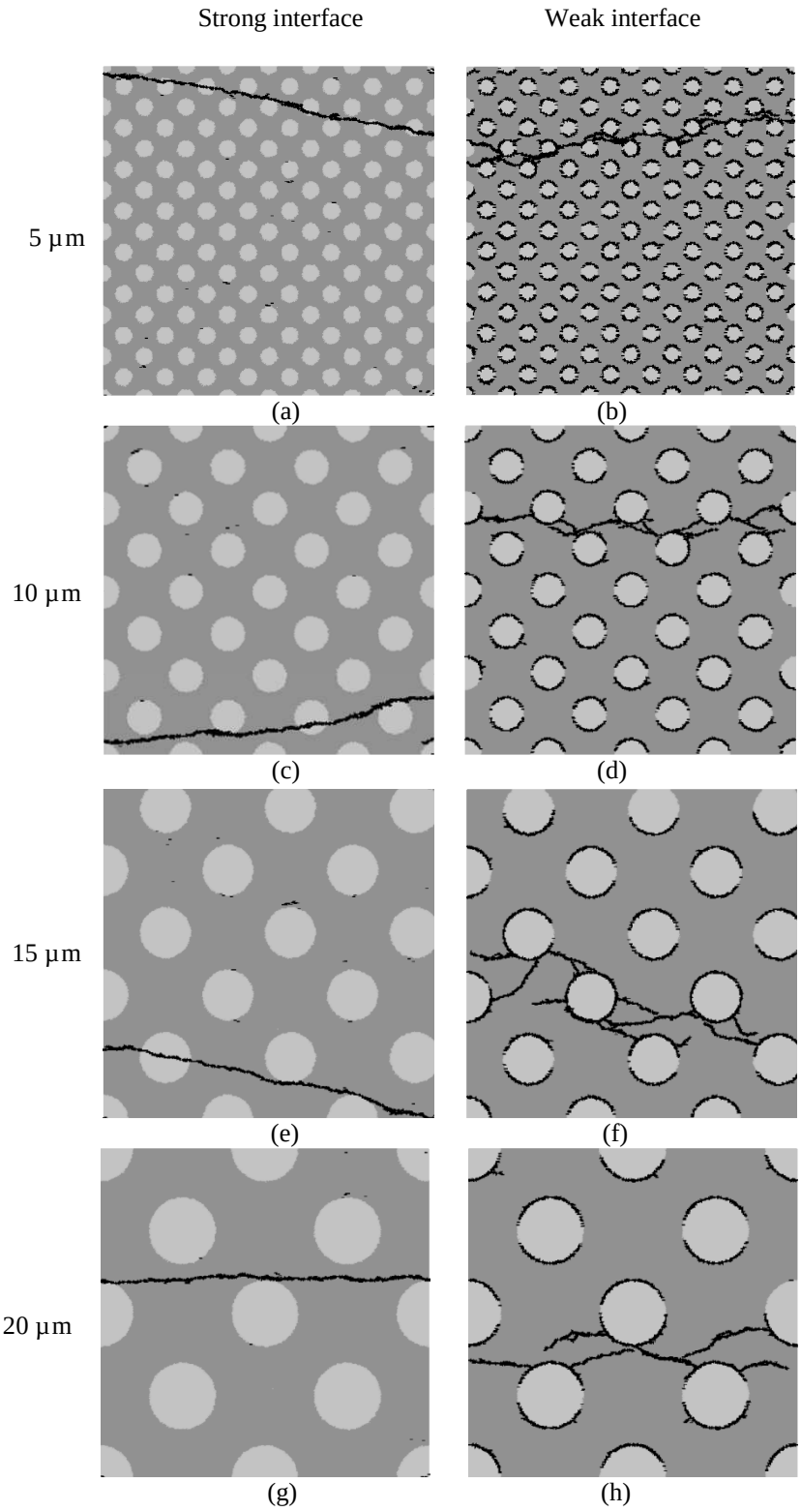

Fig. 6.4 Micro-crack patterns of specimens with uniformly distributed filler particles and different filler particle sizes.

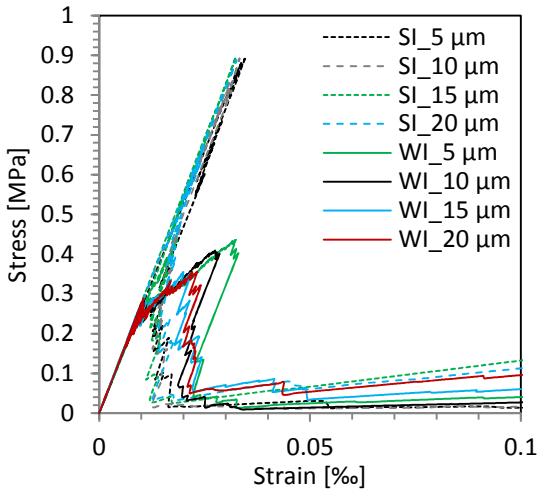

(a) Stress-strain relation(uniformly distributed)

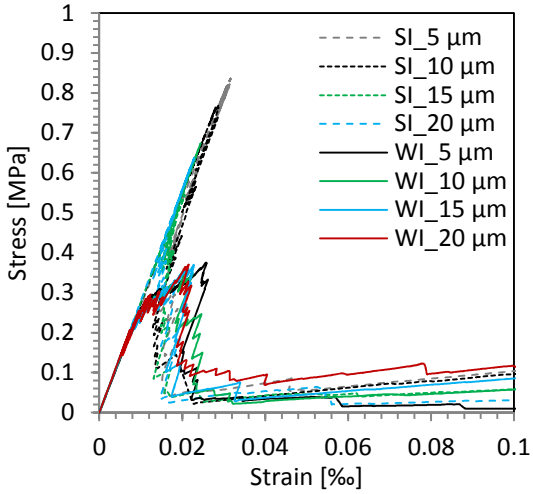

(b) Stress-strain relation(randomly distributed)

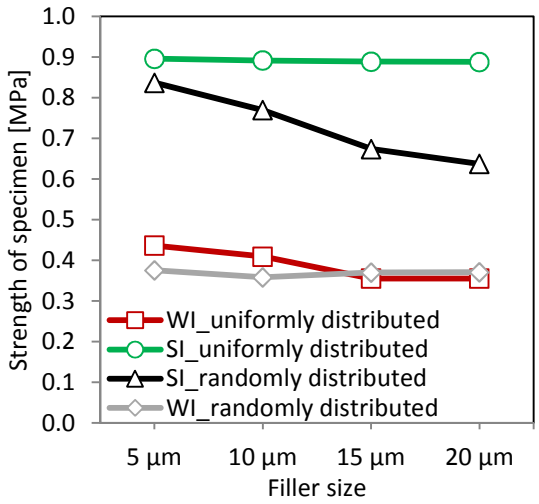

(c) Strength

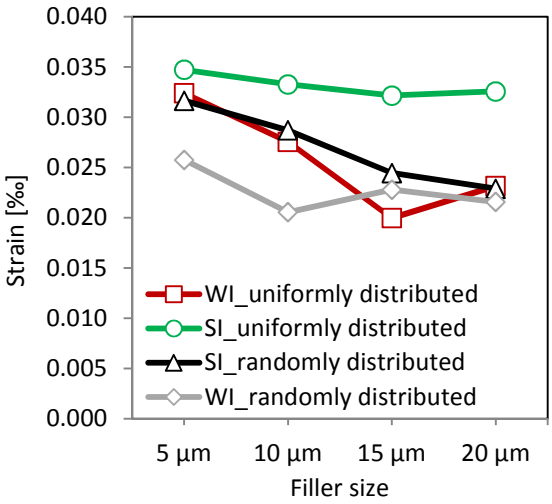

(d) Strain at peak stress

Fig. 6.5 Simulated results of the filler size effect analyses for specimens with strong interface (SI) and that with weak interface (WI) (for SI and WI, see Table 6.1).

6.3.3 Effect of filler shape

In this section the effect of the filler shape is investigated. Four different filler shapes are considered, as indicated in Fig. 6.6. They are divided into two groups: on the left is the group with strong interface (SI); on the right is that with weak interface (WI). A circular particle shape (shape 1) is used for simplicity. Arbitrary polygonal shapes (shape 2, 3 and 4) are considered close to the actual shape of filler particles. The length-to-width ratio for shape 2, 3 and 4 is about 1.0, 2.0 and 3.0, respectively. The filler volume fraction is kept constant at 25%. The diameter of circular filler particles is 10 µm.

Micro-crack patterns for the filler shape sensitivity analyses are shown in Fig. 6.6. For the specimens with strong filler-matrix interface (SI) (Fig. 6.6a, c, e and g), the micro-crack patterns are more or less similar. For the specimens with weak filler-matrix interface (WI) (Fig. 6.6b, d, f and h), the micro-crack patterns appear slightly different from each other. For the circular shape (Fig. 6.6b), the branched cracks are uniformly distributed around the filler particles and tend to encircle the filler particles. For the arbitrary polygonal shapes (Fig. 6.6d, f and h), the number of the branched cracks around the filler particles decrease with increasing length-to-width ratio of particle increases. Moreover, with increasing length-to-width ratio, it becomes increasingly difficult for cracks to propagate around and encircle the filler particles. However, the difference of the micro-crack pattern between the left and right group is much bigger. This indicates that the strength of the interface plays a more important role in the crack pattern than the shape of filler particles.

Fig. 6.7 plots the stress-strain relations (a) and variation of the strength and the strain at peak stress (b) of the specimens with filler particles with different shape. It is obvious that the filler shape has a small effect on the strength and the strain at peak stress of cement paste specimens with strong filler-matrix interface (SI). On the contrary, for the cement paste specimens with the weak filler-matrix interface (WI) the filler shape has a significant influence on the strength of the specimens. Due to the stress concentration at the sharp edges of polygonal particle shape, both the strength and the strain at peak stress of the specimens with circular filler particles are much higher than those with arbitrary polygonal filler particles. Furthermore, with increasing length-to-width ratio of the arbitrary polygonal shapes, the strength and the strain at peak stress of the cement paste specimens with the weak filler-matrix interface (WI) appear to decrease due to the increasing stress concentrations.

Although the filler shape has a significant influence on the fracture behaviour of the cement paste specimens with the weak filler-matrix interface (WI), the strength of these specimens is always much lower than that of specimens with the strong interface (SI), as shown in Fig. 6.7a. This indicates that the filler-matrix interface strength is the dominant influencing factor on the strength of the cement paste specimens compared to the influence of filler particle shape.

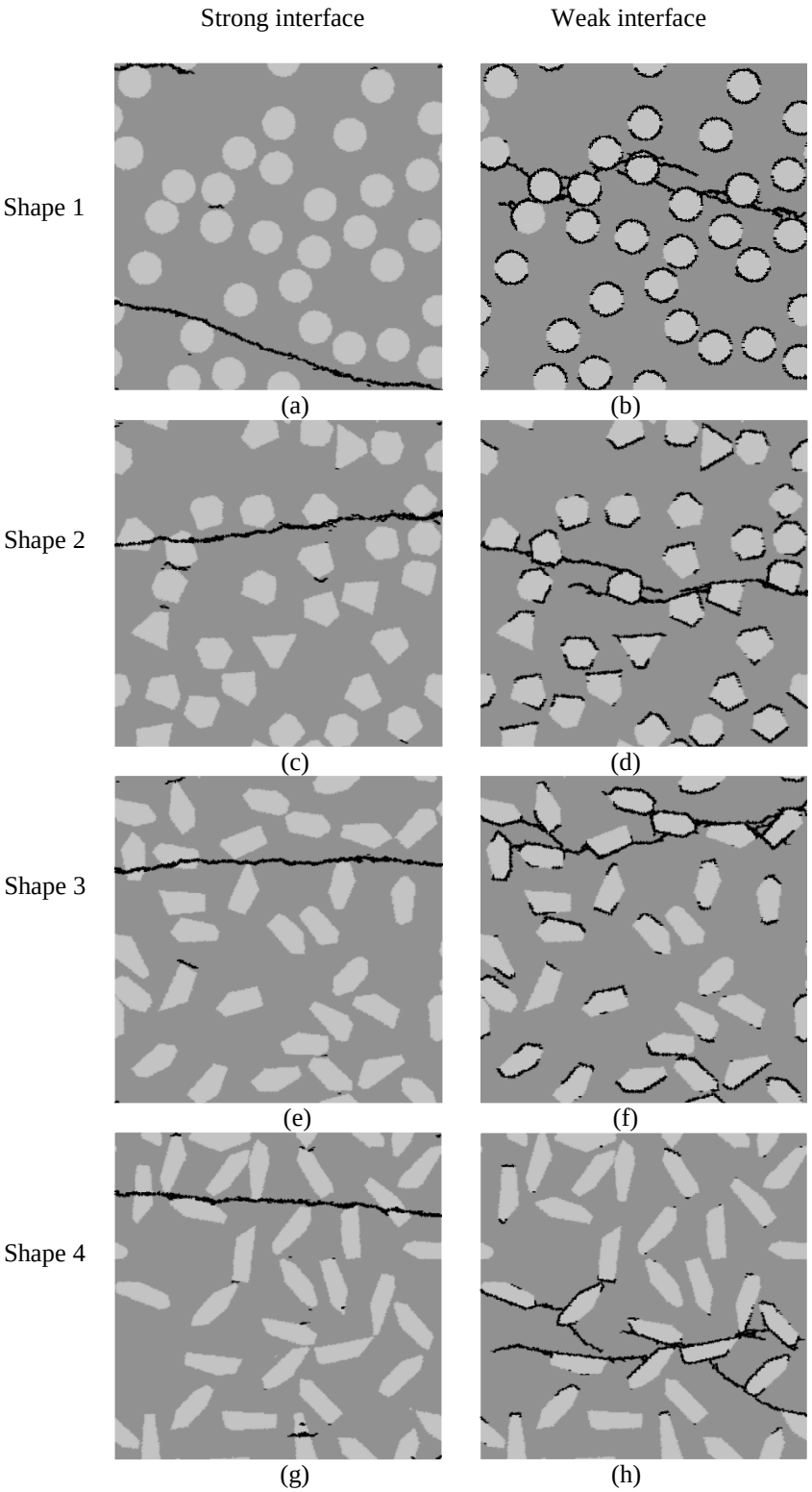

Fig. 6.6 Micro-crack patterns of specimens with strong interface (SI) and that of specimens with weak interface (WI) for different shapes of filler particles (for SI and WI, see Table 6.1).

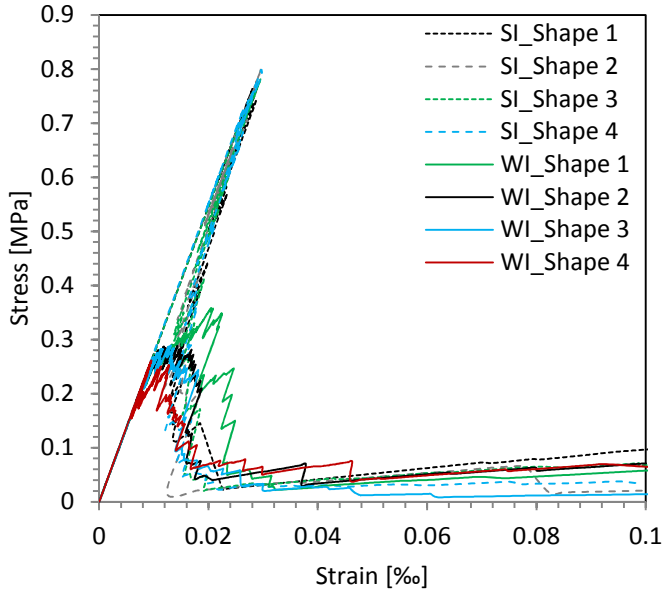

(a) Stress-strain relation for specimens with strong interface (SI) and that with weak interface (WI)

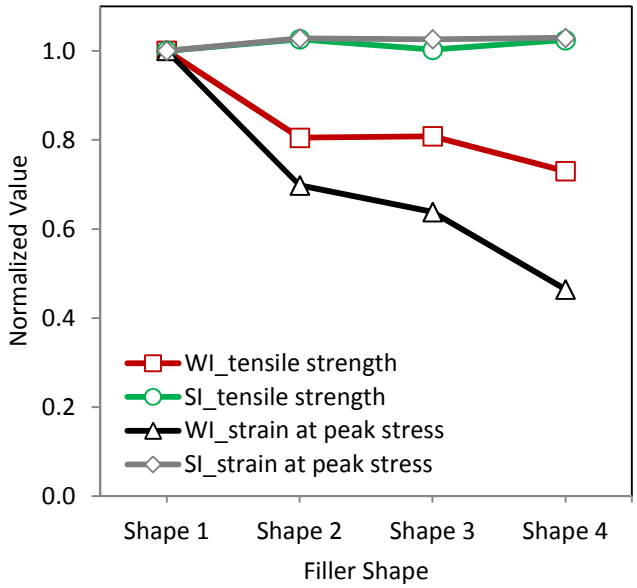

(b) Variation of the strength and the strain at peak stress for different filler shapes.

Fig. 6.7 Simulated results of the filler shape effect analyses for specimens with strong interface (SI) and that with weak interface (WI) (for SI and WI, see Table 6.1).

6.3.4 Effect of surface roughness of filler particles

The surface roughness of the filler particles is one of the important factors determining the effect of mechanical interlocking between the filler particles and cement matrix [1]. In this section the effect of the surface roughness of the filler particles on the fracture properties is analysed. Three different surface roughnesses are considered, as indicated in Fig. 6.8. They are divided into two groups: on the left is the group with strong interface (SI); on the right is that with weak interface (WI). The circular particle shape is used. The diameter of the filler particles is 10 µm. For particles with roughness 1 (Fig. 6.8a and b) the surface is smooth. For particles with roughness 2 and 3 the surfaces are rough. The surface of particles with roughness 3 (Fig. 6.8e and f) is rougher than that of the particles with roughness 2 (Fig. 6.8c and d). The filler volume fraction is kept constant at 25%.

Fig. 6.8 shows the micro-crack patterns of specimens with the filler particles at different surface roughness. For the specimens with strong filler-matrix interface (SI) (Fig. 6.8a, c and e), the micro-crack patterns are more or less similar, although the location of the crack for roughness 1 is different. For the specimens with weak filler-matrix interface (WI) (Fig. 6.8b, d and f), the micro-crack patterns appear similar. Therefore, it seems that the surface roughness of the filler has a negligible effect on the micro-crack pattern.

Fig. 6.9 shows the stress-strain relations, the strength and the strain at peak stress for different particle surface roughnesses. The figure shows that in the specimens with strong filler-matrix interface (SI) the surface roughness of the filler particles has little effect on the strength and the strain at peak stress of cement paste specimens. This is due to the fact that the interface between the filler particles and the surrounding paste is already very strong.

For the cement paste specimens with weak filler-matrix interface (WI) the surface roughness of the filler particles has a significant influence on the mechanical response of cement paste specimen. Fig. 6.9b and c show that the strength and strain at peak stress of specimens increase with increasing surface roughness.

From the simulation it is clear that in the specimens with weak filler-matrix interface (WI) the surface roughness of the filler particles can enhance the strength of the interface between the filler particles and the surrounding paste and hence improve the strength of specimens. However, even the filler particles with the highest surface roughness, the specimens with weak interface (WI) have a much lower strength than the specimens with strong interface (SI), as shown in Fig. 6.9b. This indicates that the strength of the interface can be improved by increasing surface roughness of filler particles but the improvement is limited.

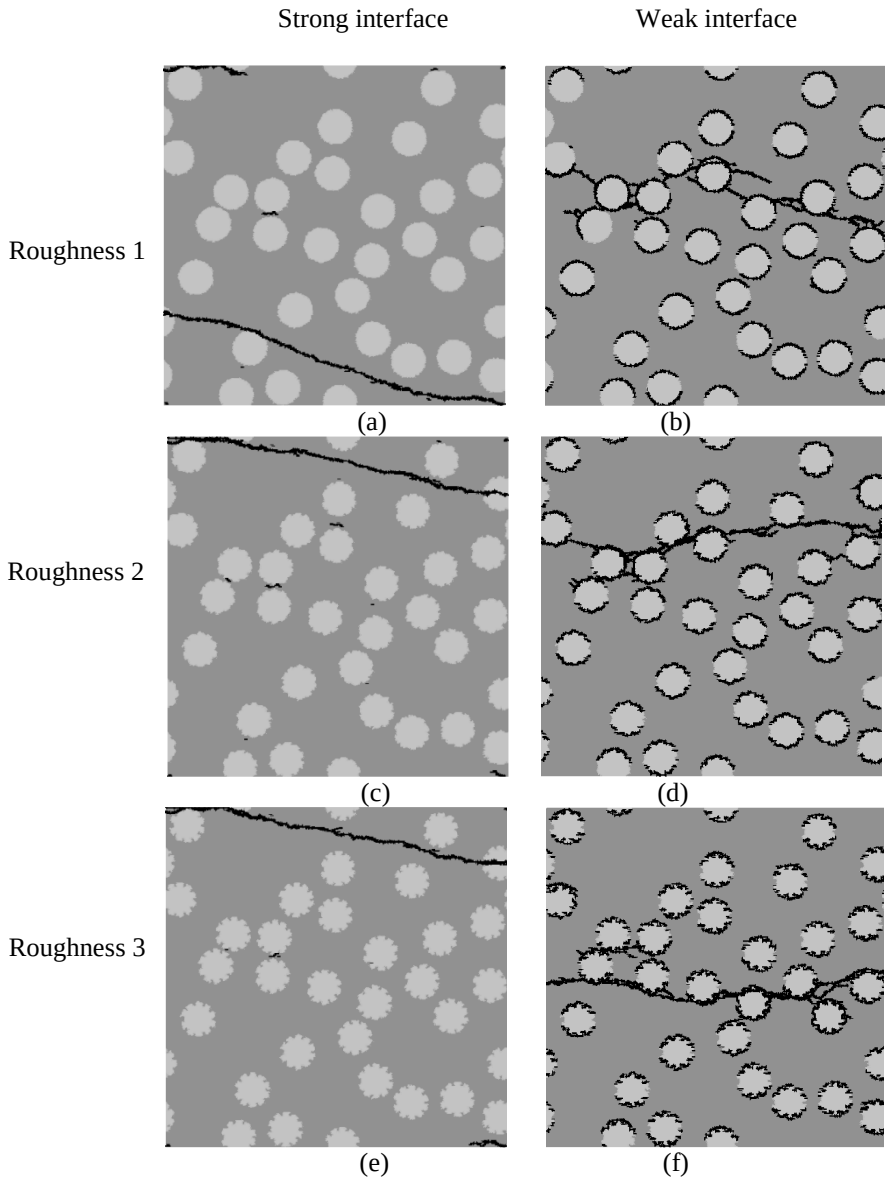

Fig. 6.8 Micro-crack patterns of specimens with strong interface (SI) and that of specimens with weak interface (WI) for different surface roughness of filler particles (for SI and WI, see Table 6.1).

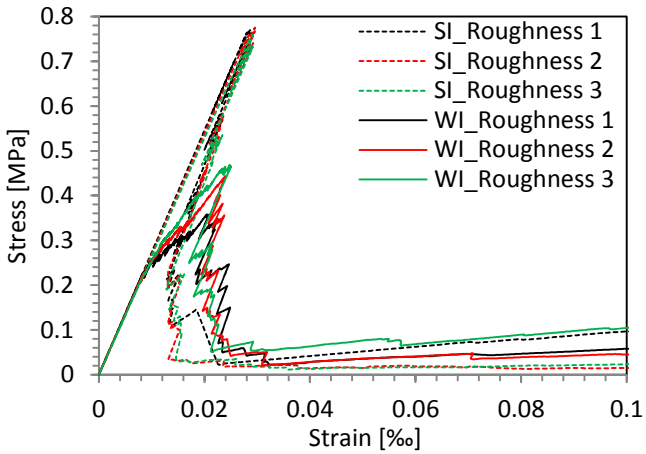

(a) Stress-strain relation for specimens with strong interface (SI) and that with weak interface (WI)

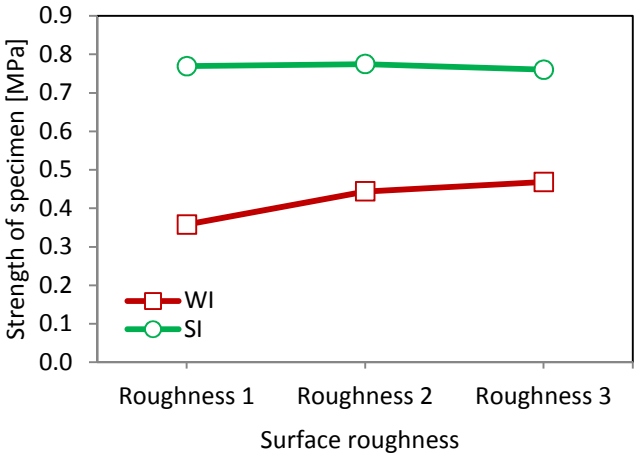

(b) Strength of for specimens with strong interface (SI) and that with weak interface (WI)

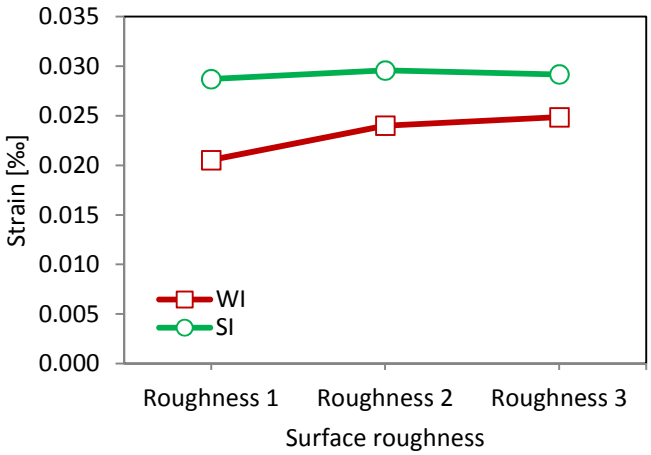

(c) Strain at peak stress of for specimens with strong interface (SI) and that with weak interface (WI)

Fig. 6.9 Simulated results of the filler surface roughness effect analyses for specimens with strong interface (SI) and that with weak interface (WI) (for SI and WI, see Table 6.1).

6.3.5 Effect of filler volume fraction

The effect of the filler content on the fracture behaviour of cement paste specimens is examined in this section. Five different volume fractions are considered: 5%, 15%, 25%, 35% and 45%. They are divided into two groups as indicated in Fig 6.10 and 6.11: on the left is the group with strong interface (SI); on the right is that with weak interface (WI). The filler particles in Fig. 6.10 are randomly distributed. As reference specimens are used with uniformly distributed filler particles (Fig. 6.11). The diameter of the filler particles is kept constant at 10 µm.

Micro-crack patterns of the specimens with different filler content are shown in Fig. 6.10 and 6.11. These figures show that the spatial distribution of filler particles has little effect on the crack pattern. For the specimens with strong interface (SI), the crack patterns in all specimens are more or less similar regardless the filler content. In the specimens with high volume of filler, cracking through filler particles can be observed. For the specimens with weak interface (WI), the crack patterns are slightly different. For the specimen with 5% filler, the crack is not branched. For the specimen with a high filler volume fraction (15%, 25%, 35% and 45%), the cracks are distorted and branched.

The stress-strain relations, the strength and strain at peak stress for different filler content are shown in Fig. 6.12. Fig. 6.12c shows that the uniform distribution of filler particles improves the strength of specimen, especially for the specimens with strong interface. The filler volume has little effect on the strength for specimens with strong filler-matrix interface (Fig. 6.12c). However, the strain at peak stress decreases with increasing filler volume fraction (Fig. 6.12d). This is because of the Young's modulus of cement paste specimens increases with increasing filler content. By contrast, for the specimens with weak interface (WI) the filler content has a significant influence on the strength. The strength decreases with increasing filler content. This is due to the increase of weak filler-matrix interfaces. This promotes propagation of crack and hence reduces the strength of the cement paste specimens.

Although the filler content has a significant influence on the strength of specimens with weak filler-matrix interface, the strength of specimens is always lower than that with strong filler-matrix interface, as shown in Fig. 6.12c. Even with a filler volume fraction of 5%, the strength of the specimens with weak interface (WI) is about 30% lower than that of the specimens with strong interface (SI). This indicates that the interface strength has more effect on the strength of the cement paste specimens than the filler volume fraction (5, 15, 25, 35 and 45%).

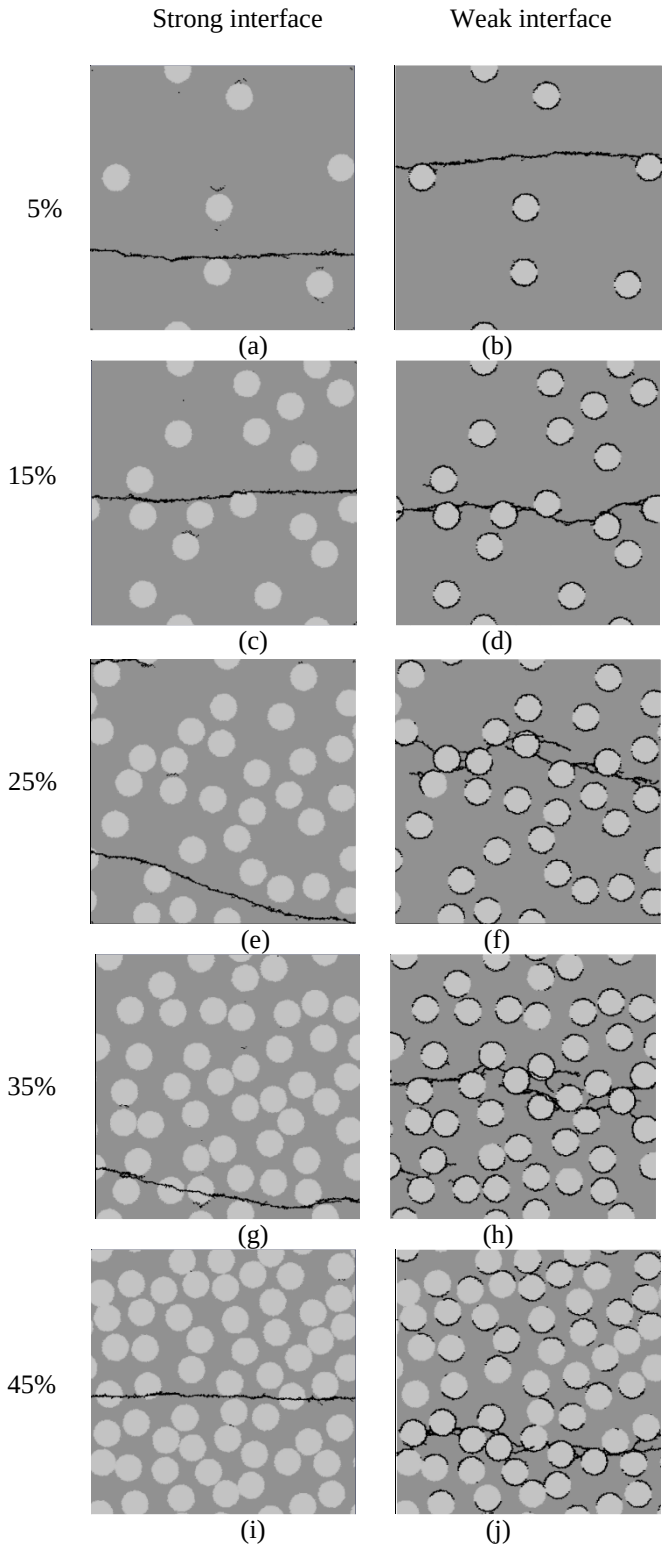

Fig. 6.10 Micro-crack patterns of specimens with randomly distributed filler particles and different filler volume fractions.

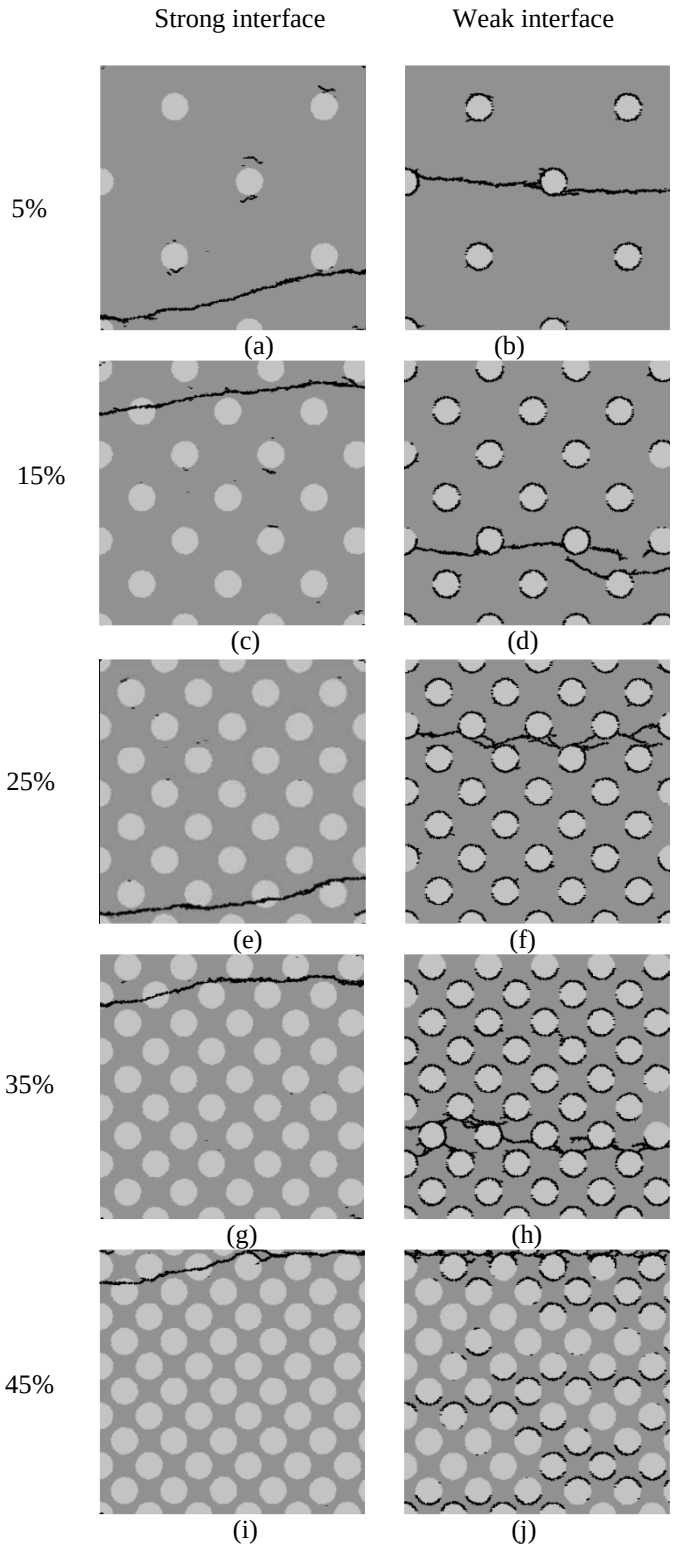

Fig. 6.11 Micro-crack patterns of specimens with uniformly distributed filler particles and different filler volume fractions.

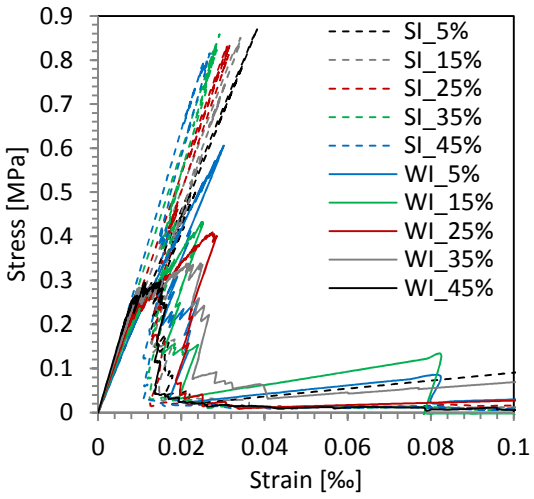

(a) Stress-strain relation(uniformly distributed)

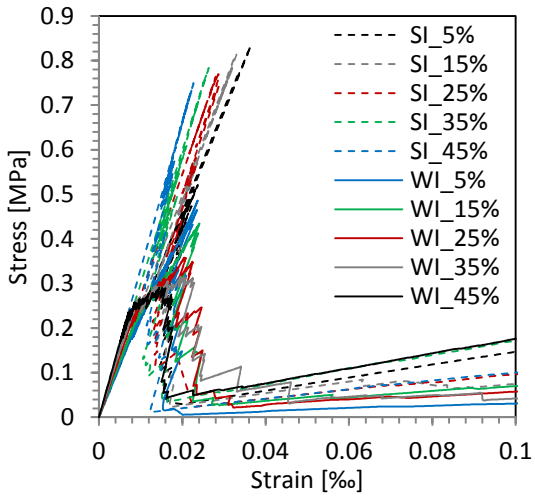

(b) Stress-strain relation(randomly distributed)

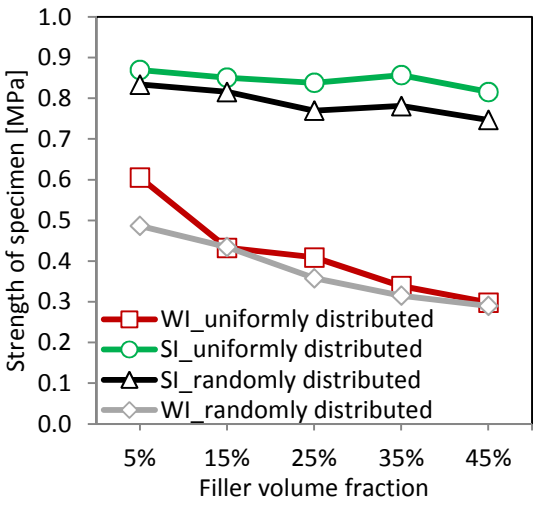

(c) Strength

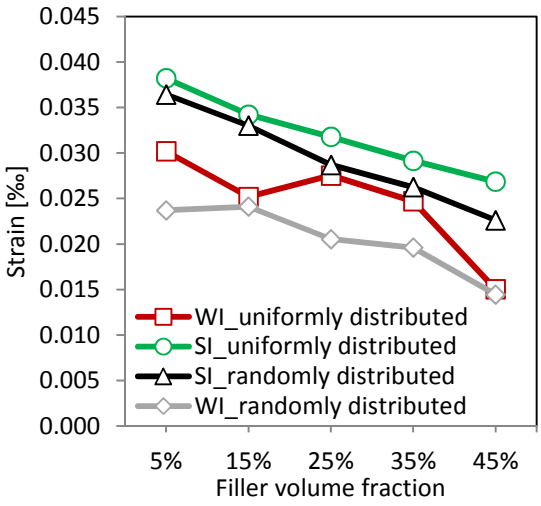

(d) Strain at peak stress

Fig. 6.12 Simulated results of the filler volume effect analyses for specimens with strong interface (SI) and that with weak interface (WI) (for SI and WI, see Table 6.1).

6.4 Conclusions and outlook

The influence of particle size distribution, size, shape, surface roughness and volume fraction of filler on the tensile strength and micro-crack pattern in blended cement paste specimens with strong and weak filler-matrix interfaces were systematically investigated by using the lattice model. Based on the numerical analyses, the following observations are made.

Strength of cement paste specimens with weak filler-matrix interface:

- Randomly distributed filler particles can result in stress concentration and hence decrease the strength of cement paste.
- In the investigated range of particle size of the filler (5, 10, 15 and 20 µm), the influence of the particle size on the strength of specimens is not noticeable.
- Due to stress concentrations at the sharp edges of polygonal particles, both the resulting tensile strength and the strain at peak stress of the cement paste specimens with arbitrary polygonal filler particles are lower than that of specimens with circular filler particles. Furthermore, with increasing length-to-width ratio of arbitrary polygonal particles, the tensile strength and the strain at peak stress of the cement paste specimens appear to decrease due to increasing stress concentrations.
- With increasing surface roughness, the effect of mechanical interlocking between the filler particles and cement matrix increases. This leads to the increase of the strength of the paste, but this increase is limited.
- With increasing filler content, the strength of the specimens decreases.

Strength of cement paste specimens with strong filler-matrix interface:

- The particle size distribution has an influence on the strength of specimens but the influence is not remarkable. The strength of specimens with uniformly distributed filler particles is only a little higher than that of specimens with randomly distributed filler particles.
- In the case of the specimens with uniformly distributed filler particles, the influence of the particle size on the strength of specimens is small. However, in the case of the specimens with randomly distributed filler particles, the strength decreases with increasing filler particle size.
- The particle shape, roughness and content of filler have little effect on the strength of specimens.
- The influence of particle size distribution, size, shape, surface roughness and volume fraction of filler on the strength of the specimens with strong interface is much smaller than on the strength of the specimens with weak interface.

Micro-crack pattern:

- With either weak or strong interface, the crack patterns are similar regardless the particle size distribution, size, shape, surface roughness and volume fraction of filler, although the location of the main cracks may change.
- The micro-crack patterns of the cement paste specimens with strong filler-matrix interface are very different from that of the specimens with weak filler-matrix interface.

The numerical simulations indicate that the strength of the filler-matrix interface, rather than the particle size distribution, size, shape, surface roughness and volume fraction of filler, plays a dominant role in the crack propagation and the strength of blended cement paste. These observations support previous findings that the strong interfaces between limestone particles and hydration products are due to the superior bond between limestone and hydration products rather than microstructural features of the filler particles, such as shape and surface roughness. Moreover, this study indicates the direction for optimization of the performance of fillers in cement paste in view of microcracking and strength. To improve the performance of fillers in blended cement paste in term of strength, priority should be given to improving the bond strength between filler particles and hydration products, not to modifying the microstructural features of filler.

References

1. Kim, S.-M. and R.K. Abu Al-Rub, *Meso-scale computational modeling of the plastic-damage response of cementitious composites.* Cement and Concrete Research, 2011. **41**(3): p. 339-358.

7

Retrospection, Conclusions and Prospects

This chapter summarises the work presented in this thesis. General conclusions and prospects are presented. In the end, suggestions for further research are given.

7.1 Retrospection

Use of fillers, such as limestone and quartz powder, as a replacement for Portland cement can make concrete cheaper and more environment friendly [1-3]. Additions of limestone or quartz powder have been reported to exert a limited chemical effect on cement hydration [4, 5]. The main quasi-chemical effect of added limestone and quartz powder is that they accelerate cement hydration by facilitating nucleation and growth of reaction products at their surfaces [1, 5-8]. Finer fillers in cement paste can result in improvements in strength because of a denser packing [9, 10]. However, the use of fillers in paste with constant water-to-binder ratio also results in dilution of Portland cement particles and their strength-providing reaction products in the paste. This 'dilution' effect will lead to a higher porosity. Above a critical amount of filler, the effect of dilution exceeds the effect of packing, resulting in a lower strength of the hardened paste or concrete [1, 11]. These effects (porosity, packing and dilution) on the strength of cement paste have been studied intensively [1, 9-13]. However, they (porosity, packing and dilution) cannot explain the difference in performance of different fillers.

The adhesion strength between filler particles and reaction products, which depends on the physical and chemical properties of the filler, also has an influence on the strength of blended cement paste. However, the role of filler-hydrates adhesion properties in the strength of blended cement paste attracted relatively little attention yet. This is attributed to the fact that the gel-space ratio plays the primary role in strength of blended cement paste and the contact area between filler particles and reaction products is very small. Various studies [14-16] report on the effect of the chemical and physical nature of fillers on the adhesion strength. However, the basic questions how the chemistry and surface characteristics of fillers affect this adhesion, and why filler particles and reaction products adhere to each other in cement paste, are rarely addressed yet.

Improvement of the effect of fillers in cementitious materials, especially their effect on the properties of the interface between filler and hydration products, is a big issue and challenge today. Clarifying the role of filler-hydrates adhesion properties in the strength of blended cement paste and understanding the adhesion mechanisms between fillers and hydration products is, therefore, important. The aim of this project was to study the filler-hydrates adhesion properties in blended cement paste system. Two main subjects were dealt with: *the filler-hydrates adhesion mechanisms, and the influence of filler-hydrates adhesion properties on the performance of blended cement paste in view of strength*.

In chapter 3, the effect of the filler-hydrates adhesion properties on the strength of blended cement paste was quantified. The compressive strength of cement paste blended with limestone powder and micronized sand was studied experimentally. The contact area between hydrating cement particles and that between hydrating cement particles and filler particles in blended cement pastes were quantified numerically. The relationship between the measured compressive strength and simulated contact area between particles was then analysed. Based on this relationship, the influence of the

filler-hydrates adhesion properties on the strength of blended cement paste was elucidated. This helps us to better understand the role of filler-hydrates adhesion properties in the strength of blended cement paste.

In chapter 4, the filler-hydrates adhesion properties were studied at the microscale. Crack paths and fracture surfaces of loaded cement pastes were investigated by scanning electron microscopy (SEM) observation. Parallel with the SEM observations, the influence of interface's mechanical properties on crack propagation, tensile strength and fracture energy was studied numerically by using a lattice model. Based on these SEM observations and simulation results, the mechanical properties of the interface between filler particles and hydration products were evaluated. Meanwhile, the study in this chapter provided a validation for the concept of the contact area.

In chapter 5, the filler-hydrates adhesion mechanisms were studied. The influence of the chemical properties of filler on the interaction between main ions, e.g., Ca^{2+}, SO_4^{2-}, in the pore solution of blended cement paste and filler surfaces was investigated via zeta potential measurements. Meanwhile, microscopic observations of the nucleation and growth of C-S-H on the surface of these filler particles were performed by scanning electron microscopy (SEM) to further elucidate these interactions. The important findings of this study concern the influence of surface chemical properties on filler-hydrates adhesion properties and information about the bonds between filler surface and C-S-H.

In chapter 6, based on the knowledge obtained in previous chapters, the fracture behaviour of blended cement paste with strong and weak filler-matrix interfaces was investigated by means of microscale numerical simulations performed with a lattice model. The effect of the microstructural features (size, shape, surface roughness), particle size distribution and volume fraction of filler on the crack patterns and strength of blended cement paste with either strong or weak filler-matrix interface was analysed and discussed.

7.2 Conclusions

The general conclusions of this research are as follows:

- A good correlation was found between the strength and contact area between filler particles and reaction products. With this correlation, the influence of the filler-hydrates adhesion properties on the strength of blended cement paste has been analysed. It was found that the contact area between micronized sand particles and hydration products had no contribution to the compressive strength. By contrast, the contact area between limestone particles and hydration products in cement paste had a substantial contribution to the compressive strength. It implies that limestone powder has much better adhesion properties than micronized sand.
- Surface analysis techniques and mechanical modelling were used to evaluate the mechanical properties of the interface between filler particles and hydration

products. It was found that the bond between limestone particles and hydration products is much stronger than that between micronized sand particles and hydration products. Meanwhile, it provided a validation for the concept of the contact area and justified the findings in chapter 3.

- From the results of zeta potential measurement it was concluded that micronized sand and C-S-H particles have very similar surface properties. This is due to the fact that the surfaces of both micronized sand and C-S-H particles are rich in silicate. Micronized sand and C-S-H have no affinity for Ca^{2+} ions. This was illustrated by the fact that the adsorption of Ca^{2+} and SO_4^{2-} ions onto micronized sand and C-S-H surfaces is similar. Only a few dispersed nuclei, generated on micronized sand and C-S-H surfaces, further supported it. The reason for this is that the adsorption of Ca^{2+} ions onto micronized sand and C-S-H surfaces is mainly driven by relatively weak electrostatic interaction.
- Compared to micronized sand and C-S-H, the surface of a limestone particle has a higher affinity for Ca^{2+} ions. This was confirmed by the zeta-potential measurement. A high amount of C-S-H nuclei, as observed on the limestone surfaces, is an additional supportive evidence. This is mainly due to a strong acid-base (donor-acceptor) interaction between the adsorbed Ca^{2+} ions and the active surface site.
- With regard to the relation between surface chemical properties and the strength of the C-S-H/filler bond, it was concluded that chemically adsorbed Ca^{2+} ions at limestone surface led to the formation of a relatively strong bond (most likely, ionic-covalent bond) between a limestone particle and C-S-H. By contrast, relatively weak electrostatically adsorbed Ca^{2+} ions at micronized sand surface resulted in an attractive ion-ion correlation force between a micronized sand particle and C-S-H.
- The fracture behaviour of cement paste with strong and weak filler-matrix interfaces was simulated at micro-scale by using a lattice model. The simulation results indicated that the strength of the filler-matrix interface plays a more important role in the crack propagation and strength of blended cement paste compared to the effect of the particle size distribution, size, shape, surface roughness and volume fraction of the filler.

7.3 Contributions to science and engineering

The main contributions of this study to science and engineering are as follows:

- A good correlation was found between the strength and contact area between filler particles and reaction products. The strength-contact area correlation was used to quantify the effect of fillers on the strength of blended cement paste. It was found that the contact area between micronized sand particles and hydrating cement particles had no contribution to the compressive strength, whereas the contact area between limestone particles and hydrating cement particles had a

substantial contribution to the compressive strength. These findings were validated. The strength-contact area correlation can be used to quantify the effect of inert fillers on the strength of blended cement paste.

- The mechanical properties of the interface between filler particles and hydration products were qualified by using a combined approach of SEM observations and mechanical modelling (lattice fracture model). It is concluded that the interface between limestone particles and hydration products is much stronger than that between micronized sand particles and hydration products, even stronger than hydration products themselves.
- Basic questions why filler particles and reaction products adhere to each other in blended cement paste, and how the surface properties of fillers affect this adhesion, were addressed in this study. Ca^{2+} ions chemically adsorbed at limestone surface lead to the formation of a relatively strong bond (most likely ionic-covalent bond) between a limestone particle and C-S-H. By contrast, Ca^{2+} ions electrostatically adsorbed at micronized sand surface result in an attractive ion-ion correlation force and hence a relatively weak bond between micronized sand particle and C-S-H.
- With this research insight is gained into the mechanism of nucleation and growth of C-S-H on filler particles. The C-S-H nucleation and growth at the filler surface also due to the interactions between a filler surface and calcium ions in the pore solution. A strong chemical bond of calcium ions to a limestone surface resulted in high volume and uniformly distributed C-S-H nuclei. Ca^{2+} ions electrostatically adsorbed at micronized sand surface led to only a few dispersed nuclei on micronized sand surfaces.
- The approach for the combined use of zeta potential test and SEM observations, which were used in this project to study the adhesion mechanisms, can be applied to investigate the adhesion properties of other fillers and the adhesion forces between these filler particles and reaction products. This approach is efficient and less expensive compared to AFM studies on adhesion mechanisms between filler particles and reaction products.
- The information about the filler-hydrates adhesion mechanisms is very important for the search for new fillers and for improving the performance of existing fillers. For example, based on the knowledge acquired in this study, carbonation can improve the performance of hardened cement paste powder when it is used as a filler in cement paste. This is because carbonation can turn the silicate and CH phase of the surface of the hardened cement paste powder into calcite phase. This enhances the adhesion properties between hardened cement paste particles and new hydration products.
- The fracture behaviour of cement paste with strong and weak filler-matrix interfaces was analysed by using a lattice model. The simulations indicate that the bond strength between filler particles and matrix, rather than the effect of the microstructural features, particle size distribution and volume fraction of filler, plays a dominant role in the crack propagation and the strength of blended

cement paste. The knowledge acquired here can provide a clue, or direction, for improving the performance of fillers in blended cement paste. For example, to improve the performance of fillers in cement paste in term of strength, priority should be given to improving the bond strength between filler particles and matrix, not to modifying the microstructural features (i.e. shape, surface roughness) of filler.

7.4 Prospects

From this study several aspects are recommended for further research:

- The adhesion forces between filler surface and hydration products were studied *indirectly* in this thesis. The *direct* experimental investigation on the adhesion forces at nanoscale requires more advanced techniques.
- In this thesis, only two types of filler (micronized sand and limestone powder) were used to study the filler-hydrates adhesion mechanisms in blended cement paste system. In further research, more fillers need to be studied, such as recycled concrete powder.
- Investigating the adhesion mechanisms between filler particles and reaction products in cementitious materials blended with other binder materials, such as fly ash and slag, is needed, since reaction products of these materials are different from that of Portland cement hydration.
- Recently, geopolymer has become a research focus in view of developing green cementitious materials. Different from the cement gel (C-S-H), the geopolymer gel is sodium aluminosilicate hydrate (N-A-S-H). It is important to get insight into the adhesion mechanisms between filler particles and geopolymer gel.
- It is inferred from this study that the bond between limestone particles and hydration products is much stronger than that between micronized sand particles and hydration products, and even stronger than hydration products themselves. Theoretically, cement paste with a high content of limestone powder can achieve the same strength as Portland cement paste. However, if the water-to-binder ratio is kept constant, the cement paste with a high content of limestone powder has a higher porosity and a lower strength compared to the cement paste with less limestone powder. Optimization of packing can reduce porosity. What is more, the development of more efficient superplasticizers allows increased amount of fillers to be used [17]. Making a cement paste or concrete with high content of limestone powder while maintaining proper strength is challenging, but doable.

References

1. Bonavetti, V., et al., *Limestone filler cement in low w/c concrete: A rational use of energy.* Cement and Concrete Research, 2003. **33**(6): p. 865-871.
2. Nehdi, M., S. Mindess, and P.C. Aitcin, *Optimization of high strength limestone filler cement mortars.* Cement and Concrete Research, 1996. **26**(6): p. 883-893.
3. Justnes, H., et al., *Microstructure and performance of energetically modified cement (EMC) with high filler content.* Cement & Concrete Composites, 2007. **29**(7): p. 533-541.
4. Lothenbach, B., et al., *Influence of limestone on the hydration of Portland cements.* Cement and Concrete Research, 2008. **38**(6): p. 848-860.
5. Bentz, D.P., *Modeling the influence of limestone filler on cement hydration using CEMHYD3D.* Cement & Concrete Composites, 2006. **28**(2): p. 124-129.
6. Gutteridge, W.A. and J.A. Dalziel, *Filler cement: The effect of the secondary component on the hydration of Portland cement.* Cement and Concrete Research, 1990. **20**(5): p. 778-782.
7. Soroka, I. and N. Stern, *Calcareous fillers and the compressive strength of portland cement.* Cement and Concrete Research, 1976. **6**(3): p. 367-376.
8. Berodier, E. and K. Scrivener, *Understanding the Filler Effect on the Nucleation and Growth of C-S-H.* Journal of the American Ceramic Society, 2014: p. n/a-n/a.
9. Moosberg-Bustnes, H., B. Lagerblad, and E. Forssberg, *The function of fillers in concrete.* Materials and Structures, 2004. **37**(2): p. 74-81.
10. Kronlöf, A., *Filler effect of inert mineral powder in concrete.* VTT PUBLICATIONS, 1997.
11. Lawrence, P., M. Cyr, and E. Ringot, *Mineral admixtures in mortars - Effect of inert materials on short-term hydration.* Cement and Concrete Research, 2003. **33**(12): p. 1939-1947.
12. Taylor, H.F., *Cement chemistry*1997: Thomas Telford.
13. Igarashi, S., V. Kawamura, and A. Watanabe, *Analysis of cement pastes and mortars by a combination of backscatter-based SEM image analysis and calculations based on the Powers model.* Cement & Concrete Composites, 2004. **26**(8): p. 977-985.
14. Mehta, P. and P.J.M. Monteiro, *Concrete: Microstructure, Properties, and Materials*2006: McGraw-Hill Education.
15. French, C.W. and A. Mokhtarzadeh, *High strength concrete: Effects of materials, curing and test procedures on short-term compressive strength.* PCI Journal, 1993. **38**(3): p. 76-87.
16. Bentz, D.P., et al., *Multi-scale investigation of the performance of limestone in concrete.* Construction and Building Materials, 2015. **75**: p. 1-10.
17. Lagerblad, B. and C. Vogt, *Ultrafine particles to save cement and improve concrete properties*2004: Cement och Betong Institutet.

Summary

Fillers, such as limestone or quartz powder, are used as a replacement of Portland cement. Their application can make concrete more environment friendly and possibly cheaper. Additions of limestone or quartz powder have been reported to exert a limited chemical effect on cement hydration. The main quasi-chemical effect of added limestone and quartz powder is that they accelerate cement hydration by facilitating nucleation and growth of reaction products at their surfaces.

Fine fillers in cement paste can result in improvements in strength because of a lower porosity and a denser packing. At the same time, however, the use of fillers results in dilution of Portland cement particles and their strength-providing reaction products in the paste. This 'dilution' effect will lead to an increased porosity. Above a critical amount of fillers, the effect of dilution exceeds the effect of packing, resulting in a lower strength of the hardened paste or concrete. These effects (porosity, packing and dilution) on the strength of cement paste have been studied intensively, but they (porosity, packing and dilution) cannot explain difference in performance of different fillers. Also adhesion between filler particles and reaction products has an influence on the strength of blended cement paste. However, filler-hydrates adhesion properties and their effect on the strength of blended cement paste are not quite well understood yet. The basic questions why filler particles and reaction products adhere to each other in blended cement paste, and how the chemistry and surface characteristics of fillers affect this adhesion, are rarely addressed and need further research. The aim of this project is to study the filler-hydrates adhesion properties in blended cement paste system.

Firstly, the influence of the filler-hydrates adhesion properties on the strength of blended cement paste has been analysed. The compressive strength of cement paste blended with limestone powder and micronized sand was studied experimentally. The contact area between different solid phases in these cement pastes was quantified numerically. The relationship between the measured compressive strength and simulated contact area was analysed ("contact area concept"). Based on this relationship, the influence of the filler-hydrates adhesion properties on the strength of blended cement paste was quantified. It was found that micronized sand-hydrates contact area had no contribution to the compressive strength. By contrast, the limestone-hydrates contact area in cement paste had a substantial contribution to the compressive strength.

Secondly, the filler-hydrates adhesion properties were studied at the microscale. Crack paths and fracture surfaces of loaded cement pastes were investigated by scanning electron microscopy (SEM) observation. Parallel with the SEM observations, the influence of interface's mechanical properties on crack propagation, tensile strength and fracture energy was studied numerically by using a lattice model. Based on these SEM observations and simulation results, the mechanical properties of the interface

between filler particles and hydration products were evaluated. Meanwhile, this provided a validation of the 'contact area concept'.

Then, the filler-hydrates adhesion mechanisms in blended cement paste system were investigated. The influence of the chemical nature of fillers on the interaction between main ions, i.e., Ca^{2+}, SO_4^{2-}, in the pore solution of blended cement paste and filler surfaces was investigated via zeta potential measurements. Meanwhile, microscopic observations of the nucleation and growth of C-S-H on the surface of these filler particles were performed by SEM. It was concluded that Ca^{2+} ions chemically adsorbed at limestone surfaces led to the formation of a relatively strong bond (most likely, 'ionic-covalent' bond) between a limestone particle and C-S-H. By contrast, Ca^{2+} ions electrostatically adsorbed at micronized sand surfaces resulted in an attractive ion-ion correlation force and hence a relatively weak bond between a micronized sand particle and C-S-H. This information about the filler-hydrates adhesion mechanisms is very important for the search for new fillers and for improving the performance of existing fillers. For example, based on the knowledge acquired in this study, carbonation can improve the performance of hardened cement paste powder when it is used as a filler in cement paste. This is because carbonation can turn the silicate and CH phase of the surface of the recycled hardened cement paste powder into calcite phase. This can enhance the adhesion properties between hardened cement paste particle and new hydration products.

Finally, the fracture behaviour of cement paste with strong and weak filler-matrix interfaces was simulated at microscale by using a lattice model. The simulations indicated that the bond strength between filler particles and C-S-H matrix plays a more important role in the crack propagation and the strength of blended cement paste compared to the role of the particle size distribution, size (5, 10, 15 and 20 μm), shape, surface roughness and volume fraction (5, 15, 25, 35 and 45%) of the filler. These findings provided support to the previous findings that the strong interfaces between limestone particles and hydration products are due to the superior bond between limestone and hydration products rather than the physical surface properties, such as shape and surface roughness. Moreover, this study indicated the direction for optimization of the performance of fillers in cement paste in view of strength. To improve the performance of fillers, priority should be given to improving the bond strength between filler particles and hydration products. Modifying microstructural features (i.e., shape, surface roughness) of filler is less effective.

Samenvatting

Vulstoffen, zoals kalksteenmeel en kwartspoeder, kunnen worden gebruikt als vervanging van Portland cement. Het toepassen van vulstoffen kan leiden tot meer milieuvriendelijke cementen, die misschien ook nog goedkoper zijn. Toevoegen van kalksteenmeel en kwartspoeder zou slechts een gering effect hebben op de chemische hydratatiereacties. Het belangrijkste quasi-chemische effect van toevoegen van kalksteenmeel en kwartspoeder is dat zij cementhydratatie versnellen door nucleatie en de groei van reactieproducten op hun oppervlakken.

Fijne vulstoffen in cementsteen kunnen resulteren in hogere sterktes als gevolg van een lagere porositeit, c.q. dichtere korrelpakking. Tegelijkertijd resulteert het gebruik van vulstoffen in ‘ruimtelijke verdunning’ van Portlandcementdeeltjes en reactieproducten in de verse cementpasta. Dit 'verdunningseffect’ leidt tot een hogere porositeit. Boven een kritische hoeveelheid vulstof overtreft het effect van verdunning het effect van de korrelpakking, wat vervolgens resulteert in een lagere sterkte van de verharde cementsteen of beton. De effecten van korrelpakking, porositeit en verdunning op de eigenschappen van cementsteen zijn intensief bestudeerd. Uit die studies blijkt echter dat genoemde effecten niet kunnen verklaren waarom het effect van de ene vulstof verschilt van het effect van een andere vulstof. Het blijkt dat ook de hechtsterkte tussen vulstofdeeltjes en reactieproducten invloed heeft op de sterkteontwikkeling van samengestelde cementen. Deze hechtsterkte tussen vulstof en hydratatieproduct is nog nauwelijks in detail onderzocht. Fundamentele vragen waarom reactieproducten zich in meer of mindere mate aan vulstofdeeltjes hechten vragen dan ook om meer onderzoek. Het doel van dit project is het bestuderen van de aanhechting tussen vulstof en hydratatieproduct in samengestelde cementen.

Eerst is de invloed van de aanhechting tussen vulstof en hydratatieproduct op de sterkteontwikkeling experimenteel onderzocht. Gekeken is naar de druksterkte van cementsteen vervaardigd van samengestelde cementen met kalksteenmeel en gemicroniseerd zand als vulstof. De contactvlakken tussen vulstofkorrels en hydratatieproducten zijn numeriek gekwantificeerd. De relatie tussen de gemeten druksterkte en het gesimuleerde contactvlak is geanalyseerd (“contactvlakconcept”). Op basis van deze relatie is de invloed onderzocht van de hechtsterkte tussen vulstof en hydratieproduct op de sterkteontwikkeling van samengestelde cementen. Geconstateerd is dat het contactvlak tussen korrels van gemicroniseerd zand en hydratieproduct geen bijdrage levert aan de druksterkte. Daarentegen draagt het contactvlak tussen kalksteenmeel en hydratenproduct wel wezenlijk bij aan de druksterkte.

Hierna zijn de aanhechteigenschappen van vulstoffen en hydratieproducten op microschaal bestudeerd. Scheurgroei en breukvlakken in cementsteen vervaardigd van samengestelde cementen werden onderzocht met behulp van een elektronenmicroscoop (SEM). Parallel aan het microscopieonderzoek werd de invloed van de mechanische

eigenschappen van de interface tussen vulstofkorrels en hydratatieproduct op scheurvervorming, treksterkte en breukenergie numeriek bestudeerd met behulp van een lattice model. Op basis van de SEM-waarnemingen en de resultaten van de numerieke simulaties werden de mechanische eigenschappen van de interface tussen vulstof en hydratatieproduct geëvalueerd. Op grond van deze evaluatie kon het 'contactvlakconcept' worden gevalideerd.

Vervolgens zijn de aanhechtmechanismen tussen vulstofkorrels en hydratatieproduct onderzocht met behulp van zeta-potentiaalmetingen. Met deze methode is de invloed onderzocht van de chemische eigenschappen van een vulstofoppervlak op de interactie tussen de belangrijkste ionen in een kunstmatige poriënwateroplossing (Ca^{2+}, SO_4^{2-}) en het vulstofoppervlak. Parallel werden microscopie-waarnemingen verricht van nucleatie en groei van C-S-H-deeltjes op het oppervlak van vulstofkorrels. Geconcludeerd werd dat Ca^{2+} ionen een relatief sterke binding hebben met het kalksteenoppervlak (meest waarschijnlijk een 'ion-covalente' binding). Daarentegen bleken Ca^{2+} ionen elektrostatisch geadsorbeerd te worden aan het oppervlak van gemicroniseerde zand. Verondersteld is dat het hier om een relatief zwakke ion-ion verbinding gaat. Deze informatie over de aanhechtmechanismen is van groot belang voor het onderzoek naar nieuwe vulstoffen en het verbeteren van prestaties van bestaande vulstoffen. Bijvoorbeeld, op basis van de verworven kennis kan men veronderstellen dat carbonisatie van gerecyclede cementsteen de prestatie van cementsteenpoeder verbetert als het wordt gebruikt als vulstof in cementsteen. Dit komt omdat door carbonisatie de silicaatfase van het oppervlak van de gerecyclede cementsteen wordt omgezet in calciet ($CaCO_3$). Dit verbetert de aanhechting tussen gerecyclede cementsteen en nieuwe hydratatieproducten.

Tenslotte is het scheurgedrag van cementsteen met sterke en zwakke aanhechtsterkte tussen vulstof en hydratatieproduct, i.c. matrix, gesimuleerd met behulp van een lattice model. De simulaties geven aan dat de sterkte van de vulstof-matrix interface een belangrijker rol speelt bij scheurgroei en resulterende sterkte van samengestelde cementen dan het effect van deeltjesgrootteverdeling, korrelgrootte, korrelvorm, oppervlakte ruwheid en volumefractie van de vulstof. Deze resultaten ondersteunen eerdere bevindingen dat de sterke interface tussen kalksteenmeel en hydratatieproduct het gevolg is van een superieure (chemische) binding tussen kalksteenmeel en reactieproduct en niet het gevolg is van (fysische) micro-structurele kenmerken, zoals vorm en oppervlakte ruwheid van de vulstofkorrels. Deze studie heeft hiermee een richting gegeven voor het optimaliseren van de prestaties van vulstoffen in cementsteen als het om de sterkte gaat. Om de prestaties van vulstoffen te verbeteren dient prioriteit te worden gegeven aan het verbeteren van de bindingssterkte tussen vulstofdeeltjes en matrix. Het modificeren van micro-structurele kenmerken (d.w.z. vorm, oppervlakte-ruwheid) van de vulstof is minder effectief.

Acknowledgements

At the end of this thesis, I would like to take this opportunity to thank all the people without whom the completion of this thesis would never have been possible. Although it is just my name on the cover, many people have contributed directly or indirectly to the research reported here and for that I would like to give them special thanks.

Foremost, I would like to express my deepest appreciation to my promotor Prof. dr. ir. K. van Breugel for providing me the opportunity to do research in Microlab at TUDelft. His patience strongly encouraged me walking out of struggles that I came across on the way. Besides, I have learnt a lot from him about scientific writing and presenting. My thesis would not be accomplished without his guidance, suggestions and persistent support. I would like to sincerely thank my co-promotor Dr. Guang Ye for his encouragement and persistent help throughout my research. His suggestions are always very inspiring. I also would like to deliver my special thanks to my co-promotor Dr. D.A. Koleva for her suggestions and generous help in both lab work and paper work during the last two years.

I also want to take a moment to thank my committee members, Prof. dr. Kefei Li, Prof. dr. ir. H.E.J.G. Schlangen, Prof. dr. Stephen Picken and Dr. Jorge S. Dolado for spending their time on reviewing my thesis, giving comments and attending my PhD defence.

I would like to acknowledge China Scholarship Council (CSC) and Delft University of Technology (TUDelft). The research work reported in this thesis was sponsored by these institutes. I also would like to express acknowledgement to Prof. Dong Ouyang and Prof. Hong Yuan at Jinan University, P.R. China. They supported me to apply this PhD position at TUDelft.

I owe gratitude to Gerrit Nagtegaal, Arjan Thijssen and John van den Berg and Maiko van Leeuwen for their help with my experimental work. A special gratitude goes to Dr. Hitham Amin Hassan and Dr. Chassagne Claire from the section of environmental fluid mechanics at TUDelft for helping me in zeta potential measurement. I am heartily thankful to Peng Gao, Dr. Zhiwei Qian, Dr. Zichao Pan, Dr. Mladena Lukovic and Dr. Branko Savija for helping me in modelling work.

I warmly acknowledge all colleagues in the Microlab. It would not be such a wonderful experience without any of them. In particular, I would like to thank secretaries: Claire de Bruin, Nynke Verhulst, Melanie Holtzapffel and Claudia Baltussen, and Franca Post from CICAT. They helped me a lot with various daily issues. I would like to give my thanks to my current office mates, Eirini Tziviloglou and Yibing Zuo. They always provided the nice atmosphere in the office. I would like to express my gratitude to Dr. Henk Jonkers, Dr. Oguzhan Copuroglu, Dr. Lupita Sierra Beltran, Dr. Marc Ottele, Dr. Mingzhong Zhang, Dr. Ying Wang, Dr. Georgi Georgiev,

Dr. Yuwei Ma, Dr. Haoliang Huang, Dr. Zhengxian Yang, Dr. Senot Sangadji, Dr. Jure Zlopasa, Dr. Zhuqing Yu, Prof. Dr. Jiangxiong Wei, Dr. Fuhai Li, Dr. Yun Huang, Dr. Chunping Gu, Bei Wu, Dr. Damian Palin, Agus Susanto, Farhad Pargar, Dr. Amir Zomorodian, Dr. Bahman Ghiassi, Renee Mors, Balqis MD Yunus, Zhipei Chen, Vladislav Omelchuk, Stefan Chaves Figueiredo, Marija Nedeljkovic, Claudia Romero Rodriguez, Kuba Pawłowicz etc. They helped me directly or indirectly on my research.

A very special gratitude goes out to my Chinese colleagues, Hua Dong, Tianshi Lu, Hao Huang (Heya Na), Jiayi Chen (Wenqin Shi), Xuliang Hou (Dr. Ying Yang), Xu Ma, Jiahua Liu, Leyang Lu, Zhenming Li, Wenjuan LYU, Hongzhi Zhang, Shi Xu (Qiling Wang), Shizhe Zhang for all the great time that we shared. The lunch time we shared every day is memorable. The good time we spent together in South France is unforgettable. Their support and help in my daily life during these years in the Netherlands are also acknowledged.

I am grateful to all the friends that I met in the Netherlands. Their friendships replace my longlines with the happiness and rich my life in the land which is far away from my hometown. I owe many thanks to Ming Li, Jinhu, Feifei, Zhen Yang, Xueming Xin Li, Lin Xiao, Xiaochen, Yuling, Jingyu, Xin Tian and Wen Yang from ‘Wolf family’. I also like to express my deep appreciation to Tao Lv, Kai Li (Shulan Shu), Kai Zhang (Li Zhu), Zilong Wei (Yan Zhou), Dr. Guangming Chen, Qujiang Lei, Dr, Xiangwei Liu, Dr. Xiaoyan Wei, Dr Wuyuan Zhang, Yang Qu, Mingjuan Zhao, Xiangming Liu, Jiakun Gong, Dr. Yuanyang Wan, etc. My life in the Netherlands could not be so colourful without them.

I want to express my greatest thanks to my parents and grandmother for bringing me up and endlessly supporting me. Last but not the least, I would like to express my deepest gratitude to my beloved wife (Cui Wei) and daughter (Shiying Ouyang). My wife left her family in China and came to the Netherlands to accompany me and support me. Without her unconditional love, support, sacrifices and endless encouragements, I would never have had this colourful and enjoyable life.

Xiaowei Ouyang
September, 2017

TU Delft Delft University of Technology